Horizontal Direction Drilling

Estimating Pipe Pulling Tensions

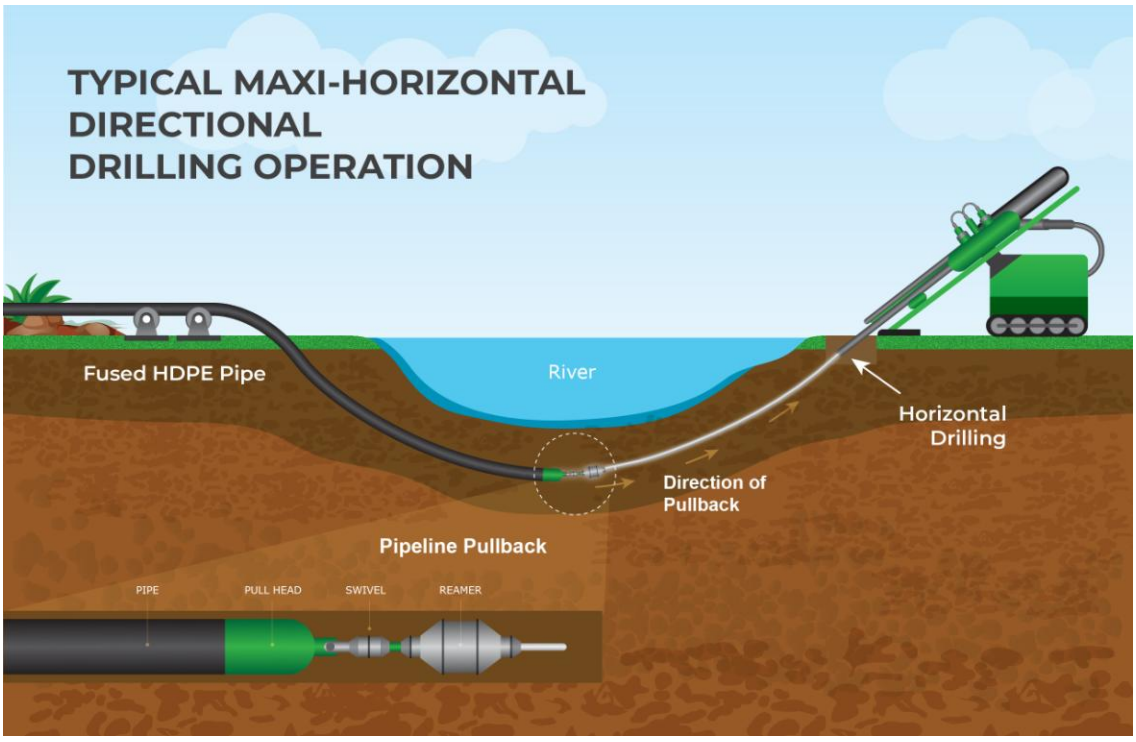

Lawrence M. Slavin, Ph.D.

Drawing on cover courtesy of Murphy Pipeline Contractors

FOREWORD

This publication is intended as an aid for engineers, users, contractors, code officials, and other interested parties in the use of horizontal directional drilling (HDD) for the design, construction and installation of piping systems, and especially those of high-density polyethylene (HDPE). The local utility or engineer may need to modify the information in this book to adapt the results to local conditions, operations, and practices.

The information in this book is offered in good faith and believed to be accurate at the time of its preparation, but is offered "as is" without express or implied warranties, including WARRANTIES OF MERCHANTABILITY AND FITNESS FOR A PARTICULAR PURPOSE. Any reference to a specific manufacturer's product is merely illustrative, and not intended as an endorsement of that product. Reference to a proprietary product should not be construed as an endorsement by the author, who does not endorse the proprietary products or processes of any manufacturer. Users are advised to consult the manufacturer for more detailed information about the specific manufacturer's products. The information in this document is offered for consideration by all interested parties in fulfilling their own compliance responsibilities. The author assumes no responsibility for compliance with applicable laws and regulations.

Please send suggestions of improvements to Dr. Lawrence M. Slavin, at LSLAVIN@IEEE.ORG.

CONTENTS

PREFACE

This book provides analyses and methods for estimating the pull forces on a product pipe being installed by horizontal directional drilling (HDD). The results may be used for selecting the pipe strength, as determined by its wall thickness, for a given size (diameter) pipe or conduit. This force also represents a significant portion of the required force exerted at the drill rig, which equipment must also overcome resistance due to the pulling of the drill rods and the reamer. The focus of the book is on long-distance, "maxi-HDD" operations, using high density polyethylene (HDPE) pipe, but short distance, "mini-HDD" installations are also discussed.

The original basis for the tension calculations is provided in ASTM F1562, *Standard Guide for Use of Maxi-Horizontal Directional Drilling for Placement of Polyethylene Pipe or Conduit Under Obstacles, Including River Crossings*. It is understood that the model used and associated assumptions are approximations of a complicated process, but is intended to provide conservative estimates for design purposes. This model has also been extended to geometries and applications not directly considered in the original standard, using techniques and analyses presented and described in technical papers previous published by the author (and co-authors), with some revisions, as necessary, to provide more recent considerations as well a consistent, integrated presentation of the various issues addressed. While originally intended to be applied to carefully engineered, well-controlled maxi-HDD installations, further assumptions and mathematical simplifications provide a practical means of estimating the peak pull load for the more ubiquitous mini-HDD applications.

The relative effect of the various parameters on the magnitude of the pull load are examined, allowing the user to focus on the most efficient means of minimizing the required tensions, and/or determining the most cost-effective HDPE pipe product to meet the project needs. While the ASTM method ignores the possible effects of the pipe bending stiffness, the effect of this characteristic is investigated, and found to generally not be a major consideration. However, since a non-level grade, or different elevations of drill entry and exit points, will not be an unusual occurrence, it is important to consider the implications of this situation, both with and without the use of ballast, a commonly used technique to reduce pull loads. Two chapters are devoted to understanding and evaluating the effects of the associated phenomena.

Because of its ability to be provided in continuous lengths, or be conveniently fused with little or no loss in tensile strength and the absence of local bulges due to mechanical connectors, as well as its low bending stiffness, polyethylene pipe is the most commonly used product for HDD projects. The examples and quantitative results are therefore based on the installation of HDPE pipe, for which the assumed physical properties (e.g., strength and stiffness) are generally consistent with the PE4710 material, as presently being incorporated into an upcoming revision of ASTM F1962, unless otherwise stated. Other materials, however, are routinely installed using HDD, for either the long (maxi) or short (mini) installations.

The information in this document is believed to be accurate at the time of its preparation, but is provided without any warranty, expressed or implied.

August 25, 2022

Lawrence M. Slavin, Ph.D.
Rockaway, NJ 07866
LSLAVIN@IEEE.ORG

ABOUT THE AUTHOR

Dr. Lawrence (Larry) M. Slavin is Principal of Outside Plant Consulting Services, Inc. which was established in the year 2002 to help meet the needs of the telecommunications, power and pipeline industries, in establishing standards, guidelines and practices for related outside plant (outdoor) facilities and products. Larry has extensive experience and expertise in such activities, based upon his many years of service at AT&T/Lucent Bell Telephone Laboratories (Distinguished Member of Technical Staff) in telecommunications product design and development, followed by a career at Telcordia Technologies (now Ericsson, formerly Bellcore) in its research and professional service organizations. As Principal Consultant and Manager/Director of the Network Facilities, Components and Energy Group at Telcordia, he provided technical leadership in developing installation practices and "generic requirements" documents, introducing new construction methods, and performing analyses on a wide variety of technologies and products. Throughout his long career, Larry has had a leading role in the evolution of many telecommunications related fields and disciplines, for both overhead and belowground lines, as well as in the placement of underground conduit and pipelines for general utility applications. Larry received his Bachelor's degree in mechanical engineering from The Cooper Union for the Advancement of Science and Art, and his Master's and Ph.D. degrees from New York University. He lives with his wife, Helen, in White Meadow Lake in north central New Jersey.

ACKNOWLEDGEMENT

The author expresses his sincere appreciation to Camille Rubeiz and the Plastics Pipe Institute and its Municipal Advisory Board for their continuing support of industry efforts to help advance the state-of-the art of horizontal directional drilling. It is hoped that this book will be useful in this endeavor.

CHAPTER 1
INTRODUCTION

1.1 BACKGROUND

"Horizontal Directional Drilling" (HDD) is a form of "trenchless technology" for installing product pipes or conduits, below ground using a surface-mounted drill rig that launches and places a drill string at a shallow angle to the surface and has tracking and steering capabilities. The drill string creates an initial (pilot) borehole in an essentially horizontal path or shallow arc which may be enlarged during a secondary operation, or sequence of such operations, through use of a reamer. The product pipe may be installed during the final reaming operation, or, if necessary, as a separate, last step in the process. Figure 1-1 shows a simplified drawing of the pipe installation process.

The predetermined path of the bore is maintained by tracking the path of the pilot bore and performing steering and path corrections by controlling the orientation of the drill head. Soil penetration is accomplished using high pressure, low volume fluid jets and/or mechanical cutting. The drilling fluid volume is controlled to avoid or minimize the creation of voids during the initial boring and back-reaming operations. The drilling fluid serves several purposes, including stabilization of the borehole, removal of cuttings, lubrication for the drill string and product pipe, and cooling the drill head and internal electronics. Typically, the resultant slurry created by the combination of the drilling fluid and soil cuttings gradually solidifies into a solid mass encapsulating the product pipe.

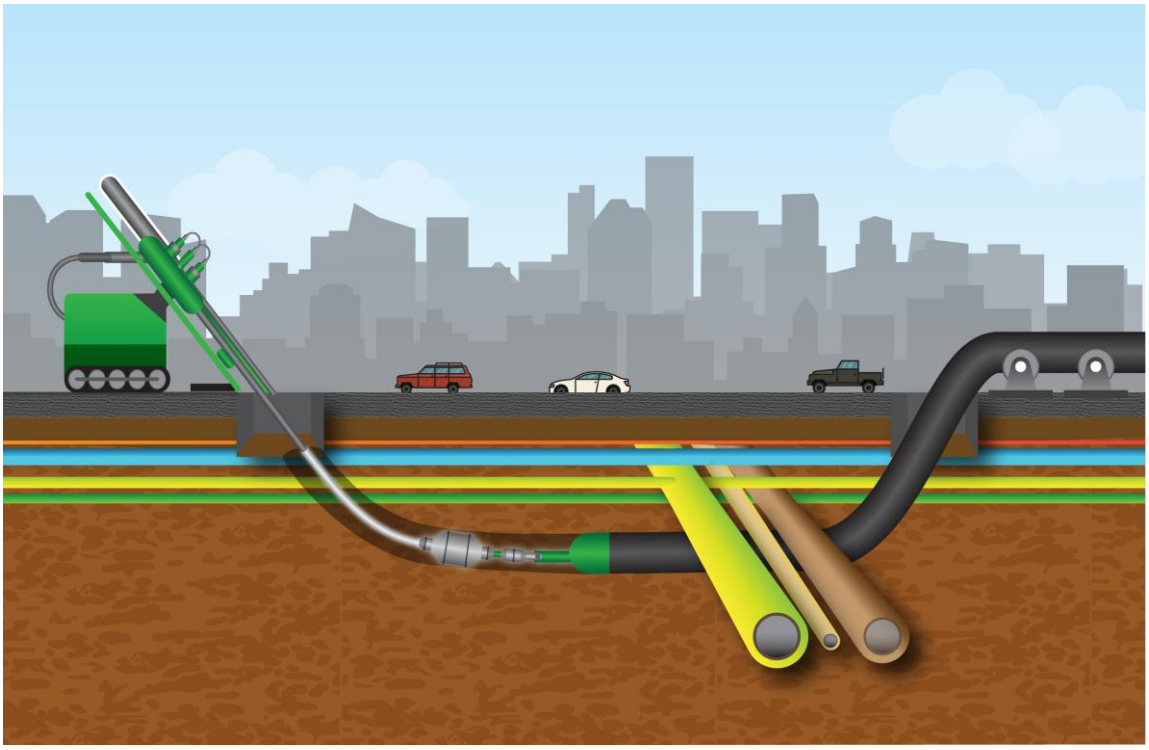

Figure 1-1. Typical HDD Operation.
(Courtesy of Murphy Pipeline Contractors)

Horizontal directional drilling encompasses a wide range of equipment and capabilities, ranging from small rigs used for distribution and service applications to large machines able to install pipelines up to 48-inches or greater, for distances as long as one or two miles, including beneath rivers or other obstacles. HDD operations and equipment on the smaller scale are sometimes referred to as "mini-horizontal directional drilling" (mini-HDD), and are typically employed for boring segments less than 600 feet in length, such as distribution lines beneath streets, placing pipes or conduits up to 12 inches diameter; see Figure 1-2.

Figure 1-2. Typical HDD Machine.
(Courtesy of Ditch Witch®, Inc.)

The HDD operations and equipment at the larger end are commonly referred to as "maxi-horizontal directional drilling" (maxi-HDD), using equipment such as illustrated in Figure 1-3. The primary focus on the book is on maxi-HDD.

Figure 1-3. Typical Maxi-HDD Machine.
(Courtesy of American Augers, Inc.)

1.2 ASTM F1962

ASTM F1962, *Standard Guide for Use of Maxi-Horizontal Directional Drilling for Placement of Polyethylene Pipe or Conduit Under Obstacles, Including River Crossings*, was originally approved in 1999, following development within the F17.67 Trenchless Technology Subcommittee of the ASTM organization[1], and reissued with minor revisions in 2005 and 2011, and reinstated in 2020. A detailed description of ASTM F1962, and its application, was provided during NO-DIG 2006 (Petroff, 2006), with another article in 2010 describing its "decade of success" (Petroff, 2010).

The ASTM document provides overall guidelines for a maxi-HDD operation, addressing preliminary site investigation, safety and environmental considerations, regulations and damage prevention, bore path layout and design, implementation, and inspection and site cleanup. One of the most significant contributions of ASTM F1962 is the provision of a rational, analytical method for selecting the polyethylene (PE) pipe strength based upon the estimated installation loads on the polyethylene pipe. Thus, ASTM F1962 provides a means of determining project feasibility, as well as initial design information. Such results could be further refined by competent engineering expertise, including an analysis of pipe and soil characteristics and interaction, often including the use of relatively sophisticated software tools.

ASTM F1962 attempts to make reasonable or conservative assumptions in the process of estimating the loads associated with the HDD pipe placement process as applied to the pipe. The loads are compared to the corresponding strength to evaluate the ability of the pipe to withstand the loads, with a reasonable margin of confidence. There are essentially two categories of loads to be considered. The pipe must withstand the peak pulling stresses experienced during the

[1] Originally known as the American Society for Testing and Materials.

installation process, as well as the laterally or radially imposed forces due to the drilling fluid/slurry pressure, or possible subsequent soil loads, without collapse. The guide addresses both of these possible failure modes. However, it is the evaluation of the former condition (tensile failure) that has received most of the attention in the industry due to the loads being so uniquely characteristic of the HDD process, and is therefore the focus of this manual.

Although other methods developed within the HDD industry for estimating the pulling load (Huey et al, 1996; Cheng, 2007) are based upon generally similar concepts, the theoretical model in ASTM F1962 is somewhat different and is, in part, based upon cable installation principles from the communications and electric power industries. The convenience of the methodology has led to its widespread usage throughout the industry for maxi-HDD installations, including internationally (Xiao et al, 2012; Zeng et al, 2013). The procedure is straightforward and has been incorporated into various software tools (e.g., Vermeer Boreaid®, PipeEng) as an engineering and design aid for such projects (Bayat et al, 2011).

The ASTM guide specifically addresses polyethylene pipe (PE). Relevant material properties for PE pipe, such as safe pull stress, are also provided in the document. Because of its ability to be provided in continuous lengths, or be conveniently fused with little or no loss in tensile strength and the absence of local bulges due to mechanical connectors, as well low bending stiffness, polyethylene pipe, particularly high density polyethylene (HDPE), is the most commonly used product for HDD projects. Nonetheless, ASTM F1962 has been adopted or applied to pipes constructed of other materials, with apparent success.

Chapter 2 of this manual reviews the methodology and basis for the corresponding formulae related to the pulling loads and their usage within ASTM F1962, and also discusses various issues that have arisen in their application. Chapter 3 discusses the results of a parametric study, to help understand the relative effects of the values of significant bore path characteristics on the magnitude of the required tension. A basic assumption in ASTM F1962 is that the pipe bending stiffness is very low (e.g., PE), such that any bearing forces, and associated frictional drag, at route bends are insignificant. Since this document has been used for evaluating the pull forces developed when installing non-PE products, Chapter 4 estimates the effect of a finite pipe bending stiffness on the required pull forces, as a function of basic material stiffness, pipe size, and route curvature. A related comparison of the results using ASTM F1962 with those of another popular procedure, explicitly considering pipe stiffness, is provided in Chapter 5. Although ASTM F1962 is intended for carefully designed, well-controlled maxi-HDD installations, the methodology has been extended, via appropriate assumptions and mathematical simplifications, to provide a simpler methodology that may be advantageously applied to typical, less well-controlled, mini-HDD projects, as discussed in Chapter 6. Indeed, this relatively simple procedure may provide better agreement with practical mini-HDD installations than the more detailed method of ASTM F1962, if the latter were to be applied to such projects.

Since the basic geometry assumed in the model is a level grade – i.e., that the entry and exit points for the drilling operation are at the same elevation – it is also of interest to consider the impact of a non-level grade (i.e., different elevations of entry and exit points). Chapter 7 investigates the simpler case, if internal (water) ballast is not used, while Chapter 8 considers the potential effects if ballast is employed, a commonly used procedure to reduce the buoyant weight of an otherwise empty pipe, in an attempt to reduce the corresponding drag and required pull

forces. The results in these two chapters are considered to be especially important, since they are not necessarily intuitive and such applications are not uncommon.

Quantitative results are presented throughout the book to illustrate the various issue(s) being addressed within the individual chapters. A glossary of terms is provided as an aid to the reader.

CHAPTER 2
ASTM F1962 METHODOLOGY[2]

2.1 PROCEDURE

Figure 2-1 illustrates a typical geometry for a maxi-HDD operation, in this case corresponding to a river crossing. The indicated bore/pipe path comprises three segments spanning the pipe entry (point A) to its exit point (point D), with horizontal projected distance L_{bore}, equal to the sum of the three horizontal (projected) segments L_2, L_3 and L_4. There is an additional length L_1 exterior to the drilled path which allows for handling at both ends and possible other effects (path curvature, thermal contraction, ...). The intermediate horizontal segment, L_3, may be of zero length.

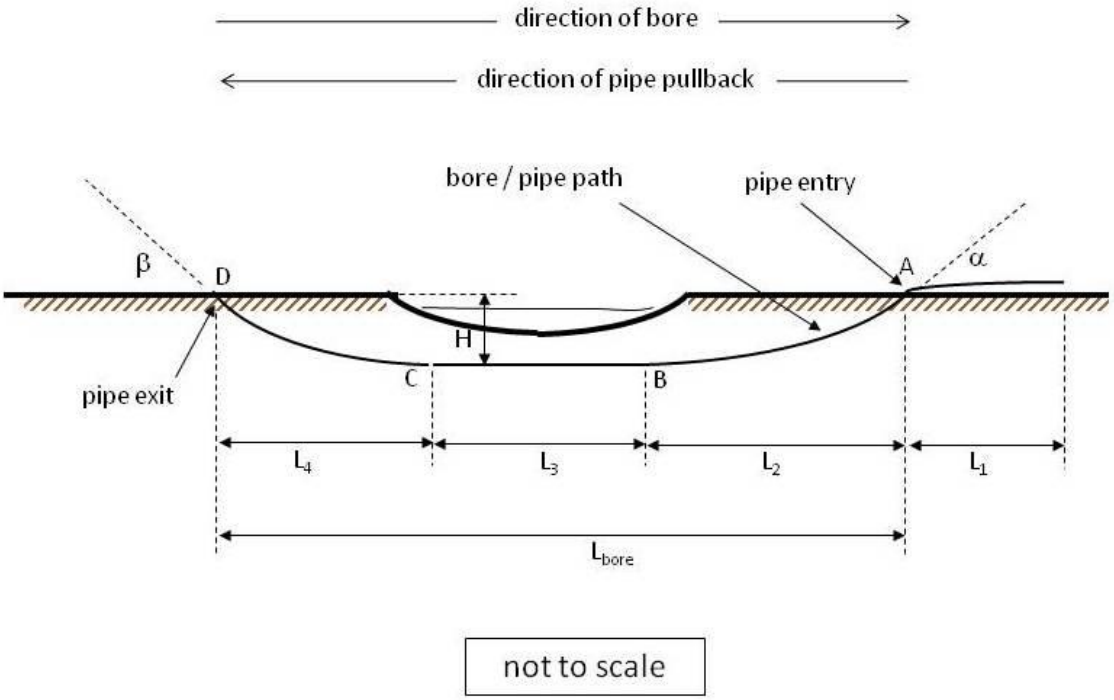

Figure 2-1. Typical Maxi-HDD Route (Obstacle or River Crossing)
(Courtesy of Outside Plant Consulting Services, Inc.)

Referring to Figure 2-1, ASTM F1962 provides a set of relations used to estimate the required pull force – T_A , T_B , T_C , and T_D – corresponding to the leading end of the pipe reaching point A, B, C and D:

$$T_A = e^{\nu_a \alpha} \cdot \nu_a \cdot w_a \ (L_1 + L_2 + L_3 + L_4) \qquad [2\text{-}1a]$$

$$T_B = e^{\nu_b \alpha} \ (T_A + \nu_b \cdot |w_b| \cdot L_2 + w_b \cdot H - \nu_a \cdot w_a \cdot L_2 \cdot e^{\nu_a \alpha}) \qquad [2\text{-}1b]$$

$$T_C = T_B + \nu_b \cdot |w_b| \cdot L_3 - e^{\nu_b \alpha} \nu_a \cdot w_a \cdot L_3 \cdot e^{\nu_a \alpha} \qquad [2\text{-}1c]$$

$$T_D = e^{\nu_b \beta} \ [T_C + \nu_b \cdot |w_b| \cdot L_4 - w_b \cdot H - e^{\nu_b \alpha} \ \nu_a \cdot w_a \cdot L_4 \cdot e^{\nu_a \alpha}] \qquad [2\text{-}1d]$$

[2] Ref. "Discussion of ASTM F1962 or 'How are the Pulling Load Formulas Derived and How are they Used?' ", Slavin and Petroff, NO DIG 2010, Chicago.

where w_a and w_b are the empty (positive downward) and buoyant (positive upward) weights of the pipe, respectively, and ν_a and ν_b. are the corresponding "coefficients of friction", as defined below. The pipe entry (i.e., pilot bore exit) angle α and pipe exit (i.e., drill rig side) angle β are expressed in radians, for which one radian equals $180^o / \pi$. Although Equations [2-1] are well-defined, their complexity requires care in performing the calculations in order to avoid errors.

These formulae account for the frictional drag acting on the pipe along the surface of the borehole, and are sufficiently general to consider the possible implementation of anti-buoyancy measures to reduce the otherwise high values of w_b for vacant PE pipe. The use of the absolute value symbol in the term $|w_b|$ is generally unnecessary for PE pipe, since the buoyant weight will always be positive in practical applications, but is provided in anticipation that the methodology may be used for other situations or applications.

While these equations account for the majority of the drag forces resisting the pipe's movement into the borehole, there is an additional term, ΔT, that is added to the above terms at the individual stages of progress (points A, B, C, and D). This incremental tension is intended to account for the ("fluidic drag") effect of the mud slurry flowing along the surface of the pipe, and is estimated by:

$$\Delta T = \Delta P \cdot (\pi/8) \cdot (D_{hole}^2 - D^2) \qquad [2\text{-}2]$$

where D_{hole} is the diameter of the borehole and D is the outer diameter of the pipe. The term ΔP is the incremental drilling fluid (hydrokinetic) pressure in the borehole at the leading end of the pipe during the pullback operation, which is in addition to the hydrostatic pressure corresponding to the head (depth) of the relatively dense resulting slurry.

The incremental tension, ΔT, is added to the local tension T_A , T_B , T_C , or T_D as specified in Equations [2-1] for each of the four points, but is *not cumulative*; e.g., the value of T_A inserted into Equation [2-1b] is that given by Equation [2-1a], as written, and *not* $T_A + \Delta T$, etc. This is clearly indicated in ASTM F1962, but is not always properly implemented by users. In any case, this estimate of ΔT is usually low compared to the tension components given by Equations [2-1], as based on a conservatively recommended value of 10 psi in ASTM F1962; values of ΔP are typically 4 – 8 psi (Svetlik, 1995). In the absence of ballast, the maximum total calculated tension will typically occur towards the end of the installation; e.g., at point C or D.

Although the bending stiffness of polyethylene may be considered insignificant with respect to developing bearing forces and associated drag forces at route bends, the local bending stresses induced within the pipe are considered in ASTM F1962, and should added to the average stress corresponding to the results of Equations [2-1] and [2-2]. This effect is relatively minor for the flexible PE pipe, for the relatively large radii of curvature generated by the steel drill rods. The net resulting peak tensile stress is required to be less than the safe pull stress (SPS) of the PE pipe (Petroff, 2006).

2.2 THEORETICAL BASIS FOR MODEL

The theoretical model used to estimate the required pull force assumes that frictional drag forces on the pipe are directly related to the local bearing forces applied at the pipe surface. Such bearing forces may be a reaction to the dead weight of the pipe where above ground or the

buoyant weight of the submerged pipe. For an empty PE pipe, the latter weight results in the primary drag effects, and which are usually the dominant contributor to the required pull force. The buoyant weight, however – and the associated drag forces – may be mitigated by anti-buoyancy measures, such as filling the submerged portion of the pipe with ballast, most conveniently using water. Additional frictional drag effects may possibly result from the bearing/bending forces associated with pulling a relatively stiff (e.g., non-PE) pipe around a curve, but especially from the bearing forces resulting from (previously induced) axial tension, which tends to pull the pipe snugly against any locally curved surface. In addition, to these frictional drag effects, the drilling fluid/slurry flowing along the length of the pipe, as reflected in Equation [2-2], results in fluidic drag, somewhat increasing the required pulling force. Greater details are provided below.

2.21 Frictional Drag Due to Weight and Buoyancy

The tension values in Equations [2-1] are determined assuming conventional "Coulomb" friction, which assumes that drag forces on the pipe are proportional to the local normal bearing forces, with the proportionality constant defined as the "coefficient of friction". In the absence of anti-buoyancy techniques, the frictional drag developed within the borehole is generally much greater than that developed outside, even assuming a possibly higher coefficient of friction outside the borehole, due to the very large buoyant weight for the empty PE pipe within the borehole. The basic methodology for calculating the combined effects of weight and buoyancy, and the resulting frictional drag resistance, has been provided by Svetlik (1995), and, with the exception of the various exponential terms, is equivalent to Equations [2-1]. Suggested values for the coefficients of friction are provided in ASTM F1962, consistent with industry recommended values (Svetlik, 1995). In particular, the suggested value for ν_b of 0.3 for the coefficient of friction within the borehole is also consistent with more recently obtained values based upon controlled laboratory studies (El-Chazli et al, 2005). For the coefficients of friction, ν_a, external to the borehole, values of 0.5 and 0.1 are suggested for PE pipe resting on the ground surface or rollers, respectively.

The buoyant weight of the submerged pipe is a major factor in determining the required pull force. ASTM F1962 provides formulae for determining the buoyant weight under various conditions, including the use of internal liquid (e.g., water) ballast to reduce buoyancy, and is a direct function of the density of the slurry. For the purpose of design calculations, a conservatively high specific gravity of 1.5 is suggested, although such a high density is not generally recommended during actual operation due to increased required pumping pressure and corresponding elevated risk of drilling fluid leakage from the borehole and to the surface.

2.22 Pipe Stiffness at Bends

Bearing/bending forces may possibly be significant for pipes with high material stiffness and/or large diameter when installed in pulled into boreholes with limited clearance or relatively sharp bends. However, for flexible PE pipes, installed in boreholes with recommended minimal clearances (e.g., 50% of pipe diameter), along gradually curved paths created by the relatively stiff steel drill rods, such effects may be ignored. For other applications, the magnitude of the effect of the pipe bending stiffness on the pulling force may be estimated as discussed in Chapter 4.

2.23 Capstan Effect at Bends

Somewhat independent of the pipe stiffness effect at bends described above, is another, considerably more important, effect associated with discrete route bends, or gradual path curvature, that should not be ignored. Tensions induced in the pipe as it negotiates the bore path, become amplified at such curves due to the tensile forces tending to pull the pipe against the curved surface, resulting in increased local bearing forces, and increased frictional drag. This phenomenon is referred to as the "capstan effect" since it is the operating principle of the capstan winch, as illustrated in Figure 2-2. This magnitude of this effect primarily depends upon the bend angle, and is independent of the pipe stiffness, pipe diameter, borehole clearance, radius of curvature or direction of curvature. Bends in opposite directions do not cancel, but are cumulative, with the total cumulative angle traversed being the significant parameter.

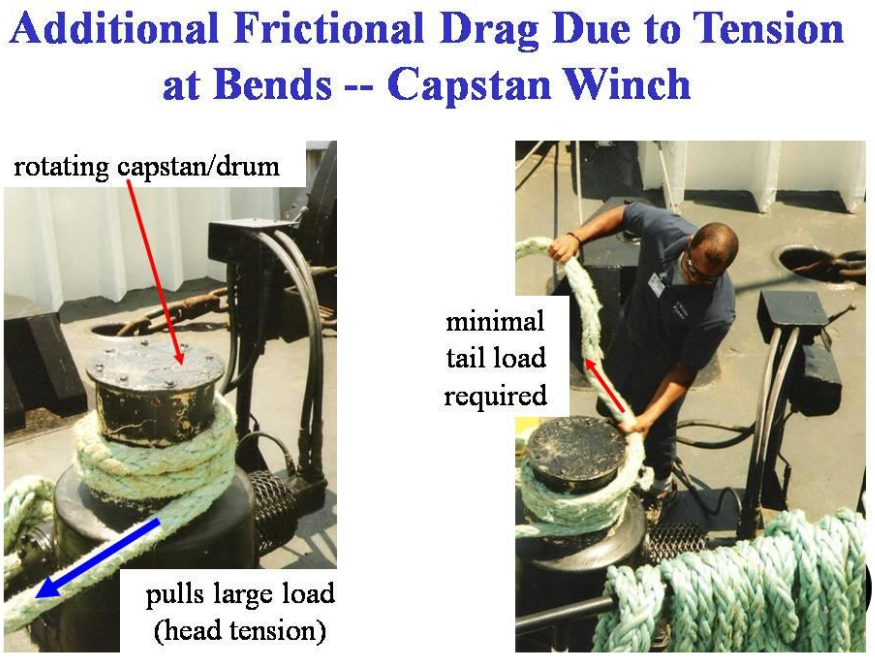

Figure 2-2. Example of "Capstan Effect"
(Courtesy of Outside Plant Consulting Services, Inc.)

The basic phenomenon of tension amplification at a bend – for the placement of a weightless, flexible item, such as rope, cable or PE pipe – may be quantified by:

$$T_2 = T_1 \cdot e^{\nu\,\theta} \qquad [2\text{-}3]$$

where T_1 represents the axial tension ("tail load") present at the beginning of a bend of magnitude θ (radians), ν is the local coefficient of friction between the (sliding) item and wall surface of the cavity, and T_2 is the required axial tension at the end of the bend. The exponential term $e^{\nu\,\theta}$ represents an amplification factor due to the discrete or cumulative bend angle θ. In practice, the effect of the actual weight of the pipe, or possible finite stiffness, may be reflected in the preceding tension, T_1. However, any weight (or buoyancy), or possible stiffness, effects occurring along the bend itself are conveniently ignored.

Detailed discussions of this mechanism and associated formulae for various path geometries are provided in the literature of the utility cable industry (Buller, 1949; Rifenburg, 1953; Griffioen, 1993), which consider the more complex case of a flexible cable, but with finite weight, as it is pulled around a horizontal or vertical bend. In practical applications, this phenomenon can have an insidious, compounding effect along a path with continuously distributed curvatures. Indeed, for conventional cable installation methods, when pulling a cable into a nominally "straight" duct, but which realistically contains deviations, the tensions rapidly escalate. Thus, whereas a small, light weight, flexible fiber-optic telecommunication cable may be predicted to be able to be installed several miles by a simple pulling operation, the tensions rapidly escalate, severely limiting the actual placement distance. A similar situation tends to arise in *mini*-HDD installations.

For the relatively well-controlled maxi-HDD operations, the capstan effect is only assumed to apply at the discrete, planned route bends shown in Figure 2-1, for which the effect, as characterized by Equation [2-3], is the source of the various exponential terms in Equations [2-1]. For convenience, the exponential amplification factor has been assumed to be applied to the pipe at entry (point A) and at the ends of the curved segments (points B and D). This tends to be a conservative procedure, in order to simplify the analysis, but is reasonable as illustrated in the more precise computer calculations presented below; see Section 2.4.

For the geometry shown in Figure 2-1, with relatively shallow entry and exit angles, and no additional deliberate path bends, the effect of the exponential terms, as reflected in Equations [2-1], is not major. However, in other cases the effect could be more significant. For example, mini-HDD applications are more likely to include paths with additional deliberate curvature due to the need to avoid known obstacles or follow a curved right-of-way. More important, for such typically less precisely controlled installations, there will tend to be subtle distributed curvatures due to unplanned path corrections. The latter (non-deliberate) curvature is a function of the soil conditions, operator skill, and equipment and is therefore difficult to accurately predict. Similar to the cable installations described above, such an effect can have a major impact and are reflected in some mini-HDD design methodologies, as discussed in Chapter 6.

2.24 Hydrokinetic Surface Drag (Fluidic Drag)

The development of Equation [2-2], for use within ASTM F1962, is also based upon a technology used to place cables into ducts, similar to consideration of the capstan effect. The "blown-cable" method refers to a technique for using high-speed air to efficiently install light-weight (fiber-optic) cables within ducts (Griffioen, 1993), without any pulling force applied to the leading end of the cable. In this procedure, high pressure air (e.g., 100 psig) is applied at one end of the duct (cable feed end) with the far end (cable exit) of the duct open to the atmosphere (0 psig). This results in a rapid movement of air in the annular space between the cable and duct surfaces, flowing from the air compressor to the opposite (open) end of the duct, which applies a useful distributed shear (fluidic drag) force to the outer surface of the cable, in this case acting in the direction of installation. This force, in combination with a cable pusher, is able to successfully place the cable into the duct, for very long distances, avoiding the limitations imposed by the capstan effect. In the analysis of this technique, the magnitude of the total shear force ΔF applied to the cable surface within the duct is estimated as:

$$\Delta F = \Delta P \cdot (\pi/4) \cdot (D_{duct}^2 - D_{cable}^2) \cdot D_{cable} / (D_{duct} + D_{cable}) \qquad [2\text{-}4]$$

where D_{duct} and D_{cable} represent the inner diameter of the duct and outer diameter of the cable, respectively. In this case, ΔP is equal to the pressure difference at the opposite ends of the cable, as it traverses the duct path. Since this pressure differential will vary from 0 psi as it enters the duct to the full applied pressure (e.g., 100 psi) when exiting the duct, the corresponding shear force ΔF will vary accordingly, with the maximum installation force occurring as the cable exits.

Equation [2-4] is based upon the convenient assumption that the rapidly moving air mass in the annular space is approximately in equilibrium. Therefore, the forces (due to the air pressure) applied to the annular cross-section at the ends of the cable are balanced by the shear forces acting upon the annular air mass by the duct and cable surfaces. These shear forces are assumed to be uniformly distributed across the duct and cable surfaces, such that the fraction applied to the cable is equal to its fraction of the combined surface areas; i.e., $D_{cable} / (D_{duct} + D_{cable})$. This simple model focuses on the gross macroscopic behavior corresponding to the pressure differential across the length of cable in the duct, ignoring the detailed microscopic behavior at the cable surface due to the moving fluid (air) as not directly relevant. This approach is an obvious oversimplification of a complex process but has the advantage of allowing a useful estimate of the effective shear force acting on the cable, as based on a known or assumed pressure differential.

In the case of the cable in the duct, the direction of fluid (air) flow is towards the leading end of the cable, helping to drag the cable into the duct. In contrast, when pulling the pipe into the borehole, the direction of drilling fluid/slurry flow is assumed to be in the opposite direction, away from the leading end of the pipe, such that the shear forces tend to inhibit the placement of the pipe into the borehole, resulting in an incremental tension load ΔT. Using the above model, this additional force may be estimated as:

$$\Delta T = \Delta P \cdot (\pi/4) \cdot (D_{hole}^2 - D^2) \cdot D / (D_{hole} + D) \qquad [2\text{-}5]$$

where ΔP now corresponds to the hydrokinetic pressure at the leading end of the pipe in the borehole. The fraction $D / (D_{hole} + D)$ in Equation [2-5] is less than ½; e.g., for a borehole 50% greater than the pipe diameter, this quantity would be equal to 0.4. For simplicity, the value of ½ is conservatively assumed, resulting in Equation [2-2]. The effect of the slurry properties would be manifested in the magnitude of the ΔP term required to maintain fluid flow, which may vary (increase) as the installation progresses, corresponding to a varying value for the fluidic drag term, ΔT. However, for practical design purposes, a single reasonable or conservative value for the hydrokinetic pressure term is assumed, which, as discussed above, is considered to be on the order of 10 psi or less, assuming proper drilling fluid control and usage in a well-controlled maxi-HDD operation. Associated calculations then indicate that this effect, derived from basic equilibrium considerations, corresponds to only minimal drag on the pipe.

2.25 Industry Investigation of Fluidic Drag

The fluidic drag has been handled in a widely disparate manner within the industry. Some design procedures assign an effective shear force to be applied to the outer surface of the pipe, on the order of 0.025 lbs/in^2 or greater (Puckett, 2003; ASCE, 2014), possibly as much as 0.050 lbs/in^2 (Huey et al, 1996). The corresponding forces tend to be relatively large, and may readily dominate that due to the frictional drag associated with the effects described above (buoyancy, route bends, …), which are generally accepted to be of greater importance. Other sources (Svetlik, 1995), however, tend to de-emphasize these shear forces, indicating such

effects are usually considered to be negligible, and is more consistent with the present ASTM model. Thus, Equation [2-2] provides the additional, relatively small, drag force resisting the movement of the pipe into the borehole, representing the net effect of the shear forces directly imparted on the pipe by the flowing drilling fluid/slurry. The general validity of the present ASTM F1962 procedure is supported by the reasonable agreement of predictions, based on a related method as extrapolated to mini-HDD applications, with actual field data, including tension measurements using load cells mounted at the leading ends of the pipes (Slavin, 2007).

The convenience of the above method notwithstanding, there have been various investigations in the industry attempting to evaluate the magnitude of the fluidic drag, including both theoretical and those based on field data. The latter, for example, comprised monitoring the pulling force applied to the pipe, possibly deduced from the loads applied at the drill rig, and essentially subtracting the contributions due to all other effects. In particular, Adedamola et al (2002) conducted field experiments using PE pipe, and Puckett (2003) evaluated the effect based upon actual installations with steel pipe. While working with "real" data offers advantages, the proper interpretation – including the assignment of the measured overall resistance to the appropriate individual effects – is a non-trivial task. In order to quantify the component due to the fluidic drag, it is necessary to quantify the contribution of the frictional drag, as well as, or perhaps ignore, the capstan effect, pipe stiffness, etc. As a result, the determined values tend to be unreliable, and may be inordinately high if they reflect the impact of other effects that may not have been explicitly considered in the employed model.

The derivation of Equation [2-5] (and resulting Equation [2-2]) is an admitted oversimplification of a complicated fluid flow process, including the assumption that the slurry always flows towards the rear of the pipe. Since the direction of the flow does change during the pipe installation process – i.e., when the pipe has reached the "crossover" point where the resistance to flow out of the pipe exit point is less than that towards its entry – the assumption is not correct. Duyvestyn (2009) provided a detailed explanation and analysis including the crossover point. Nonetheless, the resulting parametric dependence of the incremental tension on the borehole and pipe diameters of above Equation [2-5] is remarkably similar to that provided by Duyvestyn, as obtained from his referenced Wellplan drilling analysis tool. These relationships only differ by a sign (plus vs. minus) in the denominator of the respective equations. It is not presently clear why there should be such a fundamental difference in the dependency upon these basic parameters. In any case, the peak borehole pressure, as well as the peak fluidic drag component, is apparently at a peak at the crossover point, suggesting that the estimate given by Equation [2-5] (or Equation [2-2]) is conservative, as intended for the present design purposes.

Other investigations considering rheological models have also been used to better understand and characterize the phenomenon, such as discussed by Baumert et al (2005), Faghih et al (2015) and Rabiei et al (2017). The two latter studies compare their theoretically predicted pull loads to "observed" results in actual installations, as well as to that given by ASTM F1962 and/or the method adopted for the installation of steel pipe by the American Gas Association, aka Pipeline Research Committee (PRC) method (Hair et al, 1995; Hair, 2015). While these studies provide a more detailed analysis of the fluidic behavior, it is apparent that the corresponding fluidic drag is very small, and essentially inconsequential in comparison to the conventional frictional drag, and well within the uncertainties in quantifying the overall process, and that the much greater fluidic drag used in the PRC model is overly conservative. Furthermore, the net

effect of the ASTM approach – albeit oversimplified in the assumption of a constant hydrokinetic pressure and flow direction during the entire operation – provides a reasonable estimate of the peak pulling force. It appears that the simple equilibrium condition used to derive the formula for fluidic drag results in levels often consistent with its general magnitude as predicted by the more rigorous methods, and is also consistent with its relatively inconsequential nature in the overall process.

It is noted that the magnitude of the hydrokinetic pressure has been assumed to be that necessary to maintain proper flow of the slurry. However, a non-uniform pulling rate for the pipe may cause additional incremental pressure. Such surge effects may be minimized by pulling at essentially constant speed, and any possible such incremental loads on the pipe, either radial or longitudinal, would be withstood by the greater short term strength of the HDPE product (Svetlik, 1995).

2.3 PREDICTION vs. DESIGN

In spite of attempts by the HDD industry to develop more accurate predictions of pulling loads, such results often differ significantly from actual field results. Attempts to align any predictions with field measurements, by selecting appropriate quantitative values of relevant parameters, are only useful if able to more accurately anticipate the required pulling loads in subsequent applications, using the developed model with the corresponding parametric values. The development of such a methodology is inhibited by the complexity and variability associated with operations in an environment of non-engineered materials (i.e., soil, rock, …). For example, presumably well-controlled HDD field experiments have resulted in significantly different pull loads in what would appear to be almost identical conditions (Knight et al, 2002). In a sequence of two installations in which the same pipe was pulled through the same borehole, the measured pull force, using a gauge mounted at the leading end of the pipe, varied by a factor of almost two to one. For the second installation, the pipe experienced a pull load of approximately half that of the first pipe installation, with the peak occurring at a different point along the path. The pull loads are therefore very sensitive to subtle, not necessarily apparent differences, possibly due to the second pipe pullback operation benefiting from a slightly straighter borehole path as a result of the second pass of the reamer, or a more stabilized borehole, and/or improved drilling fluid/slurry conditions. Thus, although there may be readily available explanations for significantly different pull loads in supposedly identical situations, it appears that the present state of understanding of the overall process is insufficient to allow complete characterization and accurate prediction of the pulling load experienced in any given HDD installation.

Theoretical procedures may be considered to attempt to address the apparent randomness of the pull force. For example, since all the factors affecting the installation are not readily quantified in advance of an installation, it is possible that probabilistic analyses would be the most appropriate approach, based upon what would appear to be random variations of significant parameters (coefficients of friction, slurry density, unplanned variations in path curvature, etc.). In this case, the predicted pulling load would be expressed in statistical parameters, such as expected (average) pulling load and standard deviation, for which it would still be necessary to statistically characterize the variability of the assumed individual significant parameters. (The results of the parametric study presented in Chapter 3 may provide some insight in this regard.) The resulting probabilistic distribution of the pulling load would then be used to select a

compatible pipe strength, based upon the high end of the distribution (e.g., 95th percentile load), rather than attempt to predict a single value of an inherently widely varying, somewhat random, quantity.

In the absence of such a more technically correct method, ASTM F1962 employs an admittedly imperfect model, using reasonable and/or conservative values for the various coefficients of friction, resultant slurry density and hydrokinetic pressure, recognizing the first two parameters are the most significant in estimating the required pull force (see Chapter 3). While the capstan effect is appropriately reflected in the calculations, associated with increased frictional drag at the route bends in Figure 2-1, it is assumed there is no additional (planned or unplanned) route curvature introduced during the presumably well-controlled maxi-HDD operation. ASTM F1962 then compares the corresponding peak axial stress, including the contribution of the local peak bending stresses, to the safe pull stress for the PE pipe. This strength level is conservatively selected to avoid permanent deformation under assumed load duration and temperature. Due to the combination of these effects, no additional safety factor is proposed, although the engineer may decide to apply a "load factor" (> 1.0) to the estimated pull force to provide greater assurance of success.

2.4 "MORE EXACT" CALCULATIONS

Equations [2-1] represent a simplification with respect to the application of the capstan effect, for which the exponential amplification of Equation [2-3] is conveniently (conservatively) applied at the ends of the curved segments, rather than distributed continuously along the segment, as would be strictly correct. The discrepancy due to this simplification, however, appears to be extremely small, as based on a comparison with a more accurate solution for the case of a bore path comprising a (different) uniform radius along each of the entry and exit segments, A – B and C – D, with results illustrated in Figure 2-3. For this special case, a closed form expression may be obtained, such as provided in Griffioen (1993) for cable applications, or for HDD applications by Rabiei et al (2016), of the form:

$$T(\phi) = Ae^{\nu\phi} + w\,R\,(1 - \nu^2)\,SIN\,\phi\,/(1 + \nu^2) \; + - \; 2\,w\,R\,\nu\,COS\,\phi\,/(1 + \nu^2) \qquad [2\text{-}6]$$

where R is the borehole radius, ϕ is a measure of the local inclination angle (radians) along the curve, w is the distributed (buoyant) weight, ν is the coefficient of friction, and "A" is a constant determined by the otherwise determined tension at the entry of the curved segment. Alternatively, the "exact" solution may be obtained using a computer-generated solution simulating the distributed nature of the capstan effect.

Thus, the ASTM F1962 method was applied to a 2,500 foot installation of 24-inch DR 11[3] HDPE pipe, at a depth of 35 feet. The excess pipe length L_1 is 100 feet and the pipe entry and exit angles are 10° and 15°, respectively. In this example, the coefficient of friction on the surface, νa, has been assumed to be 0.1, assuming roller supports for the pipe outside the borehole, and that in the borehole, ν_b, to be 0.3 – as suggested in ASTM F1962. The results of either (closed form or computer-generated) solution are in excellent agreement with the estimated tensions at point C and D, including intermediate values, as shown in Figure 2-3. Indeed, the differences are barely discernible, less than one percent in this example. While typically very small, the discrepancies depend upon the specific borehole geometry, but are

[3] See Section 3.32 for a discussion of the "Dimension Ratio", DR.

generally less than that indicated in the two examples presented in Rabiei et al (2016). The discrepancy in one of these examples, in particular, was relatively large and is likely due to differences in the borehole geometries being compared in order to simulate the geometry in Figure 2-1. In practice, however, Equations [2-1] are applicable to borehole geometries considerably more general than that illustrated in Figure 2-1, for which the length, L_3, of intermediate segment B – C may be zero, and/or the shapes of segments A – B and C – D are not restricted to uniform curvature.

The reason for the relative insensitivity of the estimated pulling tension to the precise manner in which the capstan effect is applied, is at least partially due to its usually relatively minor influence on the results, as indicated ("without capstan effect") in Figure 2-3. Nonetheless, and in spite of the uncertainty and potential variability in the pulling forces in a complicated HDD operation, it is good practice to include this effect in any estimates, as reflected in Equations [2-1]. For some cases, for which there may be additional deliberate planned route bends, as well as cumulative, unplanned path curvature resulting from path deviations and corrections, ignoring the capstan effect may lead to major discrepancies – especially in mini-HDD operations (Chapter 6).

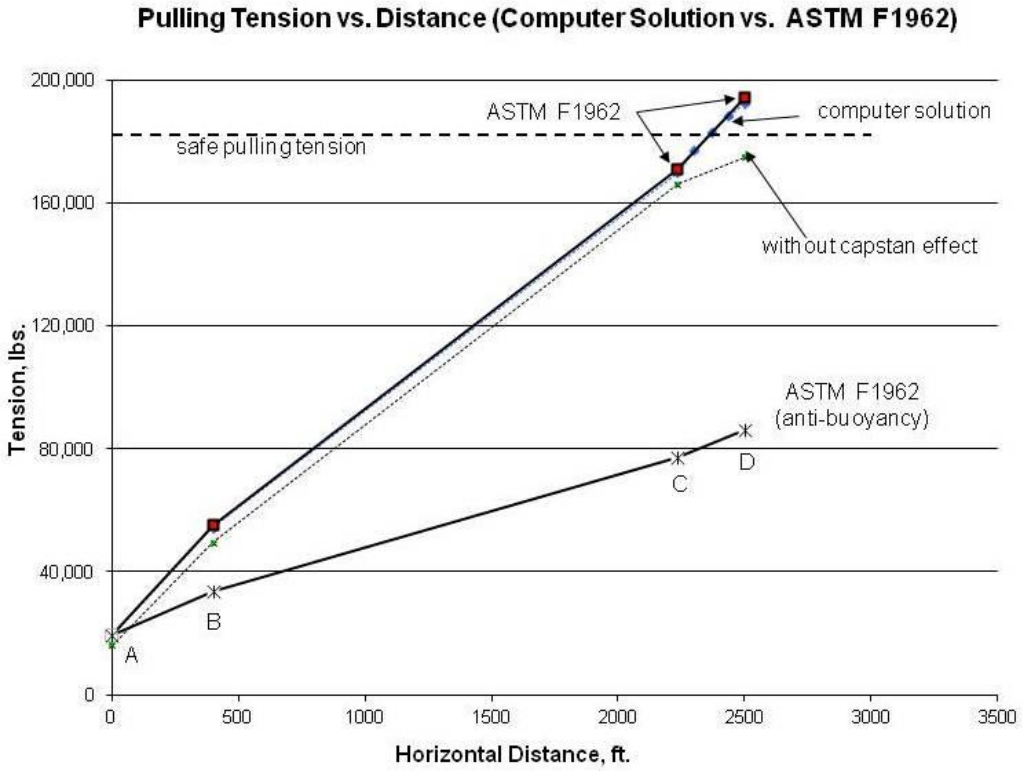

Figure 2-3. Results of ASTM F1962 and Computer Generated Incremental Model

In this example, the peak pulling load is determined to occur at the end of the bore path, at point D. However, depending upon the relative values of the various parameters, the peak tension may occur prior to the end of the installation, possibly between points C and D. It is also

noted that this tension exceeds the safe pulling tension for the assumed PE material[4], indicating that ballast (e.g., water) should be used to reduce the buoyant weight and corresponding frictional drag. The major reduction in tension clearly demonstrates the importance of this technique.

2.5 POSSIBLE MODIFICATIONS

The ASTM F1962 method has been widely and successfully used for many years (Petroff, 2010), without an obvious need for significant changes. Nonetheless, several possible modifications may be discussed, including the more technically accurate characterizations of the fluidic drag and capstan effect, as well as relatively simple adjustments to basic Equations [2-1]. Such modifications should be considered in view of the primary objective of obtaining a reasonable estimate of the peak pulling force to be applied to the PE pipe, for design purposes, in contrast to the difficulty and impracticality in determining potentially "improved" values, as discussed in Section 2.3. Thus, it is suggested that the present convenient method of accounting for the relatively complicated effects of fluidic drag and tension amplification at bends, as reflected in Equations [2-1] and Equation [2-2], be retained.

Equations [2-1] have been written in a form that relates the tension at the distinct points along the bore (B, C or D) to that at the preceding point (A, B, or C). However, an explicit relationship between the tensions and the various parameters may be readily obtained by substituting the formula for T_A into T_B, etc.:

$$T_A = e^{\nu_a \alpha} \cdot \nu_a \cdot w_a \ (L_1 + L_2 + L_3 + L_4) \qquad [2\text{-}7a]$$

$$T_B = e^{\nu_b \alpha} [e^{\nu_a \alpha} \cdot \nu_a \cdot w_a \ (L_1 + L_3 + L_4) + \nu_b \cdot |w_b| \cdot L_2 + w_b \cdot H] \qquad [2\text{-}7b]$$

$$T_C = e^{\nu_b \alpha} [e^{\nu_a \alpha} \cdot \nu_a \cdot w_a \ (L_1 + L_4) + \nu_b \cdot |w_b| \cdot L_2 + w_b \cdot H] + \nu_b \cdot |w_b| \cdot L_3 \qquad [2\text{-}7c]$$

$$T_D = e^{\nu_b \beta} \{e^{\nu_b \alpha} [e^{\nu_a \alpha} \cdot \nu_a \cdot w_a \cdot L_1 + \nu b \cdot |w_b| \cdot L_2 + w_b \cdot H] + \nu_b \cdot |w_b| \cdot L_3 + \nu_b \cdot |w_b| \cdot L_4 - w_b \cdot H\} \qquad [2\text{-}7d]$$

While it is possible this format may be helpful in understanding some of the parametric dependencies, the original format retains the relation of the tension at a subsequent point along the installation to that when the pipe had reached the previous point, which may be useful in the interpretation of the results.

It should be noted that the lengths "L_2" and "L_4" do not have precisely the same significance in their usage within Equations [2-1] or [2-7]. For example, the distance "L_2" in Equation [2-1a] should fundamentally be the length along the curved borehole segment A – B, which is slightly greater than its horizontal projected distance, as defined for use in the calculations, while its usage in Equation [2-1b] in the frictional drag term – i.e., $\nu_b \ |w_b| \ L_2$ – should be the projected distance. Similarly, the distance "L_4" in Equation [2-1a] should fundamentally be the length along the curved borehole segment C – D, which is slightly greater than its horizontal projected distance, while its usage in Equation [2-1d] in the frictional drag term, $\nu_b \ |w_b| \ L_4$, should be the projected distance. However, since the borehole entry and exit

[4] For this example, PE3608 material is assumed, with a 12 hour safe pull stress of 1150 lbs/in^2. However, the more current PE4710 material, with a safe pull stress of approximately 1300 lbs/in^2, corresponding to a safe pulling tension of 206,000 lbs, is somewhat greater than the conservatively estimated pulling load, possibly eliminating the need for anti-buoyancy measures (ballast).

angles are shallow, the differences between the projected distance and the distance along the curved segments are very small, and the additional complexity is not necessary.

In contrast to the above items, there is one issue that is potentially very significant; i.e., the effect of a non-level grade. Equations [2-1] are based on the entry and exit points being at essentially the same elevation. Since the total buoyant weight of the pipe is a major consideration in determining the pull force, any change in the overall inclination of the bore path would be expected to have an important effect, and not necessarily consistent with initial intuition. This issue is addressed in detail in Chapters 7 and 8, for which the specific quantitative results may help provide general (qualitative) recommendations in the design and/or implementation of HDD installations.

CHAPTER 3
PARAMETRIC DEPENDENCY AND TRENDS[5]

3.1 BENEFITS

ASTM F1962 provides a rational, analytical method for selecting the polyethylene pipe strength based upon the estimated installation loads on the pipe. This allows the engineer a means of determining the general feasibility of the project, as well as initial design information. The procedures and formulae provided in this document are readily adaptable for spreadsheet applications, and have been incorporated into several commercially available software tools (Bayat et al, 2011). In particular, Equations [2-1] of Chapter 2 explicitly includes the various parameters that may reasonably to be considered to impact the required tensile loads. Although the engineer or contractor will not have direct control over all of the factors, some of which will be dictated by the project or equipment limitations, a knowledge of their relative importance in affecting the pull loads would be extremely helpful in allowing their efforts to be efficiently utilized.

3.2 NOMINAL (AND REFERENCE) INSTALLATION

While the qualitative effects of some of the parameters may be evident from a perusal of Equations [2-1] and [2-2], it is of interest to verify their magnitude, as well as that of other parameters whose effect may be less apparent. For this purpose, it is convenient to specify "nominal" (or "reference") values of the parameters to serve as a basis from which the variables will be varied, within a reasonable range, allowing the magnitude and general trend of the effect to be investigated. Table 3-1 therefore defines a corresponding nominal geometry, and installation related variables, as well as the HDPE pipe characteristics. Table 3-1 also includes the range of values which are considered in the study, for which the values of some of the parameters in Table 3-1 are equal to that suggested in ASTM F1962 (i.e., coefficients of friction, specific gravity of slurry, and drilling fluid pressure), or as calculated from relationships provided in this guide (i.e., buoyant weight). Thus, in addition to the terminology defined previously, the specific gravity of the HDPE material and any liquid ballast that may be placed within the pipe, as appropriate, are included. The nominal segment lengths L_2 and L_4 are based upon a uniform borehole curvature consistent with the entry or exit angles and depth, as determined by formulae provided in ASTM F1962. Where there is more than one possible nominal value shown, the one in **bold** font is considered as the reference value.

[5] Ref. "Parametric Dependency and Trends of HDD Pull Loads", L.M. Slavin, ASCE Journal of Pipeline Systems Engineering and Practice, May 2010.

.

Table 3-1 Nominal Installation Parameters

Parameter	Nominal Value	Range	Remarks
bore length, L_{bore}	2,500 ft	1,000 – 5,000 ft	
entry angle, α	15°	5° – 25°	0.262 radians
exit angle, β	15°	5° – 25°	0.262 radians
depth, H	45 ft	25 – 160 ft	
segment, L_1	125 ft	25 – 250 ft	= 5% L_{bore}
segment, L_2	343 ft	190 – 1,215 ft	= 2H/α for uniform curvature
segment, L_4	343 ft	190 – 1,215 ft	= 2H/β for uniform curvature
segment, L_3	1,814 ft	69 – 2,120 ft	= $L_{bore} - L_2 - L_4$
diameter, D	24.0 in	----	actual IPS pipe outer diameter
thickness, DR	11	7.3 – 21	2.182-in. wall thickness
ratio, D_{hole}/D	1.5	1.025 – 3.0	50% clearance
pressure, ΔP	10 psi	----	suggested incremental pressure
incr tension, ΔT	2,827 lbs	----	= $\Delta P \cdot (\pi/8) \cdot (D_{hole}^2 - D^2)$
spec grvty pipe	0.955	----	HDPE
spec grvty slurry	1.5	1.0 – 1.7	suggested (conservative)
spec grvty ballst	**1.0** or 1.5	**1.0** or slurry	**water (Reference)** or slurry ballast
weight, w_a	61.9 lbs/ft	----	HDPE
weight, w_b	232.2 lbs/ft	134 – 271 lbs/ft	no ballast
	100.9 or 35.3 lbs/ft	140 – 2.9 lbs/ft	**water (Reference)** or slurry ballast
friction, ν_a	**0.10** or 0.50	0.0 – 0.75	rollers (**Reference**) or ground surface
friction, ν_b	0.30	0.1 – 0.55	suggested

The large difference in the possible nominal values for the buoyant weight, which has a major impact on the pull force, reflects the benefits of using anti-buoyancy techniques, as demonstrated in the example illustrated in Figure 2-3. The values indicated in Table 3-1 correspond to the absence of any ballast, or to the use of water or slurry to fill the pipe interior, with the precise values dependent on the assumed density of the HDPE pipe material, which values vary slightly. Figure 3-1 shows the tension results for three possible cases, including no ballast, water ballast, and allowing the drilling fluid/slurry to enter the pipe. As in the previous example, the tension for the empty pipe may be anticipated to exceed the safe pulling tension for the pipe, requiring the application of anti-buoyancy measures. Although the use of the slurry results in the lowest pulling force, water is more commonly used, since it simplifies the subsequent cleaning and purging process, and may remain in the pipe to provide stability until the line is operational, at which time the pipe may be pressurized, as appropriate. For this reason, the use of water ballast is considered to be the "**Reference**" case, as indicated in Figure 3-1, corresponding to the buoyant weight w_b = 100.9 lbs/ft, representing the basis for comparison for other alternatives. Similarly, the Reference case is also based on the external coefficient of friction, νa, of 0.1, corresponding to roller supports for the pipe external to the borehole, typical of maxi-HDD installations.

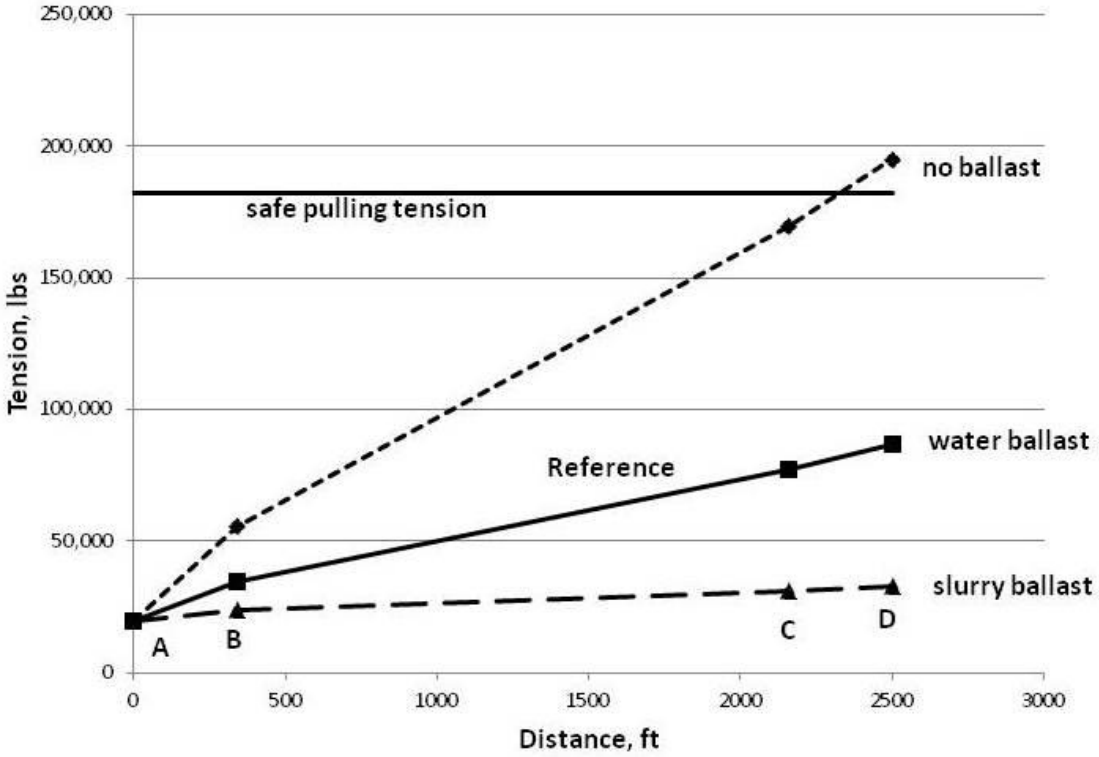

Figure 3-1. Tension vs. Installed Length

3.3 VARIATIONS FROM NOMINAL VALUES

Although the pipe diameter is a major factor in determining the required pulling force, for the purposes of this study it is not varied from the 24-in. size. Assuming insignificant bending stiffness for HDPE pipe, both the anticipated tensions and the safe pulling force are directly proportional to the square of the diameter (i.e., D^2), for given values of the other parameters in Table 3-1. This may be confirmed by an inspection of Equations [2-1], as well as Equation [2-2] for the contribution of the fluidic drag, and the relationships for the buoyant weight provided in ASTM F1962. Thus, the ability of the pipe to withstand the expected pull loads, for given values of the other parameters, including route geometry, remains unchanged with different pipe outer diameters. In this regard, the results could be normalized with respect to the D^2 term, but such a presentation would tend to obscure the physical interpretation.

3.31 Geometry

Figure 3-2 illustrates the effect of a variation in the pipe entry or pipe exit angle. While neither parameter has a major effect on the pull force, the pipe entry angle is essentially of no consequence in this regard, while the exit angle can have a small but noticeable impact, within approximately ±5%. The entry angle has an insignificant effect on the required tension because of the relatively low tail (restraining) load at point A, due to a combination of the small remaining length, L_1, at the end of the installation and the low coefficient of friction for the reference roller supports, even with the capstan effect at the entry point. In contrast, the capstan

effect at the end of the installation, where there is a large tail load, will have a measureable impact.

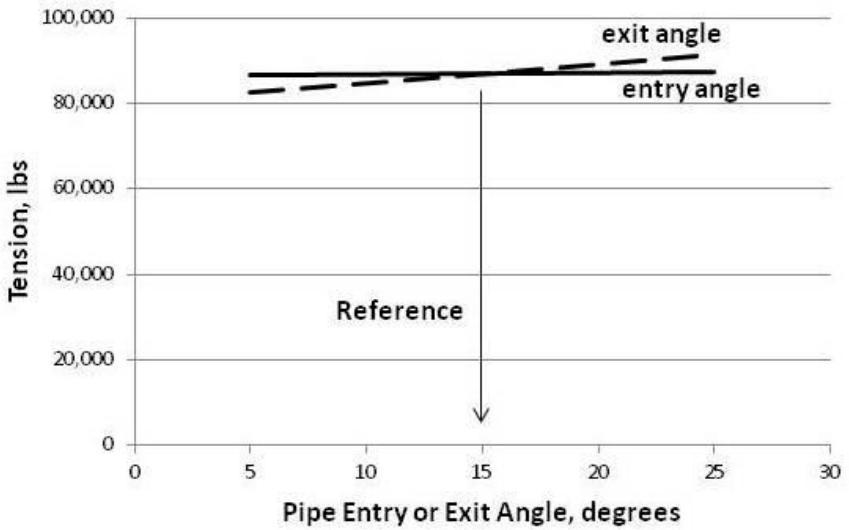

Figure 3-2. Tension vs. Pipe Entry or Exit Angle

It is interesting that greater depths, as illustrated in Figure 3-3, also do not appreciably cause higher tensions. A relatively large depth of 160 ft results in only a 4% increase in pull load, using the corresponding values of the lengths L_2 and L_4, to maintain a uniform radius of curvature, as indicated in Table 3-1. However, if these segments are assumed to remain constant, corresponding to a non-uniform entry and/or exit curvature, the change in pull load is even lower, less than 1%, because the terms including the depth, H, in Equations [2-1b] and [2-1d] almost cancel each other.

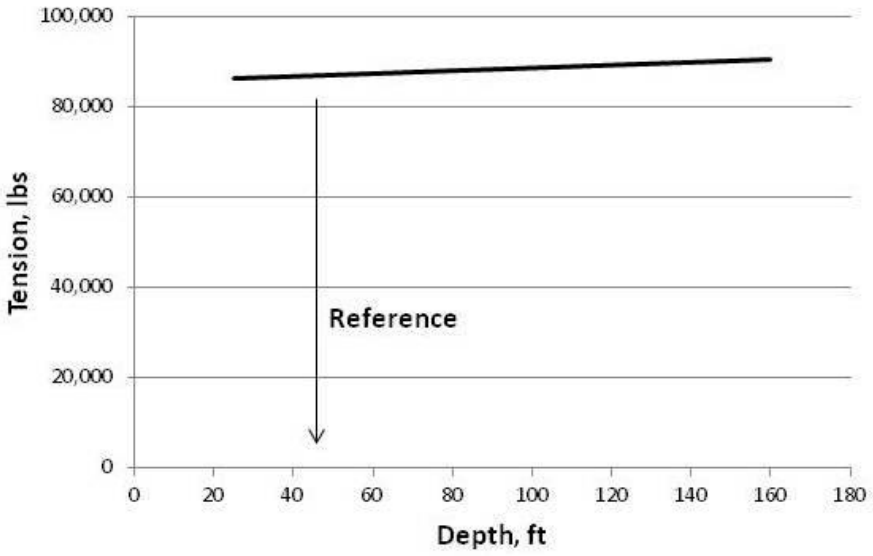

Figure 3-3. Tension vs. Maximum Depth

Similar to the minimal effect of the depth, Figure 3-4 also shows that the amount of excess length, L_1, is not an issue, especially with the low friction associated with the roller supports external to the borehole. For this condition, and the range of lengths considered, the impact is negligible; i.e., ±1%. However, as suggested by Figure 3-7 (Section 3.33), the impact will be somewhat more significant if there is greater friction external to the borehole, such as for other support conditions.

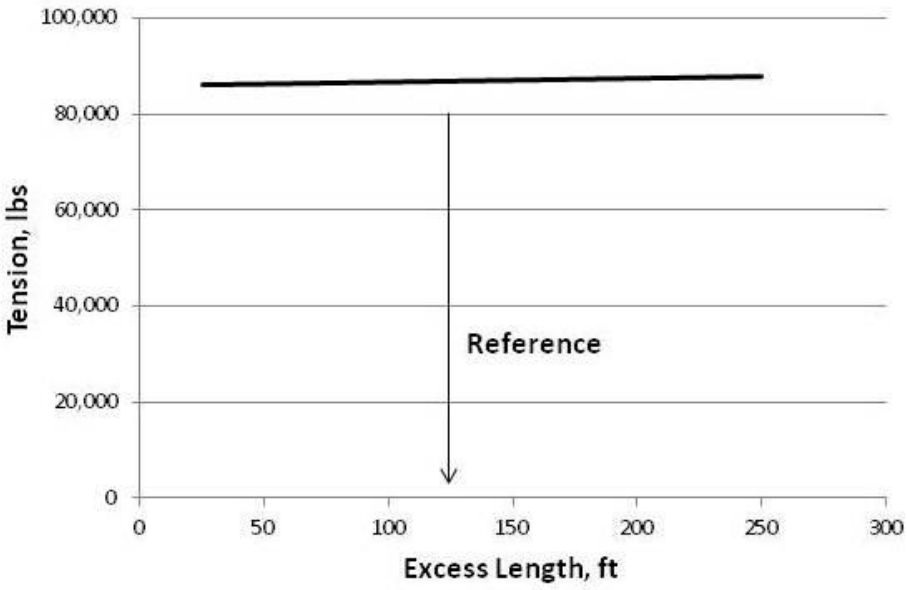

Figure 3-4. Tension vs. Excess Length

Figure 3-5 illustrates the obvious strong dependency of the pulling force on the length of the bore, for which the tension is essentially directly proportional to the bore length, and therefore the entire buoyant weight within the bore. The bore length is apparently the only geometry-related parameter that has a significant impact on the required pull force.

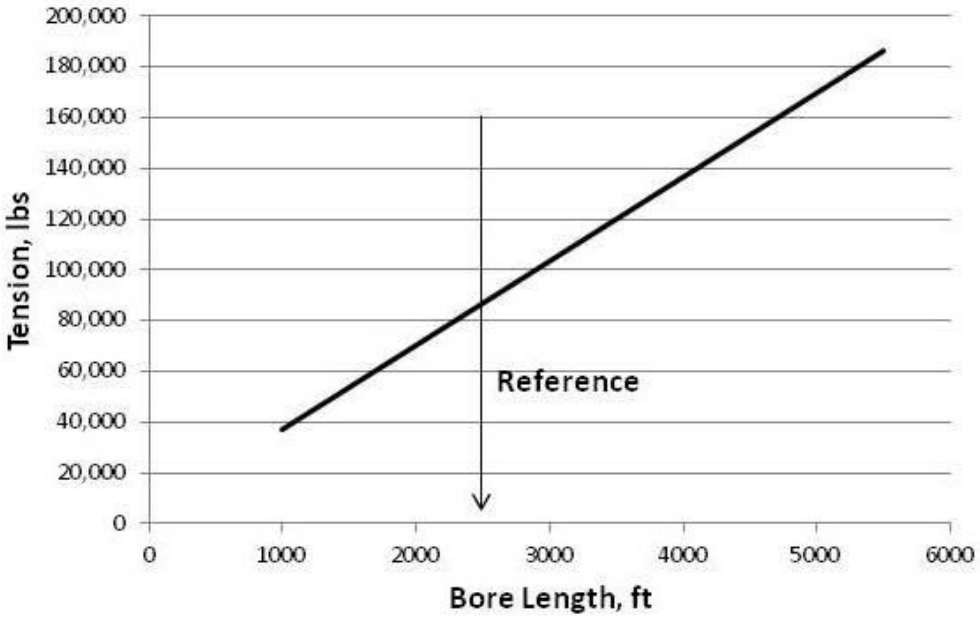

Figure 3-5. Tension vs. Bore Length

3.32 Dimension Ratio (DR)

Figure 3-6 shows both the required tension and the allowable (safe) pull force as a function of the Dimension Ratio (DR), the ratio of the pipe outer diameter to wall thickness. Whereas the safe pull force is obviously strongly dependent on the wall thickness (or DR value), the pull force itself is essentially independent of the DR value, with a variation of less than ±2%. Due to the use of the ballast, even the low strength of the DR 21 product appears to be sufficient, for the present assumed bore route and conditions. However, in general, such an extremely thin-walled product is not recommended for HDD operations (Plastic Pipelines Institute, 2020). It may also be assumed that the significantly reduced strength of the other thin-wall pipes (e.g., DR 15.5[6] or DR 17) would be inadequate for somewhat more aggressive or difficult installations, and would be most dramatically demonstrated in the absence of anti-buoyancy measures (ballast), such as illustrated in Figure 3-1, for the considerably stronger DR 11 product.

[6] DR 15.5 may no longer be available for some applications.

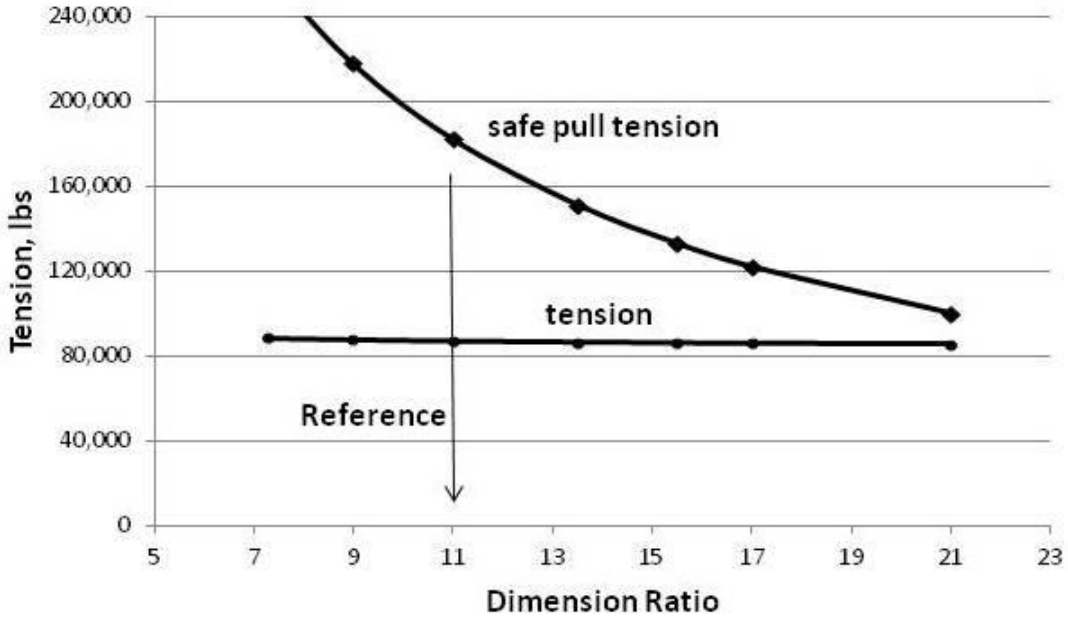

Figure 3-6. Tension vs. Pipe Dimension Ratio

3.33 Coulomb Friction

As anticipated, based on a simple consideration of the pipe's buoyant weight and the coefficient of friction within the borehole, the combination of these two parameters, plus the bore length (Figure 3-5), effectively determine the peak required pulling force. Thus, as seen in Figure 3-7, the pull load is also essentially directly proportional to the coefficient of friction within the borehole, ν_b. In contrast, the effect of the frictional drag at the surface, based on the coefficient of friction, ν_a, is low, corresponding to an increase of only 8% relative to the Reference value, for an extremely high fictional coefficient (0.75), almost an order of magnitude greater than the value of 0.1 assumed for roller supports. Figure 3-7 extends to an (idealized) value of 0.0 for ν_a, which, although not possible to physically achieve, may be considered to be equivalent to a pipe on rollers that is also subject to a push force at the entrance, effectively resulting in the absence of a tail load at point A.

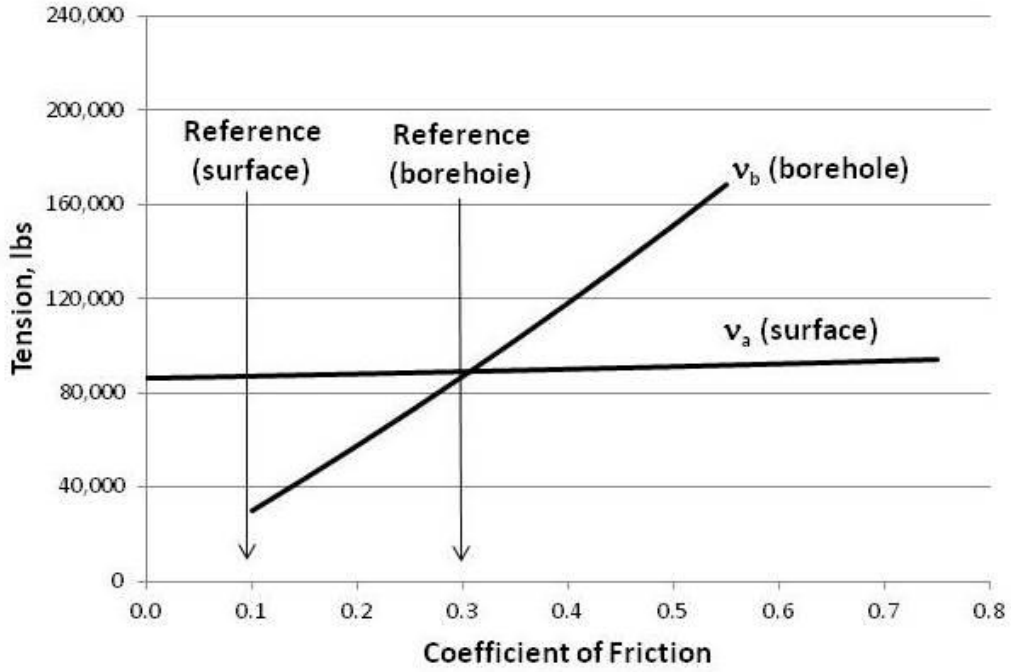

Figure 3-7. Tension vs. Coefficient of Friction

3.34 Drilling Fluid/Slurry Density

Since the buoyant weight is directly related to the density of the slurry, the strong dependence on this parameter is also anticipated, independent of whether any ballast is used, or the type of ballast. Thus, Figure 3-8 illustrates the different magnitudes of the pulling force, for the same three types of ballast indicated in Figure 3-1: none (vacant pipe), water (Reference) or slurry (enters open pipe). At the Reference density of the slurry (specific gravity = 1.5), the peak tension in the absence of ballast is double that corresponding to the use of water ballast, which is itself almost triple that of using the drilling fluid/slurry itself as ballast. However, since the Reference value of 1.5 is recognized to be relatively high, as part of a conservative design procedure (Section 2.3), in practice, the magnitude of the required pull force will tend to be lower than those indicated, for each of the three alternatives. For the lower slurry densities, the ratio of the pull forces without ballast, to those with ballast, dramatically increases, while the benefit of the slurry ballast relative to the water ballast decreases, as may be expected. For example, maintaining a maximum slurry density corresponding to a specific gravity of only 1.2 (HDD Consortium, 2008), would reduce the pull load, using water ballast, to less than half that otherwise calculated at the higher value (i.e., specific gravity of 1.5).

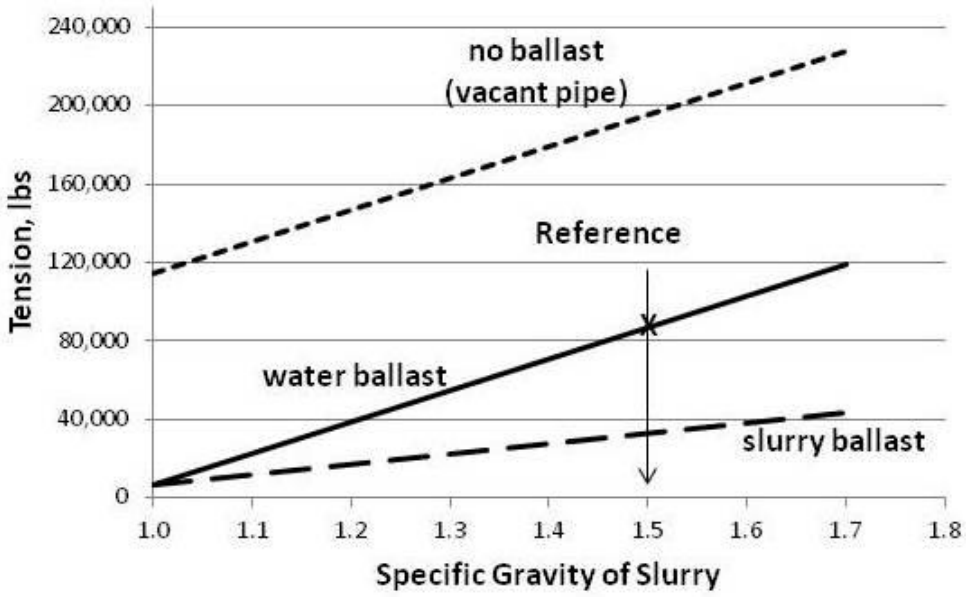

Figure 3-8. Tension vs. Slurry Density

3.35 Hydrokinetic Surface Drag (Fluidic Drag)

The effect of the fluidic drag associated with the drilling fluid/slurry, with magnitude given by Equation [2-2], is discussed in Sections 2.24 and 2.25. This model of the fluidic drag results in the incremental pull force, ΔT, as illustrated in Figure 3-9, for the nominal 10 psi level for the hydrokinetic pressure, and is a function of the borehole clearance, D_{hole} / D. The resultant loads are generally very small compared to the overall estimated tension, with the possible exception of the combination of low density slurry and the use of ballast (Figure 3-8), especially for a much larger than necessary borehole, assuming the 10 psi pressure is maintained. Proper HDD practices suggest a borehole clearance of 50% minimum relative to the pipe diameter in order to help ensure proper circulation of drilling fluid and spoils removal, although a maximum clearance of 12 inches is recommended by the HDD Consortium (2008), corresponding to the 50% reference value in these examples. Larger clearances will facilitate passage of the pipe and minimize any pipe stiffness effects (see Chapter 4). However, larger than necessary boreholes will also add to the difficulty of the overall HDD operation (reaming, spoils removal, …). Engineering judgment and experience may be used to select an optimum borehole size.

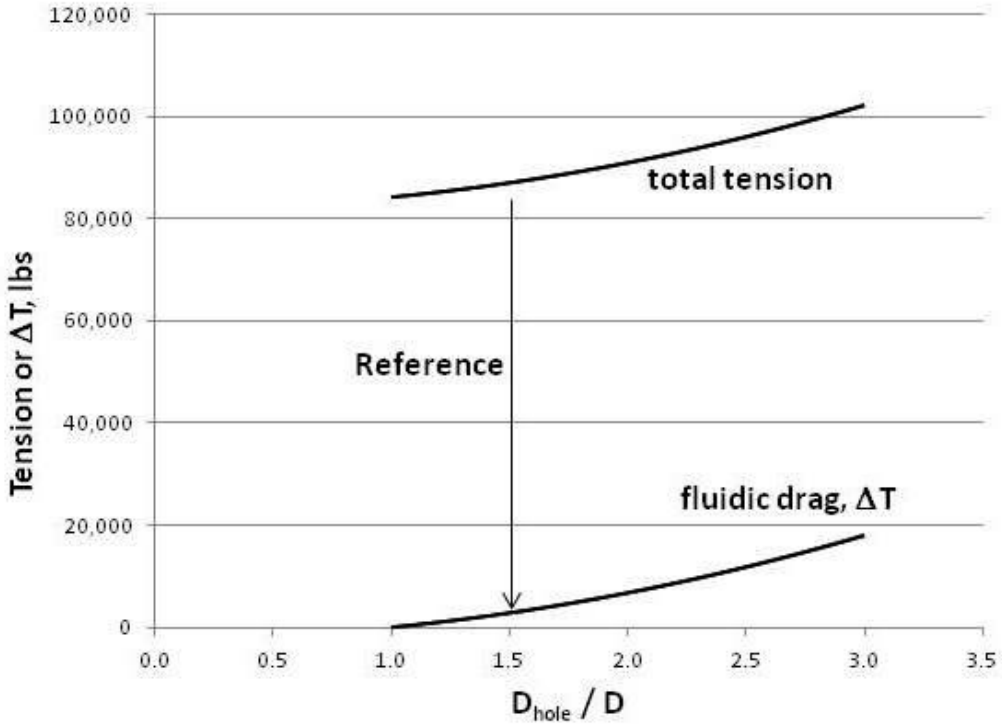

Figure 3-9. Incremental Tension (Fluidic Drag) vs. Borehole Clearance

3.4 ADDITIONAL CONSIDERATIONS

The trends illustrated in Figure 2-1 and Figure 3-1 suggest that the peak pulling load generally occurs at the end of the installation, at point D. For convenience, therefore, the tensions shown in Figures 3-2 through 3-9 are those occurring at that point. However, in some cases, and in actual installations, the tension on the leading end of the pipe may peak prior to the very end of the installation. While recognizing that this situation may affect the quantitative results, the overall, and specific, conclusions regarding the relative effects of the various parameters are considered to remain qualitatively valid.

There are various possible explanations for this phenomenon to occur in practice, some of which may be merely due to variations in some of the significant factors during the course of the installation (e.g., coefficients of friction or slurry density), or possibly due to a temporary loss of circulation. However, it is also possible to explain such a pattern, without assuming such time-varying effects. Figure 3-10 shows the variability in the calculated pulling forces, as the installation progresses, for a relatively low surface friction within the borehole (i.e., $\nu_b = 0.1$ in comparison to the Reference value of 0.3), for which the estimated tension at point C exceeds that at point D, including for installations with and without the use of ballast. This result is due to the net upward assistance provided by the net buoyant forces overcoming the frictional drag along the last segment, between points C and D. It is noted that an intermediate value for the borehole friction ($\nu_b = 0.2$) does not result in the peak force occurring at point C, but again occurs towards the end of the installation, at point D.

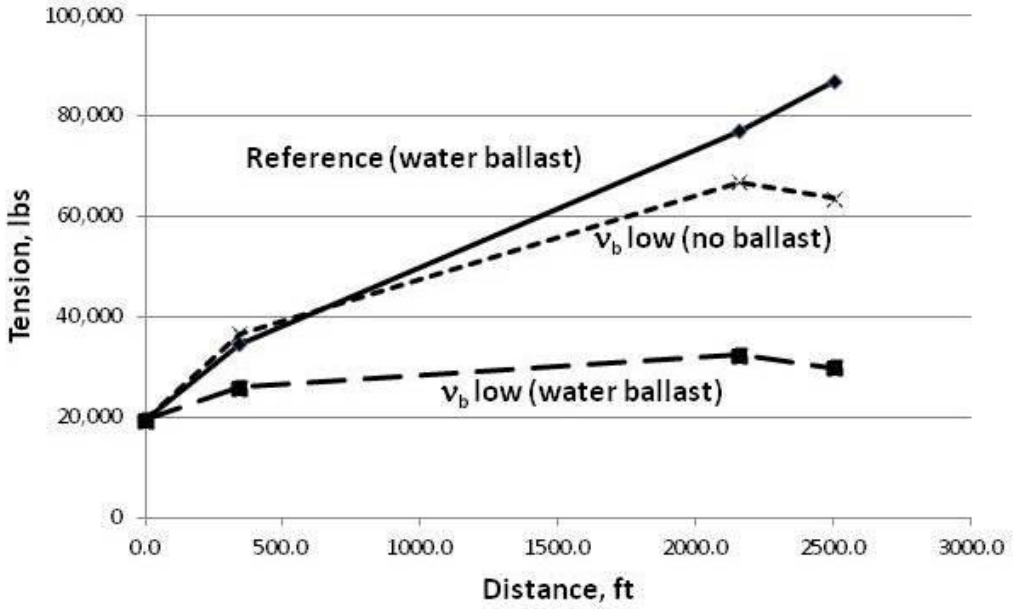

Figure 3-10. Peak Tension Occurring Prior to End of Installation (Point D)

3.5 SUMMARY

The trends and tendencies observed in the investigation described in this chapter allow a number of qualitative conclusions regarding the relative significance of various parameters in determining the peak required pulling force, some of which may not have been otherwise apparent:

- For the same DR (diameter to thickness ratio) value, the pull load is proportional to the square of the pipe diameter; thus, under similar conditions, a 36-inch pipe requires a pull force almost an order of magnitude greater than that of a 12-inch pipe.
- While the pull force for larger pipes is disproportionately greater than for smaller pipes, their relative tensile strength, for the same DR value, is similarly larger, so there is not be a significantly greater likelihood of pipe failure, for the same installation geometry.[7]
- The DR value has only a minimal negligible effect on the estimated pull force, but is the major consideration in determining its tensile strength, and the ability to withstand that force.
- The borehole clearance should be maintained at approximately 50%, consistent with HDD industry guidelines, but the precise borehole diameter has only a small effect on pull load.

[7] Assuming the typically low bending stresses for PE pipe are ignored.

- While the bore length is obviously a major factor, with the required tension essentially proportional to the total distance, other geometric details – including the depth or pipe entry or exit angle – have relatively little impact, in spite of the capstan effect.
- For a given overall bore length, the individual segment lengths, transitioning to or from the desired depth, including the excess length of pipe at the pipe entry end, do not significantly affect the peak pull load.
- Thus, for a given bore length (and DR value), the primary factors in determining the likelihood of successfully installing the pipe, without exceeding the allowable pull tension, are the borehole frictional coefficient and slurry density (buoyant weight), but for which the use of anti-buoyancy measures (e.g., internal liquid ballast) will greatly reduce the required pulling force.

While the ASTM F1962 methodology was developed to address the placement of flexible polyethylene pipe, with proper engineering judgment, some of the general conclusions and guidelines may reasonably be extrapolated to other types of pipe. Notable exceptions would apply to heavy materials (e.g., iron) which density directly affects the critically important buoyant weight, such that any trends related to the DR value or slurry density, or the use of ballast, would generally not be applicable.

CHAPTER 4
PIPE STIFFNESS[8]

4.1 BACKGROUND

As discussed, Equations [2-1] were developed assuming negligible pipe bending stiffness, as appropriate for the flexible PE material. Pipes constructed of other materials, including relatively rigid plastics (e.g., polyvinyl chloride, PVC), and especially iron or steel, may conceivably result in significant reaction forces at route bends, as the pipe is pulled along the borehole during the HDD operation. These local reaction forces correspond to additional sources of frictional drag on the pipe, impeding its placement, possibly requiring a somewhat greater installation tension than may otherwise may be necessary, considering only the frictional drag due to the pipe's buoyant weight and tension at route bends (capstan effect), as well as any contribution due to fluidic drag.

The effect of pipe bending stiffness has been considered in previous analytical methods by Huey et al (1996) and Cheng et al (2007). These methods use computer-generated solutions to estimate the pull loads as a function of various route and drilling parameters. Although these procedures may be very useful for evaluating specific cases, including consideration of possible additional effects, numerical techniques do not usually provide any insight into the quantitative dependence of the pull loads on the various parameters (e.g., pipe stiffness and borehole geometry). Such methods are also not as convenient to apply as the ASTM procedure, and the models may not be fully compatible with actual route and pipe geometric conditions. It is therefore desirable to attempt to incorporate the effect of the pipe bending stiffness into the ASTM F1962 format, which would allow an understanding of the potential quantitative impact on pull loads, including possible application to a broad range of pipe materials.

The local reaction forces of a pipe with finite stiffness may be determined by considering the pipe to be installed as an elastic beam, which must be bent in order to conform to the curvature, which is defined as the reciprocal of the bend radius, of the bore path. Such curvatures exist, for example, at point A, or more gradually along the segments A – B and C – D of Figure 4-1, which may each be of uniform curvature, but not necessarily, or possibly more localized, as in the vicinity of point B indicated in Figure 4-2. Other types of borehole curvature may include a sequence of relatively small magnitude bends, representing path undulations, but are not considered in the present analysis for a well-controlled maxi-HDD operation.

[8] Ref. "Effect of Pipe Stiffness on Maxi-HDD Pull Loads", Slavin and Najafi, ASCE Journal of Pipeline Systems Engineering and Practice, February 2012.

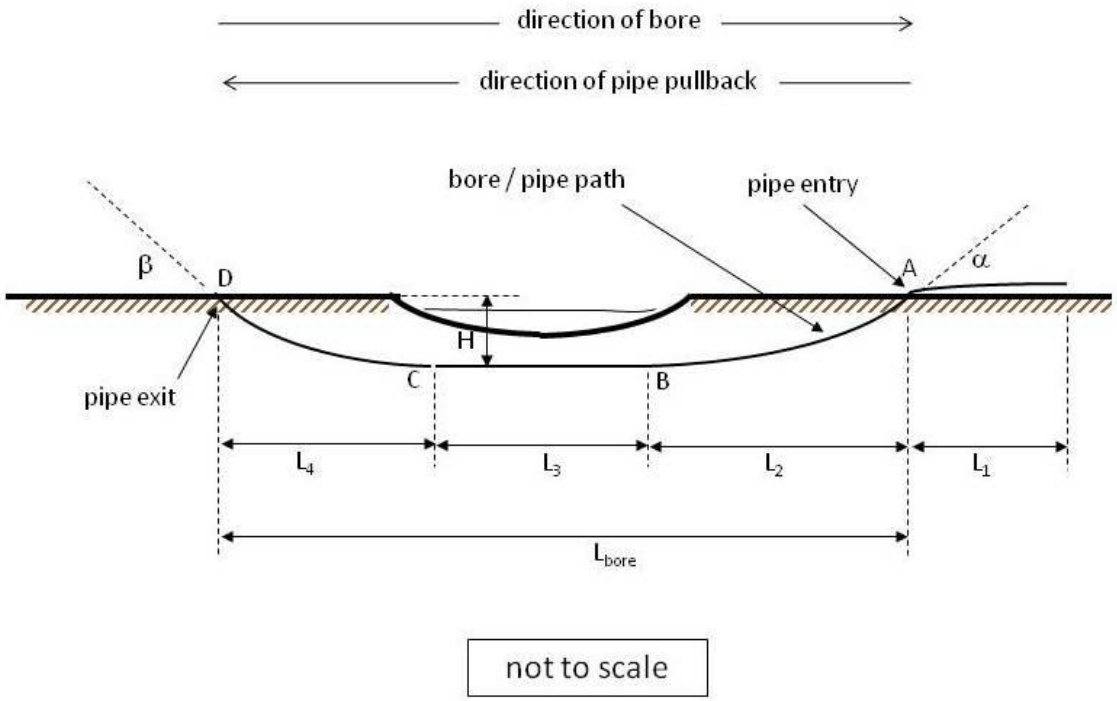

Figure 4-1. Typical Maxi-HDD Route (Obstacle or River Crossing) (Courtesy of Outside Plant Consulting Services, Inc.)

4.2 THEORETICAL DEVELOPMENT

Figure 4-2 illustrates a discrete route bend, such as along the portion of the bore path between points A, B and C, but focusing on point B and the immediately adjacent portions of the bore path. The position of the pipe in Figure 4-2, as well as the other related figures, is shown, and initially considered, in the absence of any significant buoyant forces, or tensions. The corresponding indicated local reaction forces are oriented perpendicular to the bore path at the points of contact between the pipe and the borehole, at the beginning and end of the sections of constant (uniform) curvature – i.e., where there is a change in curvature along the path.

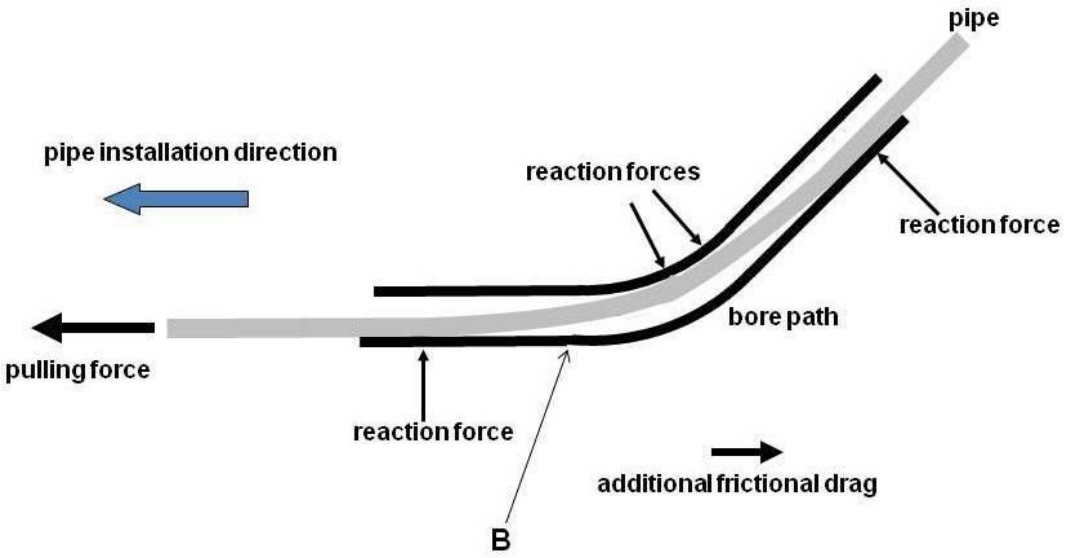

Figure 4-2. Reaction Forces at Route Bend due to Pipe Stiffness
(Courtesy of Outside Plant Consulting Services, Inc.)

It is noted that the additional reaction forces required to deflect a pipe with finite stiffness to conform to a vertical route bend, as illustrated in Figure 4-3, would be lower than otherwise required because of the beneficial effect of the distributed buoyant forces also acting vertically on the pipe, that help it conform to the local curvature. However, the pipe in Figure 4-2 is considered to be sufficiently stiff (and/or of low buoyant weight) as to be forced against the lower and upper surfaces of the borehole, as shown, resulting in the indicated local reaction forces. Similarly, any tension required to install the pipe will exert an additional bending moment that also helps reduce the otherwise required reaction forces. As a result, without direct consideration of these effects, the incremental frictional drag due to the bending stiffness may be significantly overestimated. Therefore, although a reasonable degree of conservatism is desirable and consistent with the original intent of ASTM F1962 (Section 2.3), the present investigation will also discuss these effects, as appropriate.

4.21 Discrete (Complete) Bend

The reaction forces shown in Figure 4-2 depend on the pipe bending stiffness and the curvature of the bore path, as well as the clearance between the pipe and borehole. Figure 4-3 shows a corresponding discrete "complete" bend of assumed uniform curvature (constant radius). A "complete" bend is one of sufficient extent such that the pipe curvature between the contact points **2** and **3** conforms to that of the inner radius of the borehole, and is a function of the geometry, as discussed below. Although bends of non-uniform curvature may occur in practical applications, the present model is useful for understanding the potential magnitude and significance of the effect of bending stiffness in HDD installations.

Considering only the reaction forces due to pipe stiffness (i.e., ignoring the tensions and buoyant weights), Figure 4-3, shows the geometric parameters that determine the magnitude of the indicated forces, $N_1 - N_4$, at points 1 – 4, which, in addition to the diameter of the pipe, D, and bore path, D_{hole}, include:

f = horizontal (projected) distance between point **1** and the center of borehole curvature, where **1** is at the closest contact of the pipe with the straight segment of the borehole

ℓ = horizontal (projected) distance between points (**1** and **2**) of contact of pipe with borehole (between straight and curved segments)

γ = total bend angle

θ_b[9] = partial bend angle, at point **2**, where **2** is the point of closest contact of the pipe with the borehole, from point 1, for a "complete" bend

ρ_{hole} = borehole radius of curvature of borehole center line

The details in Figure 4-3 are expanded for clarity, but it is recognized that the borehole radius of curvature would typically be orders of magnitude greater than the borehole or pipe diameter, and that the partial bend angle, θ_b, for a "complete" bend will be verified to be small; i.e., << 1 radian.

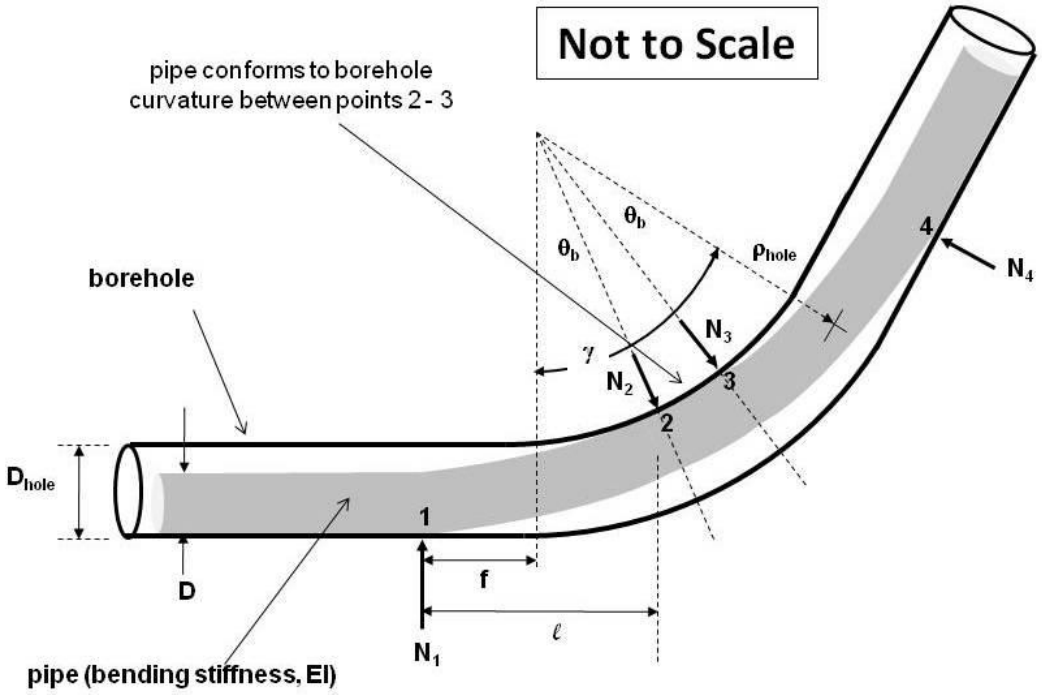

Figure 4-3. Discrete (Complete) Bend
(Courtesy of Outside Plant Consulting Services, Inc.)

For a complete bend, the total bend angle, γ, is equal to or greater than twice the partial bend angle, θ_b, with the excess corresponding to the pipe segment of uniform curvature, which is essentially equal to the curvature of the borehole itself. The pipe experiences zero curvature

[9] The use of the symbol θ or θ_b in this context is not to be confused with its use in other parts of this book, such as Section 2.23, and Section 6.3.

along its straight section to the left of point **1**, and a transition from zero to the borehole curvature between points **1** and **2**. Due to symmetry, the pipe segment between points **4** and **3,** and to the right of point **4,** is analogous to that between points **1** and **2**, and to the left of point **1**.

The bending stiffness of the pipe is denoted as "EI", the product of the pipe's effective elastic modulus, E, and its cross-section area moment of inertia, I. However, since some pipe materials may not display conventional linear elastic properties, engineering judgment may be required to select an appropriate value for the elastic modulus. For example, for a viscoelastic plastic material, such as HDPE, the effective modulus depends on the duration of the load or deflection, and, in the present application, would correspond to the time required for a portion of the pipe to enter and deform to a route bend, remain at the given curvature, and then exit from such a bend. The appropriate "elastic" moduli may therefore have a tendency to change somewhat as the pipe traverses a bend. In general, however, the time frames of interest would not be large (hours or minutes) and any change in the effective modulus would not be expected to be major (Plastics Pipe Institute, 2008). Thus, for the present purposes, the pipe segment between points **1** and **2**, (or between points **3** and **4**) may be considered to act as an elastic beam.

Long lengths of large diameter polyethylene pipe are typically joined by fusing individual lengths, resulting in a single continuous length with uniform properties. For other possible methods of joining, or pipe materials, it is assumed that the coupling flexes similar to the native pipe, or that the coupling is a local rigid element with insignificant effect on the overall size or flexibility of the joined pipeline.

4.22 Theoretical Analysis

The mechanics and related phenomena associated with pulling a pipe through a borehole are analogous to those encountered when installing a power or communications cable within a conduit or duct. Indeed, this is the motivation for considering the capstan effect incorporated into the ASTM F1962 model, as discussed in Section 2.23. Similarly, the method for determining the reaction forces associated with placing communications cables, with finite stiffness, within a duct, as applied by Griffioen (1993), is used herein to estimate those due to installing a pipe with finite stiffness within a borehole, although it is recognized that significant differences in the applications require proper interpretation of the results.[10]

Several convenient simplifications may be made in order to facilitate the analysis. Since, based on beam theory, there are no shear forces within the pipe along portions of constant curvature, the only forces acting on the pipe segment on either side of the bend in Figure 4-3 are N_1, N_2, N_3 and N_4. Furthermore, due to symmetry, and considering that θ_b is small, and again ignoring tensions and buoyant weights for this purpose, the reactions forces $N_1 - N_4$ are all approximately equal, and denoted as the reaction force, N:

$$N = N_1 = N_2 = N_3 = N_4 \qquad [4\text{-}1]$$

In addition, since the pipe and borehole dimensions, D and D_{hole}, are negligible compared the borehole radius, ρ_{hole}, the radius of curvature of the pipe, at the portion where it conforms to the inner surface of the borehole between points **2** and **3** at the bend, is essentially equal to that of the bend itself, ρ_{hole}.

[10] The original application of Griffioen's procedure is for a cable being installed in a duct without a pull line, using the "blown-cable" method.

Again, using basic beam theory (Young, 1989), the pipe is assumed to deflect elastically, with characteristic stiffness EI, as a built-in (fixed) beam at point **2**, in response to a cantilever force, N, at point **1**, where the zero curvature corresponds to the absence of any bending moment. Thus, consistent with $\theta_b << 1$ and the small deflection beam model:

$$N \cdot \boldsymbol{\ell}^3/(3\,EI) = \boldsymbol{\ell}\tan\theta_b - [\rho_{hole} \cdot (1 - \cos\theta_b) + (D_{hole} - D)]$$
$$\approx \boldsymbol{\ell} \cdot \theta_b - [\rho_{hole} \cdot (\theta_b^2)/2 + (D_{hole} - D)] \quad [4\text{-}2]$$

Since this equation has three unknowns – i.e., N, $\boldsymbol{\ell}$, θ_b – two additional conditions are necessary to provide a unique solution. Since the pipe is horizontal at point **1,** and is the slope is $\tan\theta_b$ at point **2**, the same beam theory requires:

$$N \cdot \boldsymbol{\ell}^2/(2\,EI) = \tan\theta_b$$
$$\approx \theta_b \quad [4\text{-}3]$$

Also, for a complete bend, the curvature of the pipe at point **2** is equal to that of the borehole, $1/\rho_{hole}$, and is proportional to the local bending moment, or

$$N_b \cdot \boldsymbol{\ell} / EI = 1/\rho_{hole} \quad [4\text{-}4]$$

where the designation "N_b" indicates Equation [4-4] applies only to the reaction force(s) for a complete bend. All three unknowns may now be determined by the preceding three equations.

Thus, dividing Equation [4-2] by Equation [4-3] yields:

$$\boldsymbol{\ell} = 3\,[\rho_{hole} \cdot (\theta_b)/2 + (D_{hole} - D)/\theta_b] \quad [4\text{-}5]$$

and dividing Equation [4-3] by Equation [4-4] gives:

$$\boldsymbol{\ell} = 2\,\rho_{hole} \cdot \theta_b \quad [4\text{-}6]$$

which two equations result in the following condition for a complete bend:

$$\boldsymbol{\theta_b = \sqrt{[6\,(D_{hole} - D)/\rho_{hole}]}} \quad [4\text{-}7]$$

Thus, the total bend angle, γ, of the borehole must be at least double that given by Equation [4-7] for the pipe to conform to the borehole curvature at points **2-3**. As will be seen later, it is also of interest to consider the general magnitude of the variable, $\boldsymbol{\ell}$, as given in Equation [4-6], which may be seen to be approximately double that of the distance f.

Figure 4-4 shows the magnitude of θ_b as a function of the normalized clearance $(D_{hole} - D)/\rho_{hole}$, which, for typical such values, is confirmed to be much less than 1 radian. For example, again, considering a 24-in. pipe in a borehole with 50% clearance (12-inches, or 1.0 ft.), and assuming a minimum radius of curvature of 600 ft, results in a normalized clearance of 1.0/600, or 0.00167, and a value of 0.1 radians (5.7º). For larger pipes, the combination of a possibly larger bend radius, especially for non-plastic materials, and recommended limit of 12 inch maximum clearance (HDD Consortium, 2008), corresponds to even lower values for a complete bend. Thus, it may be conservatively assumed that the total angle, γ, for the entry and exit bends, α and β, illustrated in Figure 2-1 for an HDD installation, exceeds, or is close to, that corresponding to a complete bend.

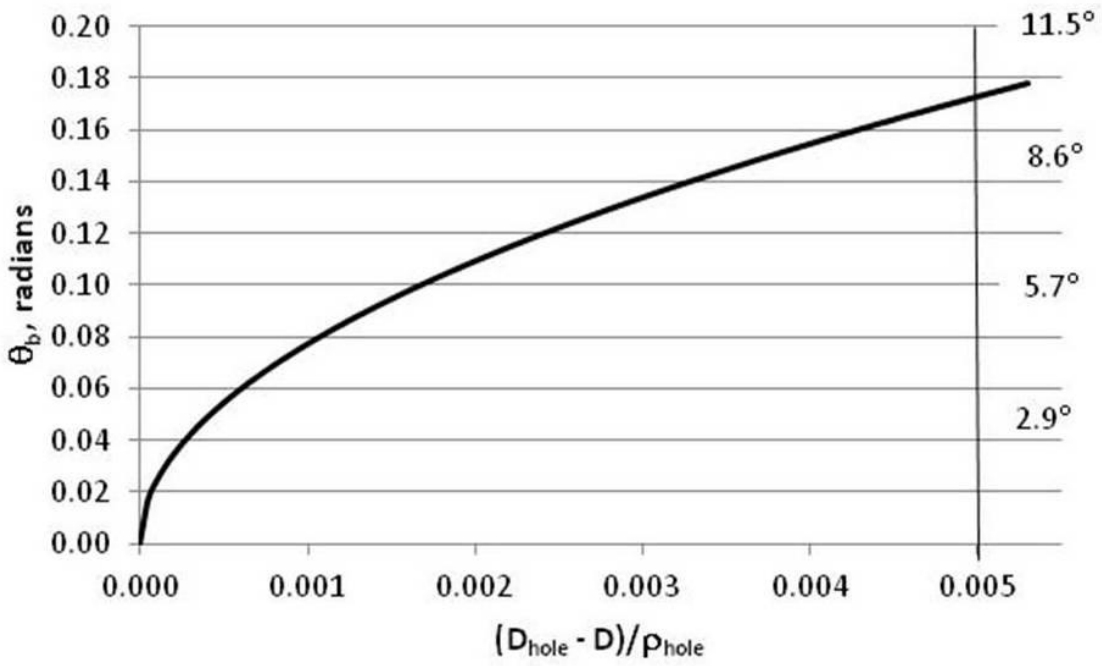

Figure 4-4. Magnitude of Complete Bend

The "characteristic reaction force" N_b for a complete bend, corresponding to the "characteristic" complete bend angle θ_b, may now be estimated by inserting the value for $\boldsymbol{\ell}$ of Equation [4-6] into Equation [4-4], resulting in:

$$\mathbf{N_b = EI / (2\,\rho_{hole}^2 \cdot \theta_b)}$$

$$\mathbf{= EI / \sqrt{[24\,(D_{hole} - D)\,\rho_{hole}^3]}} \qquad [4\text{-}8]$$

with the normalized force, $N_b\,\rho_{hole}^2/EI$, arranged as a function of the normalized clearance, as in:

$$N_b\,\rho_{hole}^2/EI = 1 / \sqrt{[24\,(D_{hole} - D)/\rho_{hole}]} \qquad [4\text{-}9]$$

and presented in Figure 4-5. A total of four times this force, or $4N_b$, acts at the bend, resulting in corresponding additional frictional drag. However, the trend in Figure 4-5 must be interpreted carefully since a brief perusal may initially suggest that larger bend radii, and therefore smaller complete bends, result in disproportionally large reaction forces, which is not correct. The opposite is true, as may be verified by observing the trend for the actual (non-normalized) force, N_b, in Equation [4-8], which shows the expected decrease for lower curvatures, or larger bend radii.

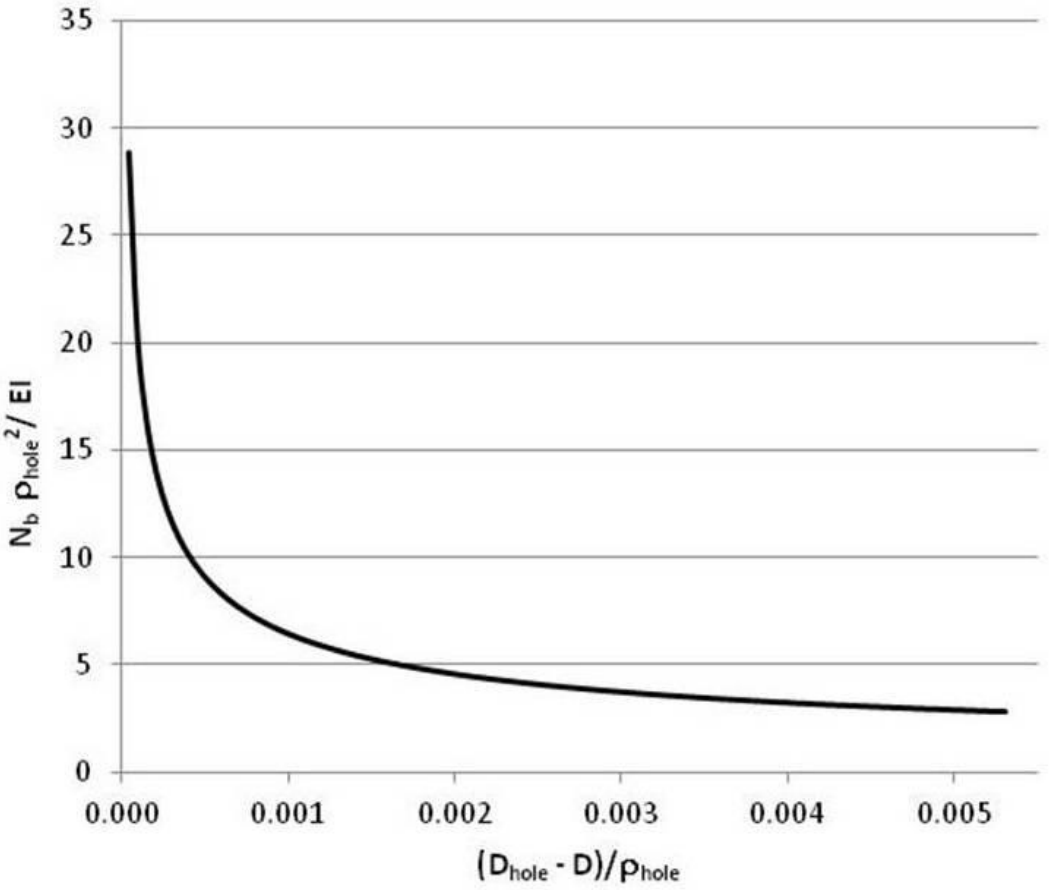

Figure 4-5. Normalized Reaction Force – Complete Bend

4.23 Incomplete (or General) Bend

For applications in which the total angle γ is less than double that of the complete bend angle θ_b of Equation [4-7], the local curvature of the pipe does not conform to that of the borehole, where it is in contact with the inner surface, as shown in Figure 4-6. This case is therefore referred to as an "incomplete" bend, for which θ is defined as half the total bend angle, or

$$\theta \equiv \gamma/2 \; < \theta_b \qquad [4\text{-}10]$$

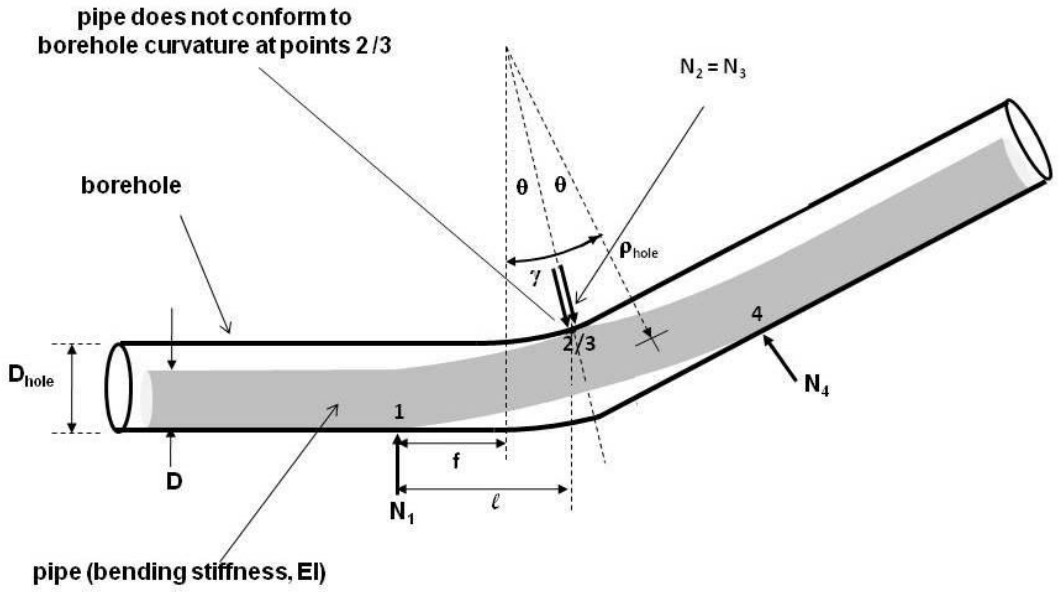

Figure 4-6. Incomplete (or General) Bend
(Courtesy of Outside Plant Consulting Services, Inc.)

As indicated in Figure 4-6, points **2** and **3** are considered to coincide, with the net reaction force at point(s) **2**/**3** interpreted as $N_2 + N_3$. Due to symmetry, Equation [4-1] is still applicable, in this case, with the reaction force $N_2 + N_3$ equal to twice that at point **1** or **4**, which is designated as $N(\theta)$, a function of the angle θ. Furthermore, Equations [4-2], [4-3] and [4-5] also remain applicable and, using Equations [4-7] and [4-8], lead to:

$$N(\theta) = 8\,EI\ (\theta/\theta_b)^3/\{\rho_{hole}^2 \cdot \theta_b \cdot[3\,(\theta/\theta_b)^2 + 1\,]^2\} \quad \text{for } \theta \le \theta_b$$

$$= N_b \quad \text{for } \theta \ge \theta_b \qquad [4\text{-}11]$$

or, again using Equation [4-8],

$$N(\theta)/N_b = 16\,(\theta/\theta_b)^3 / [3\,(\theta/\theta_b)^2 + 1]^2 \quad \text{for } \theta/\theta_b \le 1$$

$$= 1 \quad \text{for } \theta/\theta_b \ge 1 \qquad [4\text{-}12]$$

as shown in Figure 4-7. The magnitude of the reaction force increases with the value of the bend angle, reaching a maximum value when the angle is equal to θ_b. Beyond this angle, the reaction force N is equal to N_b, the value corresponding to a complete bend.

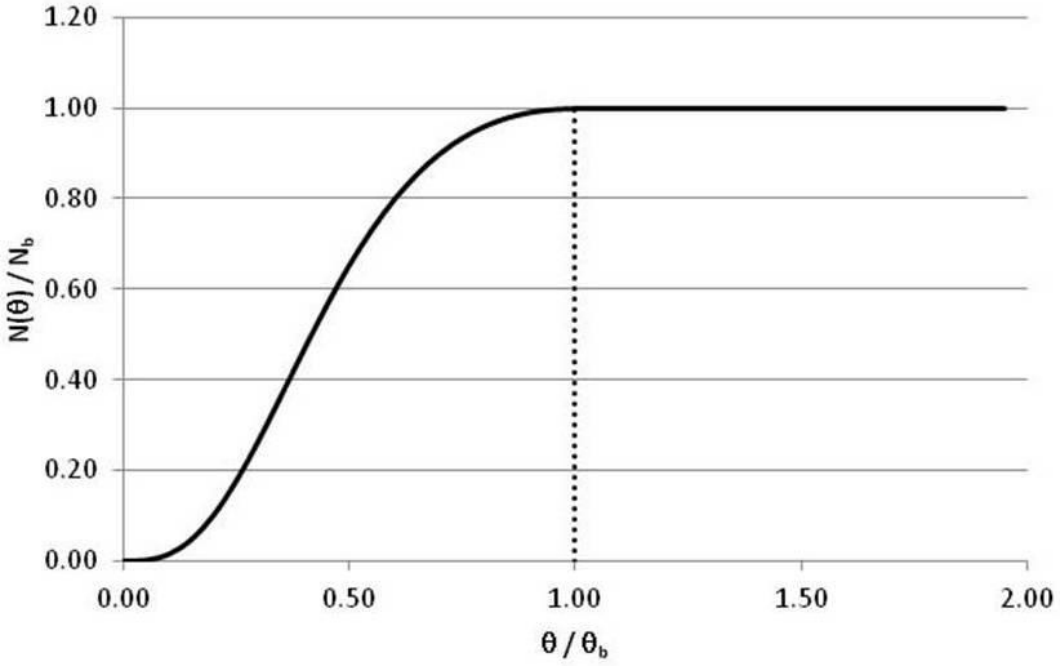

Figure 4-7. Reaction Force – General Case

Analogous to Equation [4-9], Equation [4-11] may be used to develop the following relationships:

$$N(\theta)\cdot\rho_{hole}^2/EI = 2\,\theta^3 / 9\,[\theta^2/2 + (D_{hole} - D)/\rho_{hole}]^2 \quad \text{for } \theta \le \theta_b$$
$$= 1 / \sqrt{[24\,(D_{hole} - D)/\rho_{hole}]} \quad \text{for } \theta \ge \theta_b \qquad [4\text{-}13]$$

which is presented in corresponding Figure 4-8. The effect of the clearance, relative to the bend radius of the borehole, on the reaction forces, is therefore shown in Figure 4-8, including for several bend angles, θ, less than that of a complete bend. The results for the various angles coincide at low values of clearance, since the angles approach (and exceed) the magnitude of a complete bend, θ_b, which diminishes with decreasing clearance, as illustrated in Figure 4-4. For such values of θ, or $\gamma/2 \ge \theta_b$, the reaction force reaches its peak, as indicated in Figure 4-8, independent of the magnitude of the actual total bend angle γ. For a given bend radius, ρ_{hole}, there is a rapidly increasing trend of the reaction force for decreasing clearances, which normalized clearance values relative to the bend radius, would be on the order of 0.002 or less for practical maxi-HDD installations. Similar to the case of a complete bend, a total of four times this force, or $4N(\theta)$, acts at the bend, resulting in corresponding additional frictional drag.

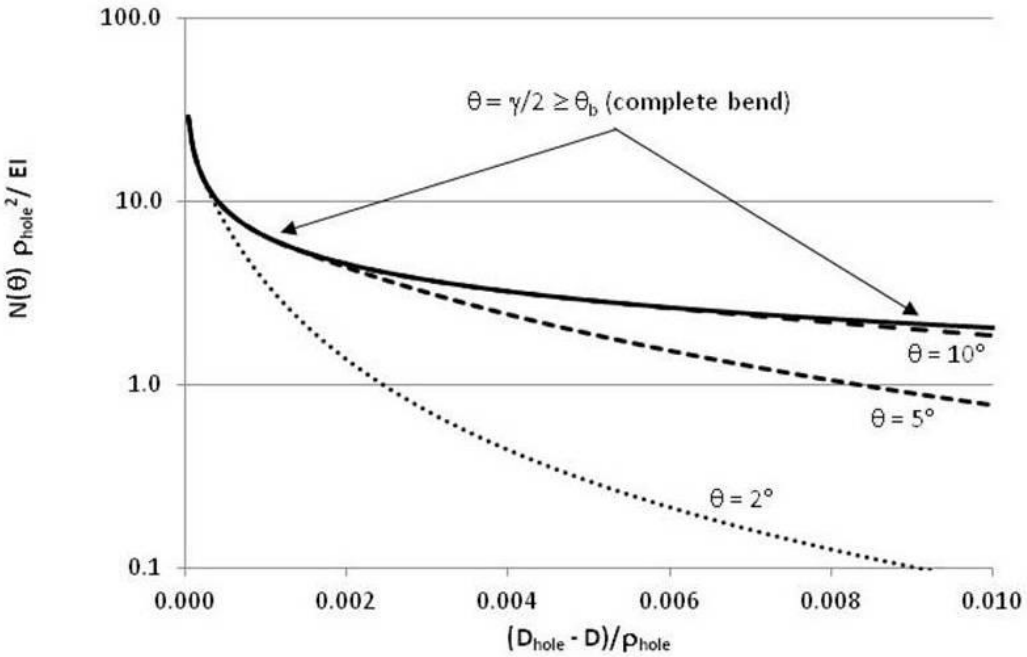

Figure 4-8. Normalized Reaction Force – General Case

4.24 End of Pipe Traversing Bend

Figure 4-3 shows the pipe in a position in which its leading end has passed the end of the bend a sufficient distance such that a portion of the pipe conforms to the straight portion of the borehole following the bend, to the left of point **1**. Figure 4-9, however, shows the leading end of the pipe as it passes through a complete bend, prior to reaching point **1**. During this transition, the reaction forces, N_1' and N_2', at points **1'** and **2'**, respectively – which locations will temporarily be somewhat behind, and to the right, of points **1** and **2** in Figure 4-3 – will be greater than that determined previously for N_1 and N_2, as by Equation [4-8]. This situation may also apply at the pipe entry or exit location, if the borehole has finite curvature at these points, or, to a somewhat lesser extent, if the straight portion is not of sufficient extent to allow the pipe to fully conform to the straight portion. Thus, if the bore path segment A – B or C – D of Figure 4-1 is of uniform curvature for most of the segment, the reaction forces at point A or D will be greater than that at point **1** or **4** of Figure 4-3. The analysis for this configuration again follows Griffioen's procedure, but with appropriate deviations from this model, including the associated adjustments presented in Section 4.25.

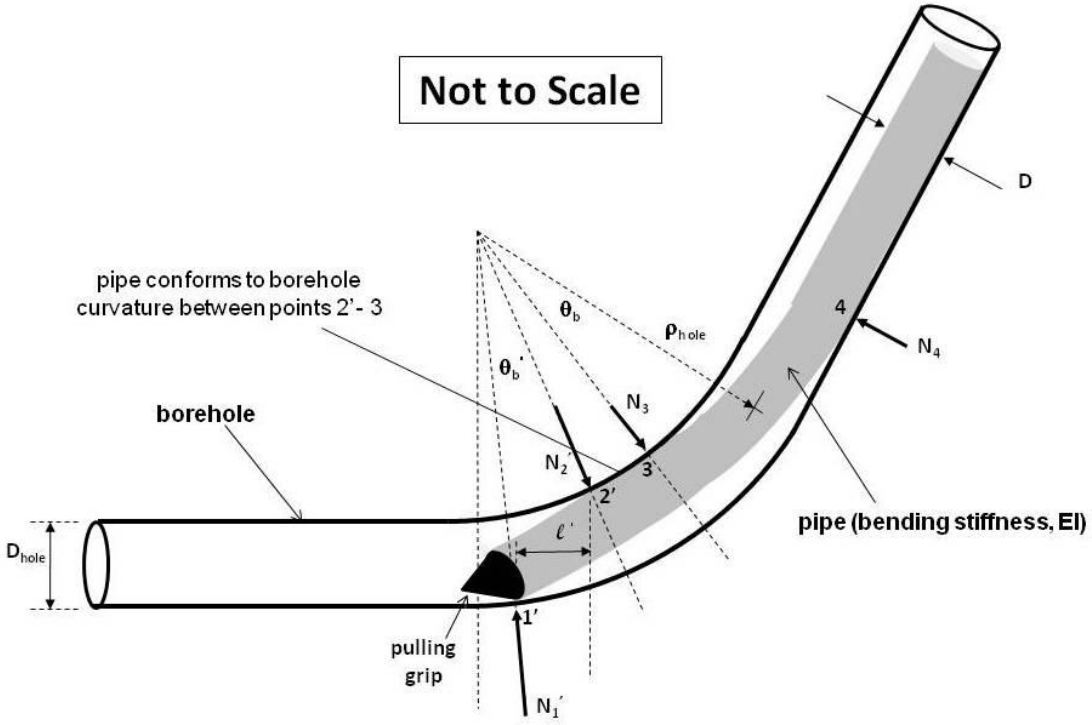

Figure 4-9. Pipe Passing through Complete Bend

For the geometry in Figure 4-9, the pair of equal reaction forces N_1' and N_2' (N_1' = N_2' = N') may not be assumed to be equal to the pair N_3 and N_4 ($N_3 = N_4$), which are each equal to the force N_b of Equation [4-8] since the geometry corresponding to this section of the bend (points **3** – **4**) is identical to that illustrated in Figure 4-3. However, considering the reactions, N_1' or N_2', on the opposite (leading) side of the bend, the beam bending relation for lateral deflection now yields:

$$N_1' \cdot (\boldsymbol{\ell}')^3 / (3\,EI) \approx \boldsymbol{\ell}' \cdot \theta_b' - [\rho_{hole} \cdot (\theta_b')^2/2 + (D_{hole} - D)] \qquad [4\text{-}14]$$

where

$$\boldsymbol{\ell}' \approx \rho_{hole} \cdot \theta_b', \qquad [4\text{-}15]$$

Since the bending moment due to the reaction force N' must again be consistent with the pipe and borehole curvature at point **2'**,

$$N_b' \cdot \boldsymbol{\ell}' / EI = 1/\rho_{hole} \qquad [4\text{-}16]$$

and for which the term N_b' is introduced to indicate this force level – i.e., N_1' or N_2' – applies to the case of the pipe end traversing a complete bend. Recognizing that the distance, or moment arm, $\boldsymbol{\ell}'$ in Figure 4-9 is less than that in Figure 4-3, it may be anticipated that the corresponding reaction forces will be greater than that of the characteristic reaction force N_b, as given by Equation [4-8]. Thus, combining these three relationships, results in:

$$N_b' \cdot \rho_{hole}^2/EI = 1 / [6\,(D_{hole} - D)/\rho_{hole}]^{1/2} \qquad [4\text{-}17]$$

or exactly twice that of Equation [4-8]. Equations [4-14] – [4-16] may then be used to verify that the condition for the pipe to conform to the borehole curvature between points **2'** – **3** is that the minimum angle of θ_b' corresponding to a complete bend is again given by the characteristic bend angle of Equation [4-7].

As the pipe end enters and traverses a complete bend, or possibly while traversing an incomplete bend, and the pipe is past the point where it contacts the upper and lower portions of the borehole, as illustrated in Figure 4-10, the subtended angle θ'' will be less than the minimum value of a complete bend. During this transition, the instantaneous total angle traversed is designated as γ'', for which:

$$\theta' + \theta'' = \gamma'' \qquad [4\text{-}18]$$

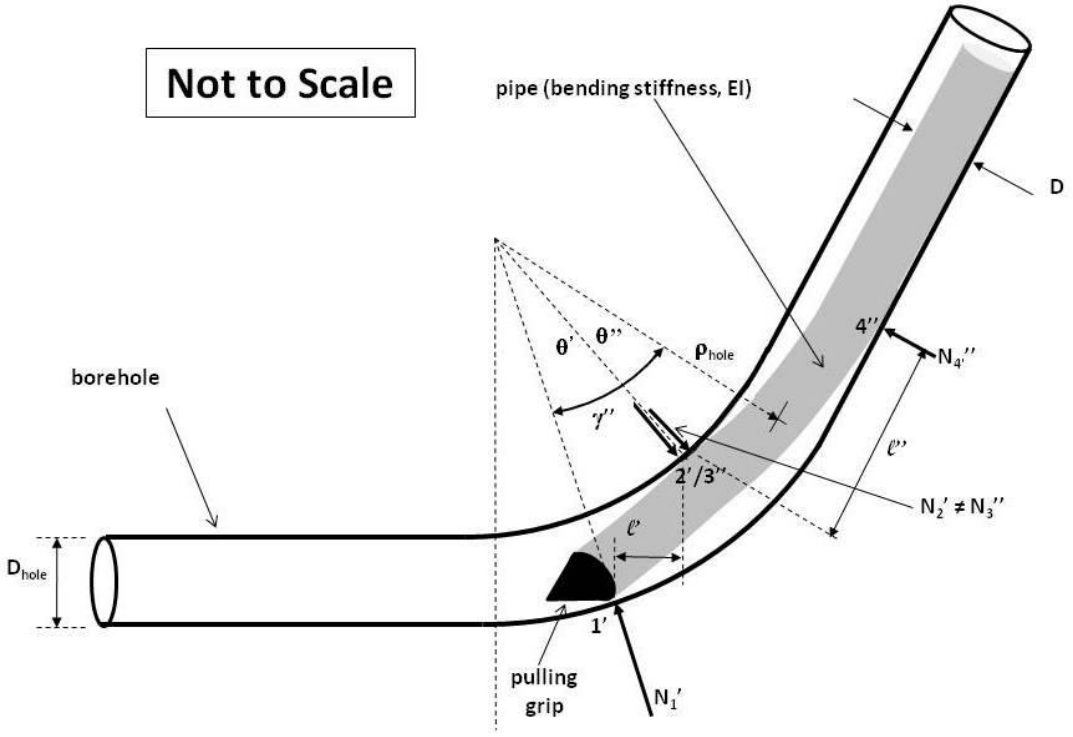

Figure 4-10. Pipe Passing through a General) Bend

In this case, points **2'** and **3''** coincide and the net reaction force at point **2'/3''** is conveniently designated as $N_2' + N_3''$.

Recognizing that Equation [4-13] applies for the segment between point **3''** and **4''**, with θ replaced by θ" in the first part of the equation,

$$N_4''(\theta'')\,\rho_{hole}^2/EI = 2\,(\theta'')^3 / 9\,[(\theta'')^2/2 + (D_{hole} - D)/\rho_{hole}]^2 \quad \text{for} \quad \theta'' \le \theta_b \qquad [4\text{-}19]$$

Another condition for the reaction force $N_4''(\theta'')$ is based on the same beam deflection equation of Equation [4-3], such that:

$$N_4''(\theta'') \cdot (\ell'')^2 / (2\,EI) = \theta'' \qquad [4\text{-}20]$$

Considering the reaction force $N_1'(\theta')$, Equations [4-14] and [4-15] give:

$$N_1'(\theta') \cdot \ell'^{\,3} / (3\,EI) \approx \ell'\,\theta' - [\rho_{hole} \cdot (\theta')^2/2 \; + \; (D_{hole} - D)] \qquad [4\text{-}21]$$

and

$$\ell' \approx \rho_{hole} \cdot \theta' \qquad [4\text{-}22]$$

Since the bending moments must be equal on both sides of the contact point **2'/3''**,

$$N_1'(\theta') \cdot \ell' = N_4''(\theta'') \cdot \ell'' \qquad [4\text{-}23]$$

Equations [4-18] through [4-23] represent six equations to determine the six unknowns (θ', θ'', N_1', N_4'', ℓ', ℓ''), as a function of the traversed total angle γ''. However, due to the increased complexity, a simple expedient is considered for the present purpose of estimating the effect of the local reaction forces. Based on the preceding results for which the reaction force $N_1'(\theta_b)$ on the leading end of the pipe passing through a complete bend (Figure 4-9) is double that trailing the bend – i.e., equal to 2 N_4 (or 2 N_1 of Figure 4-3), it is assumed that the reaction force on the leading end of the pipe passing through an incomplete bend (Figure 4-10) is also approximately double that trailing the bend, or

$$N_1'(\theta') \approx 2\,N_4'' \qquad [4\text{-}24]$$

Recognizing that the N_4'' term in Figure 4-10 corresponds to the N_4 term in Figure 4-6 and using Equation [4-13], with θ replaced by θ' or θ'', here considered as equal to half the total bend angle, or $\gamma''/2$, results in:

$$\begin{aligned} N_1'(\gamma'') \cdot \rho_{hole}^2/EI \; &\approx 4 \; (\gamma''/2)^3 / 9\,[(\gamma''/2)^2/2 + (D_{hole} - D)/\rho_{hole}]^2 \quad \text{for } \gamma''/2 \le \theta_b \\ &= 1 / \sqrt{[6\,(D_{hole} - D)\,\rho_{hole}^3]} \qquad\qquad\qquad\qquad \text{for } \gamma''/2 \ge \theta_b \end{aligned} \qquad [4\text{-}25]$$

This solution is considered to be a reasonable estimate of the reaction force at the leading end of the pipe as it traverses a bend, prior to exiting and passing beyond the bend, following which the reaction forces will be given by Equation [4-13], at half these values. In most cases, the angle θ_b corresponding to a complete bend is sufficiently low such that the reaction forces will be that corresponding to the case of $\theta \ge \theta_b$ in Equation [4-13] or $\gamma''/2 \ge \theta_b$ in Equation [4-25], which would otherwise be a conservative assumption.

Although the reaction force at point **1'** at the leading end of the pipe is double that at point **4** (or **4"**) in Figures 4-9 and 4-10, the reaction force at point **1'**, where the pipe is gripped, is absorbed within the pulling grip itself, and does not translate into a cumulative drag force along the pipe to be withstood by the strength of the pipe itself. Thus, the net reaction force of interest for Figure 4-9, with the pipe traversing a complete bend, is equal to 4 N_b, the sum of the reaction forces at point **2'** (= 2 N_b) and points **3** and **4** (=N_b each).

4.25 Adjustment for Maxi-HDD Applications

While the results for the reaction forces are consistent with that of Griffioen (1993), the assumption that the leading end of the pipe is contacting the bottom of the cavity, as shown in Figure 4-9, is not quite correct for a typical maxi-HDD operation. For example, in addition to the presence of buoyant forces and tensile loads, as discussed in Section 4.34, the pipe is usually pulled into the borehole behind a reamer, expanding or maintaining the integrity of the borehole, for which the leading end of the pipe would be gripped at the center of the borehole, as indicated

in Figure 1-1. In this case, the clearance term ($D_{hole} - D$) in Equation [4-17] would be only half of this amount, further increasing the reaction force at the leading end by a factor $\sqrt{2}$, corresponding to $2\sqrt{2}N_b$, while temporarily reducing the magnitude of the angle required for a complete bend at this point by the same factor, corresponding to $\theta_b/\sqrt{2}$. The corresponding total angle, γ, would be equal to the characteristic bend angle, θ_b, plus $\theta_b/\sqrt{2}$. Similar to the application above, where the reaction force at the pulling grip does not translate into a cumulative drag force along the pipe, the net reaction forces of interest for the lead end of the pipe traversing a bend would then be equal to $(2\sqrt{2} + 2)\ N_b$, which is the sum of the reaction forces at point **2'** ($=2\sqrt{2}\ N_b$) and points **3** and **4** ($=N_b$ each), or approximately 5Nb.

Figure 4-11 is intended to illustrate the general trend of the reaction force N_1 or N_1' (which is equal to N_2 or N_2'), normalized with respect to the characteristic reaction force N_b indicated in Equation [4-8], as the leading end of the pipe enters the (complete) bend, makes contact with the upper and lower surfaces of the borehole, and progresses around the bend, and finally exits the curved portion and progresses along the following straight section of the borehole. It is emphasized that the trends are shown only conceptually, and not based on any detailed calculations. Thus, for a complete bend, the reaction force initially increases, as the pipe enters the bend, achieving a peak value of $2\sqrt{2}\ N_b$, almost triple the characteristic force level N_b. The reaction force on the pipe end remains constant, at the peak value, until the pipe exits the bend and transitions to a subsequent straight section of the borehole, during which the reaction force decreases to the value of $\sqrt{2}\ N_b$. Beyond this point, the reaction force on the leading end of the pipe gradually vanishes as the pipe continues into the straight section of the borehole.

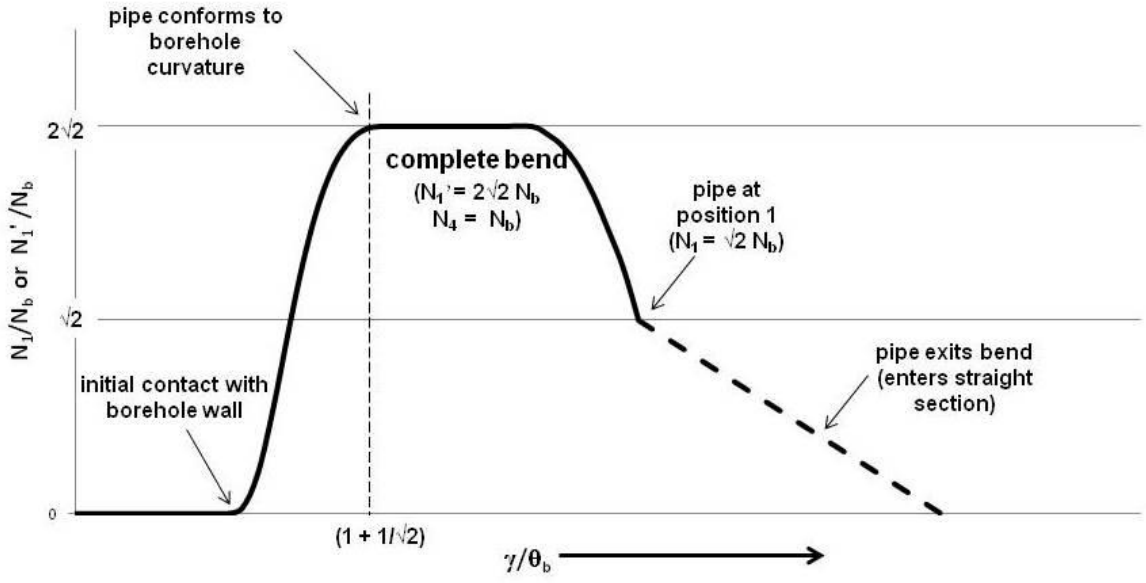

Figure 4-11. Normalized Reaction Force as Pipe Traverses Complete Bend during Maxi-HDD Operation

4.3 PIPE STIFFNESS VALUES AND IMPACT

The bending stiffness of the pipe, EI, is the product of its effective elastic modulus, E, and its cross-section area moment of inertia, I. The moment of inertia for a hollow pipe is given by (Young, 1989):

$$I = (\pi/4)\,(R_o^4 - R_i^4) \qquad [4\text{-}26]$$

where R_o and R_i are the outer and inner radii of the pipe, respectively, or

$$I = (\pi/4)\,[(D/2)^4 - (D/2 - D/DR)^4]$$

$$= (\pi/4)\,(D/2)^4\,\{1 - [(DR - 2)/DR]^4\} \qquad [4\text{-}27]$$

for which DR is the ratio of pipe (outer) diameter to wall thickness.

The results in Figures 4-5 and 4-7 have been normalized with respect to the bending stiffness of the pipe, which magnitude will determine the actual impact of this physical characteristic on the required pulling load. In addition to the elastic modulus, which is inherently very low for polyethylene material, the pipe diameter is a major factor, as may be seen by the quartic dependence of the moment of inertia on the diameter in Equation [4-27]. This strong dependence on the diameter, for a given DR value, as opposed to the quadratic dependence discussed in Section 3.5, suggests that the pipe stiffness may begin to have an appreciable effect on the pulling loads and corresponding tensile stresses for very large pipes, especially when added to the local bending stresses at the route bends. The potential quantitative effect of the pipe stiffness on the pull load, and corresponding tensile stress, is therefore discussed below for representative plastic and metallic pipes.

4.31 Plastic Pipes

In principle, some plastic pipes, such as HDPE, may be bent to a very small radius, possibly on the order of only 20 – 30 times the diameter (Performance Pipe, 2007), although for HDPE pipe with fused joints, a bend radius of times the diameter applies (AWWA 2020). In comparison, PVC pipe would require a relatively large bend radius of approximately 300 times the diameter (PWPipe, 2000).[11] Thus, with the exception of the larger PVC pipes, the bore path curvature for the installation of plastic pipes will generally be dictated by the more limited bending capability of the steel drill rods, to which the plastic pipe would readily conform. For example, the lowest bend radius term, ρ_{hole}, corresponding to the characteristic reaction forces, N_b, as in Equation [4-8] for an assumed complete bend, may be considered to be that determined by the drill rod size, such as the ASTM F1962 guideline of approximately 100 ft per inch of drill rod diameter. Assuming a fixed borehole radius, in combination with a specific borehole clearance of 12-inches for HDPE pipe sizes of 24-in. or greater (Section 3.35), the term $\sqrt{[(D_{hole} - D)\,\rho_{hole}^3]}$ in the denominator in Equation [4-8] may be assumed to be potentially of the same magnitude for this range of pipe sizes, while the stiffness term (EI) in the numerator rapidly increases at the rate of D^4 in comparison to the pipe strength increasing at the rate of D^2 (Section 3.5). Thus, the stiffness effect, as reflected in the bending reaction forces, will become increasingly significant for larger pipe sizes, increasing the total drag on the pipe and the required tensile load and corresponding average cross-sectional stress. The larger pipe sizes will also be accompanied by proportionally larger bending stresses at their outermost points relative

[11] These bend radii apply for a long-term bend, not subject to a pulling load.

to the bend. Both sources of stress are to be added, at various locations along the route, to ensure the allowable (safe) tensile stress is not exceeded.

For smaller diameter HDPE (or PVC) pipes (i.e., less than 24-in. diameter), the borehole clearance is not fixed at the 12-inch level, but is assumed to be 50% of the pipe outer diameter. The term $\sqrt{[(D_{hole} - D)\ \rho_{hole}^3]}$ in the denominator in Equation [4-8] is then equal to the quantity $\sqrt{[0.5\ D \cdot \rho_{hole}^3]}$, which *decreases* at the rate of $D^{½}$, while the stiffness term in the numerator decreases at the rate of D^4, for a net change at the rate of $D^{3½}$, which is still significant relative to the pipe strength decreasing at the rate of D^2. Thus, again in comparison to a 24-in. pipe, the stiffness effect will become increasingly less significant for smaller pipe sizes, decreasing the total drag on the pipe and the associated tensile stress, which will also be accompanied by proportionally lower bending stresses. The examples below illustrate the overall trend and dependence of the reaction forces on pipe size.

Since PVC pipe sizes of 24-in. or greater may require larger bend radii than that determined by the drill rods themselves, the trend should follow that corresponding to the metallic pipes for such sizes, as discussed below.

4.32 Metallic Pipes

In contrast to plastic pipes, steel pipes have an extremely high elastic modulus, which may be assumed to dictate the minimum bend radius to maintain the bending stresses within allowable limits – e.g., possibly 100 ft per inch of pipe outer diameter, similar to that for steel drill rods, for which ρ_{hole} will therefore vary as the pipe diameter D. For such pipes of 24-in. diameter or greater, for which a fixed clearance of 12-inches applies, the term $\sqrt{[(D_{hole} - D)\ \rho_{hole}^3]}$ in the denominator in Equation [4-8] increases at the rate of $D^{3/2}$ while the stiffness term in the numerator again increases at the rate of D^4, for a net change at the rate of $D^{2½}$, only slightly in excess of the pipe strength increase at the rate of D^2. Thus, in contrast to plastic pipes, it appears that the large size metallic pipes (> 24-in.) would be significantly less impacted by the bending stiffness effects -- essentially due to the proportionally larger bend radii considered for the bore path.

For pipes less than 24-in. diameter, for which the borehole clearance is 50% of the pipe outer diameter, the term $\sqrt{[(D_{hole} - D)\ \rho_{hole}^3]}$ may be seen to decrease at the rate of only D^2, considering the dependence of the ρ_{hole} on the pipe diameter D, while the stiffness term in the numerator decreases at the rate of D^4, for a net change at the rate of D^2. Since this is also the rate of change of the pipe strength with pipe size, there would not be any anticipated impact on the ability of the pipe to withstand the tensile stresses incurred during installation.

4.33 Results

Table 4-1 includes examples of plastic and metallic pipes, including HDPE, PVC and steel, in nominal sizes ranging from 12-inches to 48 inches, as well as the actual outer diameter D. Values of the wall thickness for representative products are reflected in the DR values for the plastic pipes, and a reasonably large DR value for the steel pipes. For the present purposes, values of the elastic modulus of 75,000 lbs/in^2 and 400,000 lbs/in^2 are assumed for HDPE and PVC pipe, respectively, and 29,000,000 lbs/in^2 for the steel pipe. The corresponding values of the stiffness EI are provided in the table.

Specific gravities of 0.955, 1.40 and 7.80 are used in the determination of the respective buoyant weights, but which also assumes the use of internal water ballast, as shown in Table 4-1.

The buoyant weights are not directly germane to the calculation of the reaction forces, but will be seen to have an important effect in reducing the potential reactions forces experienced in a practical application. For this reason, and in order to help assess the impact of the reaction forces in actual applications, a more realistic specific gravity of 1.2 (Section 3.34) is assumed for the slurry, rather than the otherwise conservatively high value of 1.5 in ASTM F1962. However, due to the greater density of the steel material, the net buoyant weight for this type pipe is negative, indicating that the pipe will rest on the bottom of the borehole. An unreasonably high slurry density would result in an overly high (plastic pipe), or overly low (steel pipe), buoyant weight, thereby reducing, or exaggerating, the impact of the actual corresponding reaction forces.

Table 4-1 Example Pipe and Borehole Characteristics (Vertical Bends)

nominal size / D (in)	**EI (lbs-in^2)**	**w_b (lbs/ft)***	**ρ_{hole} (ft)**	**$D_{hole} - D$ (in)**	**N_b (lbs)**
HDPE, DR 11, E = 75,000 lbs/in^2, specific gravity = 0.955					
12 / 12.75	5.37 x 10^7	11.9	600	6.375	7
24 / 24.0	6.74 x 10^8	42.1	600	12.0	65
36 / 36.0	3.41 x 10^9	94.8	600	12.0	329
48 / 48.0	1.08 x 10^{10}	168.5	600	12.0	1040
PVC, DR 25, E = 400,000 lbs/in^2, specific gravity = 1.40					
12 / 13.2	1.69 x 10^8	8.2	600	6.6	22
24 / 25.8	2.47 x 10^9	31.4	600	12.0	238
36 / 38.3	1.20 x 10^{10}	69.2	900	12.0	629
48 / 50.8	3.71 x 10^{10}	121.7	1,200	12.0	1265
Steel, DR 64, E = 29,000,000 lbs/in^2, specific gravity = 7.80					
12 / 12.75	4.49 x 10^9	-12.1	1,200	6.375	210
24 / 24.0	5.63 x 10^{10}	-42.8	2,400	12.0	679
36 / 36	2.85 x 10^{11}	-96.3	3,600	12.0	1871
48 / 48	9.01 x 10^{11}	-171.2	4,800	12.0	3842

* The buoyant weight is based on a slurry specific gravity of 1.2 and the use of internal water ballast.

The indicated borehole clearance is 50% of the pipe outer diameter, but a maximum of 12-in. for pipes greater than 24-in. A minimum borehole radii of curvature of 600 ft is again assumed, but is increased for steel pipe, in proportion to its outer diameter, as well as for the larger diameter PVC pipes, consistent with the 300-to-1 recommended bend radius to pipe diameter ratio. The characteristic reaction forces, N_b, are shown in Table 4-1, with the trends illustrated in Figure 4-12.

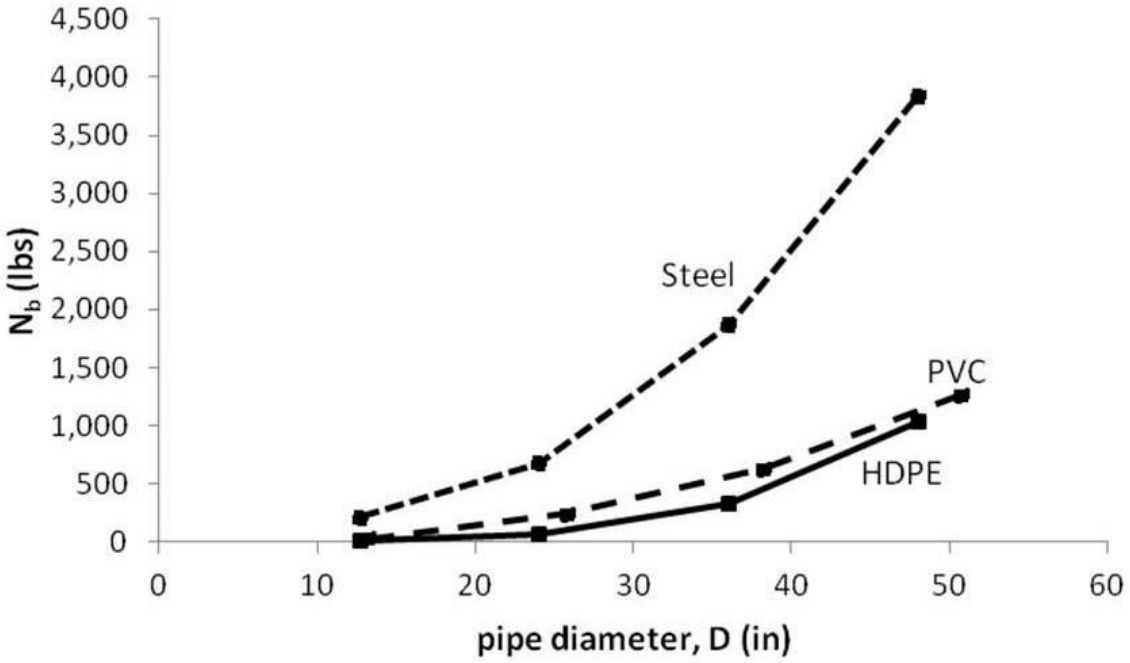

Figure 4-12. Characteristic Reaction Force N_b for Complete Bend

As anticipated, the reaction forces for the steel pipe is much greater than that of plastic pipe, but the ratio of the values tends to decrease at the larger sizes. This is due to the larger required bend radii for the steel pipe, to limit the bending stress, which is directly related to the same elastic modulus that determines the bending stiffness, EI, controlling the reaction force. Also as expected, the reaction force for PVC pipe is greater than that of the HDPE product, although the difference is reduced at the larger diameters due to the greater required bend radii for the PVC pipe.

4.34 Discussion

Based on the clearances and borehole radii for the various pipes, Equation [4-7] indicates the magnitude of a characteristic bend θ_b to be in the range of 2° to 5.7°, corresponding to a minimum total bend angle γ of 4° – 11.4°, or possibly somewhat less based on the adjustment discussed in Section 4.25 while the lead end of the pipe is traversing the bend. It may therefore be conservatively assumed that the pipe will experience a complete bend (in the vertical plane) at the entry and exit segments A – B and C – D. It is also assumed that the leading end of the pipe at point D is in fact in the process of traversing its bend along segment C – D, for which the net reaction forces of interest, on both sides of the contact points, are approximately $5N_b$ (see Section 4.25). The net reaction forces along the entry segment A – B, as illustrated in Figure 4-3, would be equal to $4N_b$, assuming the pipe is guided into the entry point with no additional or significant bending reaction forces at that point. Thus, ignoring the capstan effect, the total of these reaction forces is therefore approximately equal to $9N_b$.

Figure 4-13 shows the total possible reaction force, $9N_b$, normalized with respect to the buoyant weight, w_b, representing an effective incremental route length (ft) due to the pipe stiffness. This effective additional length corresponds to an increased frictional drag force which

should be considered during the engineering and planning stages, to the extent such reaction forces may actually be developed, as described below.

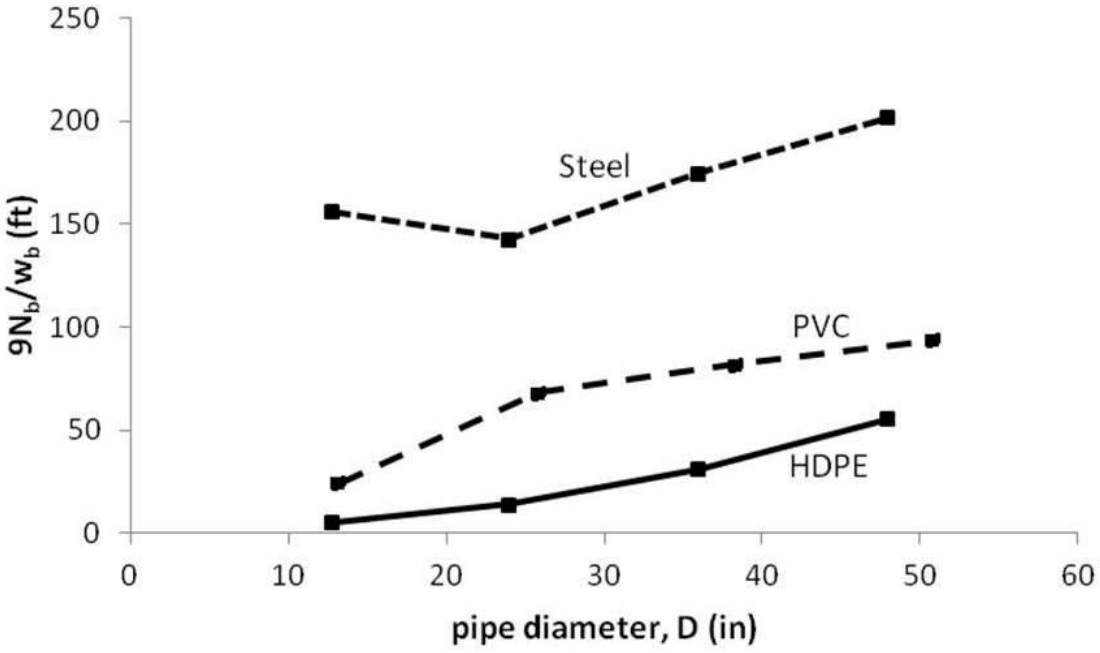

Figure 4-13. Effective Reduction in Route Length due to Reaction Forces

This frictional drag force, or corresponding potential distance, is small in spite of the conservative nature of the estimates, including the comparison to the low buoyant weights of Table 4-1, for the relatively low assumed slurry density (specific gravity = 1.2) and use of water ballast. For example, the equivalent incremental lengths for HDPE are essentially two orders of magnitude lower than the placement distances for such products, as suggested by the results in Figure 3-1 which are based on the conservatively high slurry density suggested in ASTM F1962 (specific gravity = 1.5).

Furthermore, as indicated in Section 4.2, the present model, such as illustrated in Figure 4-1, ignores the effect of the distributed vertical forces, due to gravity or buoyancy, acting along the length of the pipe, on both sides of the contact points (**2**, **3**). For a net upward buoyant weight, these forces push up, and bend the pipe about the contact points **2** and **3**, reducing, or possibly eliminating, the otherwise necessary contact and reaction forces at points **1** and **4,** potentially eliminating the detrimental effect of the pipe stiffness. Similarly, for a net downward "weight", as with heavy steel pipe, the distributed forces tend to push down, and/or bend the pipe, about points **1** and **4**, reducing the otherwise necessary contact and reaction forces. Indeed, it may be verified that the corresponding total lateral (vertical) bending forces are generally sufficient to significantly reduce, or possibly eliminate, the impact of the reaction forces, including the larger reactions experienced while traversing the bend.

In addition, any significant tension that may have previously developed at the bend will exert a beneficial local bending moment that also helps reduce the magnitude of any reaction forces. For example, the pulling force shown in Figure 4-2 tends to bend the pipe about the

contact points (e.g., point **2**, Figure 4-3), providing a bending moment helping to conform the pipe to the route curvature. Both these considerations indicate that the estimated reaction forces are likely to be significantly overestimated and, recognizing their already minor impact, may be ignored for most practical applications; see Section 4.4.

Nonetheless, there may conceivably be cases in which these effects may be more significant and should be considered or addressed. This may, for example, be applications including a combination of: thick-walled and/or very large diameter pipe, larger diameter joints resulting in reduced local clearances, very low magnitude buoyant weight, relatively small borehole radii, horizontal bends, and/or low tensile capability (e.g., weak joints) with correspondingly limited placement distance. The formulae provided herein may then be used to provide a conservative estimate of the reaction forces to determine the associated increased frictional drag force and pull load, using the method described in Section 4.4.

4.4 PROPOSED MODIFIED EQUATIONS FOR ESTIMATING PULL LOAD

To the extent they may be significant, the effect of the reaction forces due to pipe bending stiffness may be approximated by appropriate modifications to Equations [2-1]. In particular, the following term may be added to the right side of Equation [2-1b] to reflect the incremental tension when the leading end of the pipe reaches point B, due to the cumulative reaction forces acting along the curved segment A – B:

$$e^{\nu_b \alpha} \; \nu_b \, (4N_b) \, F(w_b) \qquad [4\text{-}28]$$

where $F(w_b)$ is a function of the buoyant weight, w_b, and is intended to account for the mitigating effect of the corresponding lateral (vertical) bending forces. Based on the geometry of Figure 4-3 and Figure 4-9, beam bending formulae (Young, 1989), and the discussions in Sections 4.25 and 4.34, the following conservative guideline is suggested:

$$\begin{aligned} F(w_b) &= 1 && \text{for} && |w_b| \cdot \rho_{hole} \, \theta_b \leq N_b \\ &= \tfrac{1}{2} && \text{for} \quad N_b < && |w_b| \cdot \rho_{hole} \, \theta_b < 10N_b \\ &= 0 && \text{for} && |w_b| \cdot \rho_{hole} \, \theta_b \geq 10N_b \end{aligned} \qquad [4\text{-}29]$$

In order to account for the incremental tension at the end of the installation, resulting from the reaction forces due to the pipe bending stiffness along the segment C – D, the term

$$e^{\nu_b \beta} \; \nu_b \, (5N_b) \, F(w_b) \, G(T_D) \qquad [4\text{-}30]$$

may be added to the value of "T_D" using the result of Equation [2-1d], which already includes the effect of the bending stiffness experienced along A – B by means of modified Equation [2-1b]. In addition to the term $F(w_b)$, Equation [4-30] includes the function $G(T_D)$, which is intended to account for the additional mitigating effect due to the local tensile load that has developed along the route. The magnitude of $G(T_D)$ should therefore approach 0 for relatively large values of T_D, or 1.0 for relatively low values. Again, based on the geometry of Figure 4-3

and Figure 4-9, the relationships for N_b and θ_b of Equations [4-7] and [4-8], and the following guideline may be developed[12]:

$$\begin{aligned} G(T_D) &= 1 && \text{for} && T_D \le 3N_b/\theta_b \\ &= \tfrac{1}{2} && \text{for} && 3N_b/\theta_b < T_D < 24N_b/\theta_b \\ &= 0 && \text{for} && T_D \ge 24N_b/\theta_b \end{aligned} \qquad [4\text{-}31]$$

For application of Equations [4-28] – [4-31], the appropriate value of the borehole radius, ρ_{hole}, determines the value of N_b and θ_b in each section, A – B or C – D, using Equations [4-7] and [4-8].

The suggested functions $F(w_b)$ and $G(T_D)$ are convenient, conservative, approximations intended to reflect the impact of the buoyant weight and the tension in reducing the effect of the bending reaction forces. The variability or uncertainty in quantifying the benefit is reflected in the wide ranges of values in Equations [4-29] and [4-31], which are due to the geometrical model and simplifications used to analyze the phenomena. Although the functions defined in these equations are lacking in precision, the formulae capture the essence of the phenomena, and are judged sufficient for the purposes of estimating the effects on the required pulling force for a maxi-HDD installation. Furthermore, in most practical applications, the magnitudes of the buoyant weight and pulling tension would determine the values of the proposed functions F and G to be zero. Thus, with the possible exceptions as discussed above, the relatively minor impact of the theoretical characteristic reaction forces, N_b, in combination with the mitigating factors associated with the buoyant weight and/or pulling tensions, would render the effect of the pipe bending stiffness on the required pulling force to be inconsequential. This is true even for materials otherwise having inherently large stiffness (steel, …), in large part due to the recommended procedures (i.e., allowable bend radii) in handling and installing such pipes, and their presumably thinner-walled design.

4.5 SUMMARY

While the theoretical analysis indicates that the reaction forces due to the bending stiffness of the pipes generally increase with material stiffness, wall thickness, and pipe size, as may be anticipated, the overall impact is inconsequential in most practical applications, including for non-PE materials. This conclusion is based on a consideration of the estimated magnitude of the reaction forces for appropriate borehole geometries, and the mitigating effects of the net buoyant weight and pulling tensions in helping to reduce or eliminate these forces.

These results are not surprising since it is necessary to limit the route curvatures for products with significant stiffness, in order to minimize the associated bending stresses, which restraint indirectly limits the magnitude of the reaction forces. For special cases where it may be desirable to account for the increased frictional drag due to the reaction forces, the suggested modifications of Equations [4-28] – [4-31] may be useful.

[12] The indicated magnitudes of tension produce a bending moment equivalent to that of the original reaction forces acting at the leading end of the pipe, considering the discussions in Sections 4.25 and 4.34.

CHAPTER 5
COMPARISON WITH ALTERNATE (PRC) METHOD[13]

5.1 ALTERNATE DESIGN METHODS

The results of Chapter 4 indicate that, for practical applications, pipe stiffness is not an important consideration in determining the required pull force due to the corresponding frictional drag, including for a very stiff product such as steel pipe. However, at least one widely used procedure for the installation of such pipe by maxi-HDD explicitly attempts to account for the bending stiffness of the pipe. In particular, the Pipeline Research Committee (PRC) of the American Gas Association developed a method specifically intended for such pipe. The PRC method requires an iterative technique to estimate the associated bending/reaction forces, and is therefore not quite as convenient to apply as the ASTM procedure intended for flexible polyethylene pipe, but has nonetheless been widely employed. Although each method was developed to be used for the placement of a particular material (e.g., PE or steel), both methods have been used in the industry to estimate the required pull forces for either type product. For example, Knight et al (2003) used the PRC method to estimate the required pulling force for polyethylene pipe and Zeng et al (2013) employed the ASTM method to determine the pull force on steel pipe. It is therefore of interest to further compare and analyze the results using both methods on the same type pipe – i.e., HDPE and steel – in order to help understand the differences and their implications.

5.2 PRC METHOD FOR STEEL PIPE

Huey et al (1996) describes the basic PRC method for a route geometry equivalent to that of Figure 2-1. For convenience, this procedure is represented by Equation [5-1], adopting the original nomenclature.

$$T_D = \Sigma(DRAG) + \Sigma_{straight}(|frict|) + \Sigma_{curved}(|frict|) + \Sigma(W_S\, L{\cdot}Sin\theta) \qquad [5\text{-}1]$$

Equation [5-1] therefore represents the PRC equivalent of Equations [2-1].but is only a single equation since it assumes the peak tension occurs at the end of the installation. While this is true if the pipe is continuously lengthened by adding (welding or fusing) short segments as the pipe is pulled into the borehole, it may not be the case if the entire length of pipe is initially assembled, prior to the installation. In the latter case, the peak tension may occur at an intermediate stage, depending upon the relative (buoyant) weights and frictional characteristics, as further discussed below.

The Σ summation symbols in Equation [5-1] apply to the individual segments of the pipe, including straight and curved lengths. The term $\Sigma_{straight}(|frict|)$ accounts for the friction between the pipe surface and the borehole wall, due to the net buoyant weight (up or down) of the pipe, resulting in the normal distributed reaction pressure between the pipe and the borehole, including at inclined (straight) segments of the pipe. The term with "$Sin\theta$" corresponds to the downward (or upward) tendency of gravity (or buoyancy) to inhibit or aid the movement of the pipe segment of effective (net buoyant) weight W_S, as it changes depth. The PRC method considers the fluidic "DRAG" to be based on an assumed viscous drag force distributed over the pipe outer

[13] Ref. "Which Method to Use When Estimating Maxi-HDD Installation Loads – ASTM F 1962 or the PRCI Method?", Slavin and Scholl, ASCE Pipelines 2014 Conference.,

surface. The original recommended value was 0.05 lbs/in^2 (Huey et al, 1996), but was later reduced to 0.025 lbs/in^2, based on more recent field results (Puckett, 2003; ASCE, 2014).

The most significant feature, however, is the method of determining the normal reaction forces, and corresponding frictional forces, at curved sections (route bends), including at the entry and exit segments of the bore path. The corresponding term $\Sigma_{curved}(|frict|)$ refers to the segment illustrated in Figure 5-1, for which the evaluation requires the aforementioned iterative process to determine the reaction forces, N, N_1 and N_2 at the bend, and the associated frictional force (not shown). The total effective friction along this curved segment is then considered to be double that due to the calculated value, N – i.e., 2N – presumably on the assumption that the sum of the lower reactions forces (N_1 + N_2) is also equal to N (see Section 5.5). This effect is estimated assuming a three-point beam bending configuration, and using relatively complex formulae reflecting non-linear effects associated with-the tensile loads present while installing the pipe (Roark, 1943). This calculation attempts to reflect the various effects in this pipe segment, including buoyant weight, pipe stiffness and tension at a bend (capstan effect).

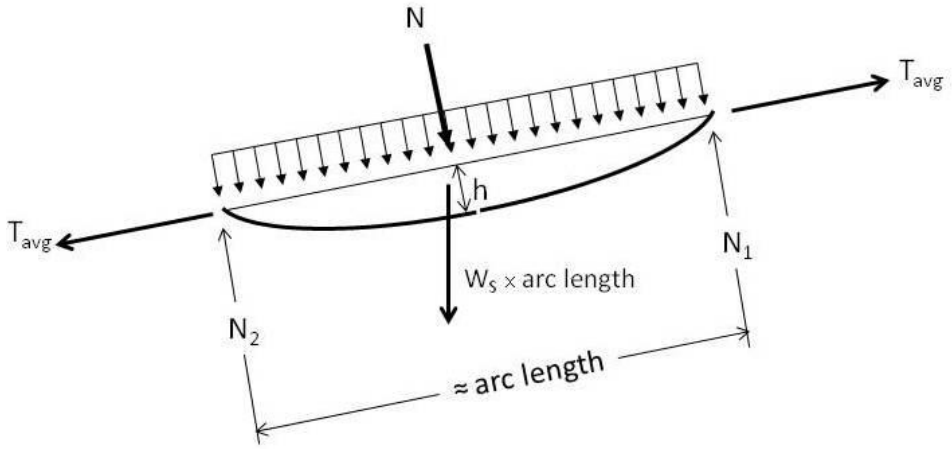

Figure 5-1. PRC Model of Pipe at Route Bend

5.3 ASTM F1962 vs. PRC

As discussed in Section 2.3, in spite of efforts by the HDD industry to develop more accurate predictions of pulling loads in practical applications, current methods often produce installation forces that differ significantly from field results. Attempts to align the predictions with field measurements, by selecting appropriate quantitative values of relevant parameters are only useful if capable of accurately predicting the required pulling loads in subsequent applications, using the developed model. This ability, however, does not presently exist, essentially because of the complexity and wide variability, and corresponding non-predictability, associated with operations in non-engineered materials and environments -- i.e., soil and rock. For instance, controlled HDD field experiments have resulted in significantly different pull loads – by a factor of almost two to one -- in what would appear to be almost identical conditions (Knight et al, 2002). It is therefore not surprising that different methods would attempt to model the complex HDD operation in a somewhat different manner, including the ASTM and PRC methods.

Both the ASTM and PRC methods are based on similar principles, including Coulomb friction, for which the frictional force is proportional to the normal reaction, and the direct effect of gravity (or buoyancy) in resisting or aiding at changes in elevation. Thus, both methods assume a coefficient of friction equal to 0.3 within the borehole and the direct effect of gravity (or buoyancy) in the W_S L·Sinθ terms is similar to those containing the depth, H, in Equations [2-1b] and [2-1d]. However, there are significant differences in the means of accounting for the fluidic drag, as well as the bending stiffness of the pipe, with the fluidic drag accounting for the most significant quantitative difference. Whereas the contribution of fluidic drag on the ASTM estimate is calculated by Equation [2-2], resulting in only a minimal effect on the calculated pull load, based on a borehole pressure of 10 psi to expel the cuttings, the present recommended viscous drag value of 0.025 lbs/in^2 for the PRC method is relatively high. In general, the drag force is related to the fluid viscosity and cuttings removal efficiency (Petroff, 2004), which depends upon the condition of the borehole. The different assumptions regarding fluidic drag may therefore be attributed to a greater degree of conservatism in the PRC estimate. In addition, the PRC model used for determining the friction at route bends, due to a pipe being pulled around the curve (Figure 5-1), is significantly different than that used in ASTM F1962 (capstan effect), and may also account for some of the discrepancies between the estimates, including the effect of pipe stiffness.

Another difference, albeit minor, is the assumed value for the density of the slurry. ASTM F1962 uses a specific gravity of 1.5, which is slightly greater than the corresponding value of 1.44 (89.76 lbs/ft^3) in the PRC analysis. These relatively high values are considered to be conservative, since they result in large values for the buoyant weights for both products, assuming no ballast is used. However, for a heavy pipe, such as steel, the combination of ballast and a greater slurry density may result in an unrealistically low buoyant weight. In such cases, the more conservative approach would be to consider lower slurry densities, possibly approaching 1.0. Furthermore, for applications with very low buoyant weights, it is also possible that the peak tension may occur prior to the end of the installation, for a fully pre-assembled pipe. This situation depends upon the combination of the (low) buoyant weight within the borehole and the corresponding frictional coefficient, compared to that of the greater dead weight of the assembled pipe length outside the borehole and the frictional characteristics of the external supports.[14] ASTM F1962 recognizes this possibility and therefore estimates the pulling load at several points in the installation. The PRC method, as described in Huey et al (1996), assumes the peak load is at the end of the installation, and calculates the pulling force at this point only. The peak tension will occur at the end of the pull, with or without the use of ballast, in the event that there are minimal external portions of the pipe, with additional sections added (fused, welded, etc.) as the pipe is pulled into the borehole.

5.4 EXAMPLES

The example presented by Huey et al (1996) was a 12.75-in. (outer diameter) steel pipe installed in a 1500 ft (horizontal projected) borehole length, without ballast. For the present purposes, however, it is more instructive to consider a 24 inch steel pipe, consistent with the size of the HDPE pipe considered in previous chapters, including a similar geometry (i.e., Table 3-1 nominal values, including 2,500 ft bore). The empty steel pipe has a net upward buoyant weight

[14] ASTM F1962 considers an additional external length, L_1, as in Figure 2-1, to allow for handling and thermal contraction of the pipe.

(no ballast added) of 187.9 lbs/ft, based on a slurry with a specific gravity of 1.44 (12 ppg). The stiffness of the (DR 11) HDPE pipe and (DR 64) steel pipe and are assumed to be 75,000 lbs/in^2 and 29,000,000 lbs/in^2 i, respectively, as in Table 4-1 or Chapter 4.

The resulting required tensile force of approximately 233,000 lbs (at the end of the installation) is illustrated in Figure 5-2 as determined by Equation [5-1], for the PRC method. The individual contributing factors are also indicated, including friction, fluidic drag, and stiffness. The fluidic "drag" is determined as discussed and the contribution due to "stiffness" was determined by redoing the calculations with a material elastic modulus equal to zero, and attributing the difference to "stiffness", as manifested by the differential reaction forces at the bends in combination with the coefficient of friction. The balance is indicated as "friction", and is considered to be that due to the reaction forces resulting from a combination of the buoyant weight along the bore path and tension at a bend. The latter procedure therefore ignores any net effect of the "W_S L·Sinθ" gravity (buoyancy) terms, which tend to approximately cancel at the completion of the installation.

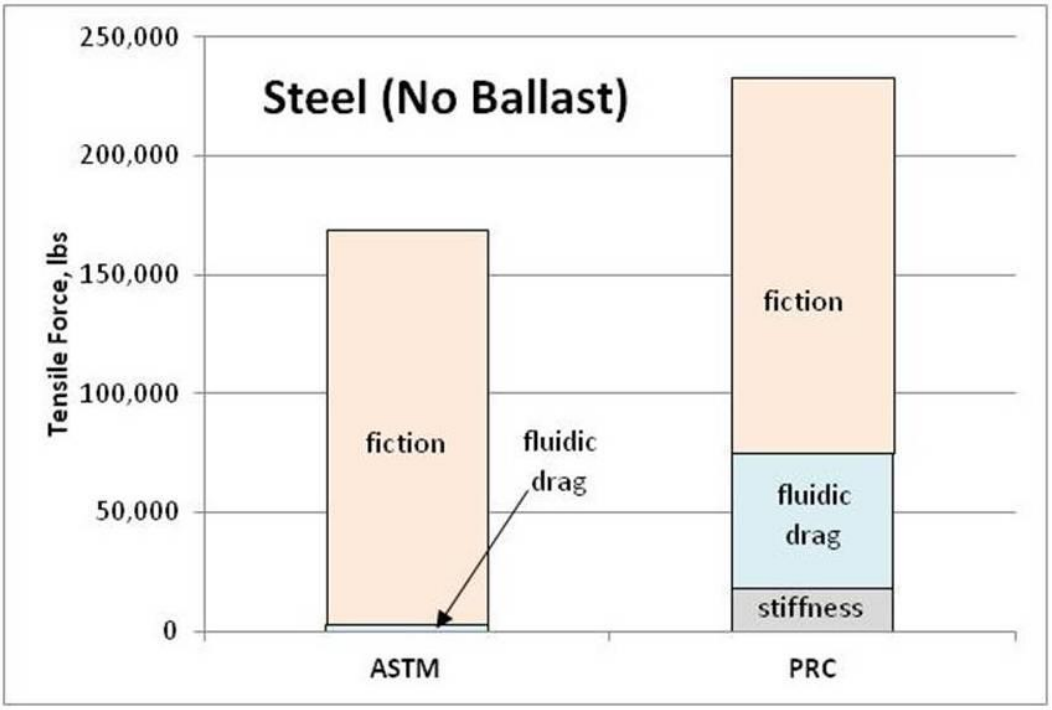

Figure 5-2. Estimated Tensile Force for Steel Pipe (No Ballast)

Figure 5-2 also shows the results of the basic ASTM method, including the relatively low estimate of the fluidic drag, but considers the possibility of bending stiffness of the pipe using the procedure proposed in Section 4.4, but which net effect is determined to be negligible in this case. The combination of the fluidic drag and pipe stiffness of the PRC method account for its approximately 35% higher estimate of the required force, for the present example.

Figure 5-3 shows the corresponding results for the installation of the HDPE pipe. The difference between the two methods is now somewhat less, approximately 25%, due to the

greater prominence of the frictional force relative to the PRC estimate of the fluidic drag, since the HDPE pipe has a considerably greater buoyant weight (232 lbs/ft) than the steel pipe.

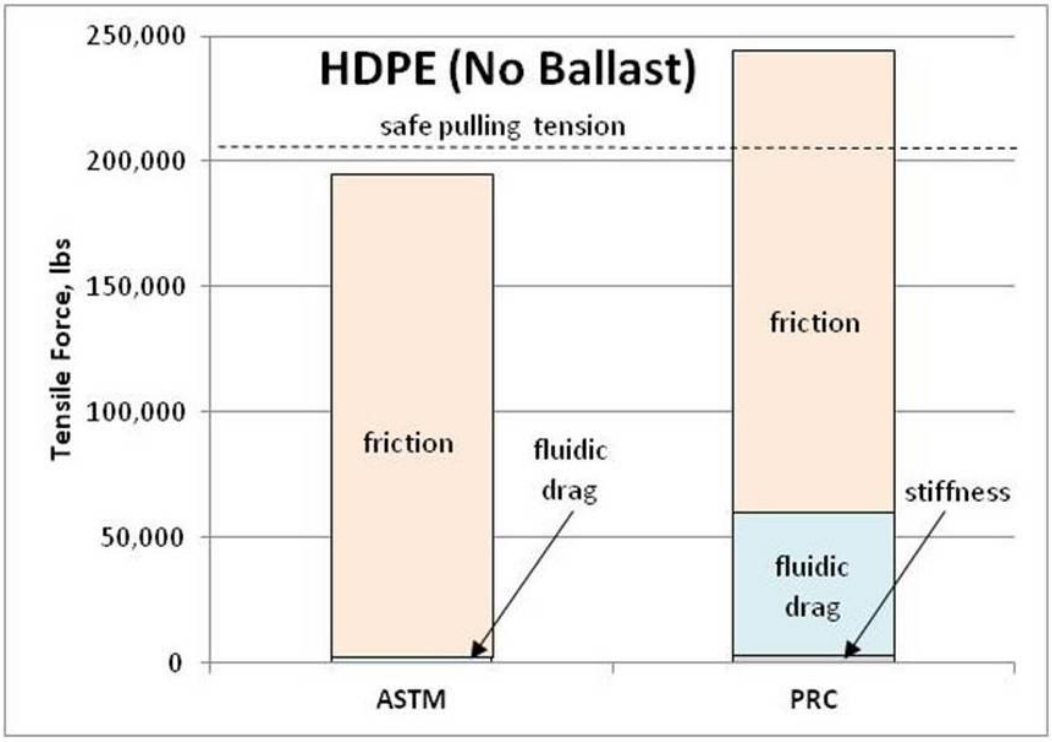

Figure 5-3 Estimated Tensile Force for HDPE Pipe (No Ballast)

As indicated in Figures 5-4 and 5-5, the use of ballast to reduce the buoyant weight, and corresponding friction, dramatically reduces the estimates of the required pulling force. This is especially the case with the steel pipe, for which the buoyant weight appears to be on the order of only 10 lbs/ft, based on the "conservatively" high assumed density of the slurry, which essentially cancels out the combination of the dead weight of the pipe filled with water ballast. This example, demonstrates that the peak tension during the placement of a pipe with a very low effective buoyant weight may (1) occur prior to the end of the installation, and (2) be significantly underestimated for a pipe of very heavy material (e.g., steel) if based on an overestimated slurry density. Thus, the ASTM results illustrated in Figure 5-4 also shows the corresponding peak tension, which is 40% greater than that at the end of the installation, as based on the low (underestimated) buoyant weight. (In this case, there is a finite contribution due to the bending stiffness of the steel pipe, again following the proposed guideline of Section 4.4.) Furthermore, and perhaps more important, a significantly lower slurry density results in a net (downward) buoyant weight of potentially much greater magnitude. For example, using the ASTM F1962 method, a more typical specific gravity of 1.2 results in an estimated peak pull force 33% greater than its peak value indicated ("mid-installation") in Figure 5-4, while the PRC method results in a peak force 14% greater than its value in Figure 5-4.

In general, the effect described above can occur with a very heavy pipe, such as steel, for which the (downward) dead weight (including internal ballast) is largely offset by the upward buoyancy of the slurry, and in principle, may also occur even without the use of ballast,

depending on the material density and wall thickness (DR value). For this example, the presumably overly conservative nature of the PRC method, due to its high assumed fluid drag, would still exceed the adjusted (increased) ASTM estimate. However, the preferred approach in such cases would be to consider the possible realistic range of slurry densities.

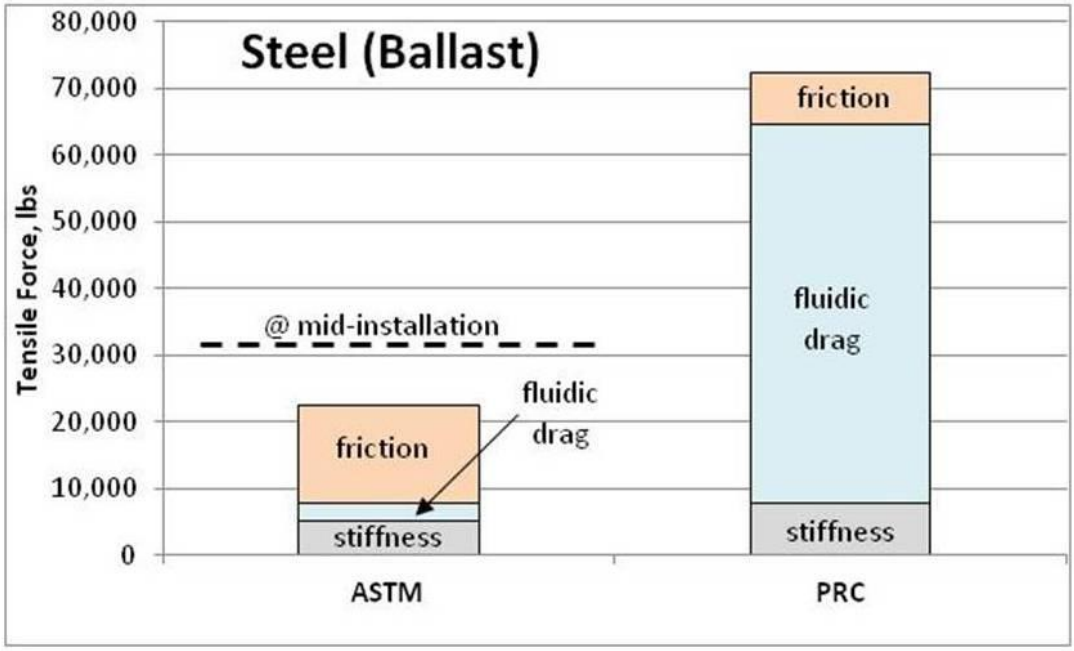

Figure 5-4. Estimated Tensile Force for Steel Pipe (with Ballast)

In contrast, HDPE pipe, will always have a significant upward net buoyancy, even filled with water ballast) due to its inherent low material density (less than water). Thus, the assumption of a relatively high density for the drilling fluid (e.g., 1.5), as suggested in ASTM F 1962, will be conservative and provide a degree of design margin; see Figure 5-5.

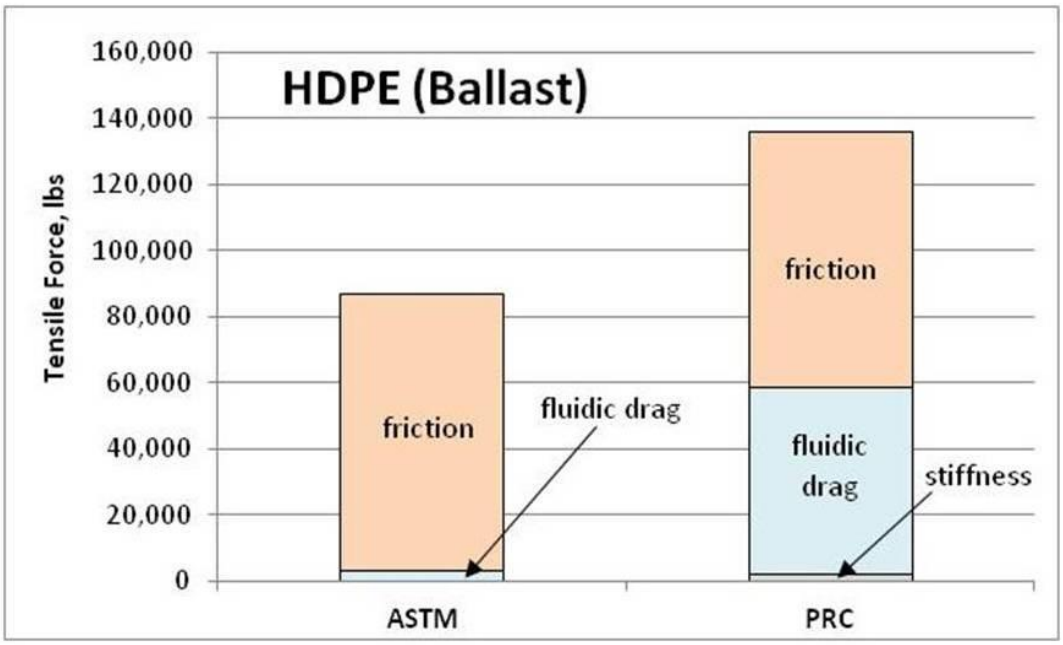

Figure 5-5. Estimated Tensile Force for HDPE Pipe (with Ballast)

5.5 DISCUSSION

As in essentially all mathematical models of physical phenomena, various convenient assumptions and approximations have been incorporated into both the ASTM F1962 and PRC methodologies. The three-point beam bending model in Figure 5-1 has the advantage of accounting for the pipe stiffness in some manner, but is not necessarily compatible with the actual interaction of the pipe with the borehole, as described in Chapter 4, including the indicated force vectors. These vectors are not aligned with the axial tension on the pipe and the (perpendicular) normal pressure applied by the borehole on the pipe surface. Nonetheless, for limiting cases (e.g., absence of material stiffness, in combination with either negligible buoyant weight or negligible local curvature), it may be verified that the resulting normal forces are as anticipated. Furthermore, as described above, the PRC method uses the "2N" term for estimating the reaction forces along the entire curved segment A – B or C – D of Figure 2-1. However, based on a direct balance of the lateral forces acting on the pipe, as indicated in Figure 5-1, it may be seen that the quantity ($N_1 + N_2$) is not equal to N, but depends on the magnitude of the upper reaction force, N, and the direction and magnitude of the buoyant weight, W_S. Thus, the overall reaction forces in the curved segments will generally not be equal to the 2N term, but may be greater or less, and presumably associated with a corresponding difference in frictional drag and estimated pulling force, which is not considered.

Although the basic ASTM F1962 model inherently ignores pipe stiffness, the proposed procedure in Chapter 4 has been applied to the examples presented, including HDPE and steel pipes, with and without the use of internal (water) ballast. The net effect of the pipe stiffness, using this modified procedure, only results in a significant increase in pulling tension for the steel pipe installation, when using ballast. In contrast, the PRC method results in a corresponding increase in tension for the steel pipe, with and without the use of ballast, but

which is still relatively small compared to the total estimated load, and an extremely small increase for the HDPE pipe.

Knight et al (2003) compared various methods of estimating the pull loads, based on three sequential laboratory field installations of HDPE and MDPE (medium density polyethylene pipe), using mini-HDD (or somewhat larger "midi-HDD") equipment. Their conclusion was that the ASTM estimate is too low and the PRC too high. While their ASTM estimate was, in fact, too low for the first installation, recent calculations show that the ASTM results are actually slightly greater than the peak tensions recorded in the subsequent two installations. These field experiments are discussed in greater detail in Section 6.6, and the results are related to the additional unplanned path curvatures (corrections/undulations), and associated frictional forces, often present in typically less-controlled mini-HDD (and midi-HDD) installations, as compared to maxi-HDD. Thus, the procedure described in Chapter 6, as applicable for HDPE pipe, should be used for estimating the required pull force for such installations, instead of ASTM F1962.

Zeng et al (2013) compares the results of three methods for estimating the pull force on (steel) pipe in four major river crossings in China, for which one method is ASTM F1962. In two cases the ASTM method over-estimated the peak load, as measured at the drill rig, but underestimated the required force in two other cases. These installations were all in problematic soil conditions, with potentially unstable boreholes, which is not considered in the ASTM method. For such cases, where problems develop, the additional conservatism of the PRC method may prove useful in better estimating the actual pull forces required.

5.6 SUMMARY

Although originally developed for specific type pipe materials, the ASTM F1962 (polyethylene) and PRC (steel) general methodologies, for estimating the maximum required pulling force during a maxi-HDD operation, may be successfully applied to other type products, with the following caveats:

- The magnitude of the fluidic drag in the PRC method is a dominant factor, while only has only a very minor impact for the ASTM method. This accounts for the major quantitative difference between the two methods.
- The pipe stiffness is a basic consideration in the PRC procedure but is ignored in the original ASTM F1962 method, which considers only PE, a very flexible material. The ASTM method may, however, be supplemented to include this effect, using the procedure provided in Chapter 4.
- The contribution effect of pipe stiffness is generally only a small (possibly negligible) fraction of the total estimated tension, using either methodology.
- For installations in which the pipe has very little net buoyant weight, due to the combination of an inherently heavy pipe material (e.g., steel), possibly with internal ballast, and the upward buoyant forces of the slurry, the peak pulling force may occur prior to the end of the installation. Although ASTM F1962 determines the corresponding tensions at mid-installation, the PRC method would have to be modified accordingly.
- In cases as above (low buoyant weight), an excessively high assumed slurry density is not necessarily conservative, and a lower, more realistic, value would correspond to a

greater net buoyant weight, and correspondingly higher frictional drag and required pulling force.

- Both methods assume a reasonably well-controlled maxi-HDD operation, with a stable borehole and minimal deviations from the nominal planned borehole path. However, the significantly greater estimated force provided by the PRC method, essentially due to the high assumed fluidic drag, provides a degree of conservatism to offset a greater degree of degradation in the operation.
- Recognizing that typical mini-HDD (or midi-HDD) operations are inherently less well-controlled than a maxi-HDD operation, including deviations (path corrections/undulations) from the nominal bore path, the basic ASTM F1962 methodology has been modified (and simplified) to be applicable to such cases. **Thus, the procedure described in Chapter 6, as applicable for HDPE pipe, albeit simpler, should be used for estimating the required pull force for such installations, instead of ASTM F1962.**

CHAPTER 6
SIMPLIFIED METHOD (MINI-HDD)[15]

6.1 INTRODUCTION

The associated equations and procedures provided in ASTM F1962, for the design and implementation of a maxi-HDD operation, represent relatively complicated formulae, and a possible tedious methodology, when considering smaller, lower cost operations associated with typical mini-HDD applications. In addition, for most mini-HDD applications, such detailed analyses are not necessary or warranted since the installations are of relatively short distance and shallow depth, and typically well within the capability of the equipment and the product being installed (e.g., HDPE pipe). Furthermore, mini-HDD operations are sometimes performed on a large scale, comprising many individual installations, with no individual installation requiring or receiving extensive planning or analysis. Isolated failures are generally not a significant problem, since the low investment in the mini-HDD process allows a subsequent re-attempt, with appropriate adjustments, at minimal cost penalty.

Nonetheless, for mini-HDD installations that may be relatively critical, or at relatively long distances, or using an unusually thin-walled product, it would be valuable to have a practical, user-friendly methodology for judging the likelihood of success of the mini-HDD operation. With one important exception, the basic principles and related equations that were provided in ASTM F1962 for maxi-HDD installations have therefore been simplified and adopted to mini-HDD applications. The resulting method represents an extremely useful tool for providing a generally conservative estimate of the required pulling force.

The mentioned exception relates the issue discussed in Section 5.5 and 5.6, which is the need to account for the additional pulling force resulting the anticipated deviations (corrections/undulations) from the nominal bore path, for typical mini- (or possibly midi-) HDD operations. Thus, although a simpler procedure than ASTM F1962, it accounts for an effect not reflected in the basic ASTM method.

6.2 SIMPLIFICATION

In order to reduce the complexity of the set of Equations [2-1] for mini-HDD installations, the procedure is limited to PE pipe without the use of ballast or anti-buoyancy techniques. In this case, it may be assumed that the pulling force at the end of the installation will be the maximum, or approximately equal to the maximum, experienced during the installation. Realistic or conservative values are then assumed for several of the parameters, and a comparison of the typical magnitudes of the individual terms in the equations allow a simplification of the predicted pull force at the end of the installation, T_D. Thus, assuming frictional coefficients υ_a and υ_b are equal to 0.5 and 0.3, respectively, and pipe entry and exit angles, α and β, are 20°, it may be shown that Equation [2-1d] can be approximated by

$$T_D \approx L_{bore} \cdot w_b \cdot (1/3) \qquad [6\text{-}1]$$

[15] Ref. "Simplified Methodology for Selecting Polyethylene Pipe for Mini (or Midi) – HDD Applications", L.M. Slavin, ASCE Pipelines 2007 Conference.

This simple expression may also be obtained by multiplying the total buoyant weight, equal to $L_{bore} \cdot w_b$, by the coefficient of friction within the borehole (0.3), but amplified by the capstan effect of $e^{\nu \theta}$ at the pipe exit, as in Equation [2-3]. Using the same coefficient of friction (0.3) and the exit angle of 20° (0.35 radians), results in an amplification factor of 1.11, which multiplied by the basic 0.3 frictional coefficient results in 0.33, or the 1/3 term indicated in Equation [6-1].

6.3 ADDITIONAL LOAD AMPLIFICATION

Equation [6-1] assumes the only route bends are those at the pipe entry and exit points. However, it is also possible that there may be deliberate (planned) route bends (e.g., in the horizontal or vertical plane), to avoid known obstacles or follow a required path, which lead to further load amplification.[16] As discussed above, due to the less well-controlled nature of typical mini-HDD operations, it is also necessary to consider the load amplifications associated with the curvatures due to small unplanned corrections/deviations from the design bore path. The load T_D must therefore be modified accordingly. These effects may be conservatively estimated by again applying the exponential term in Equation [2-3], such that

$$T_D' = T_D \cdot e^{\nu_b \theta} \qquad [6\text{-}2]$$

for which the angle θ is selected as equal to the total additional route curvature, due to both of these effects. The angle θ may be conveniently expressed as:

$$\theta = n \cdot (\pi/2) \qquad [6\text{-}3]$$

where n is interpreted as the number of additional equivalent 90° route bends due to the effective additional route curvature. Considering the assumed value of υ_b of 0.3, combining Equations [6-1] to [6-3] then yields:

$$T_D' \approx [L_{bore} \cdot w_b \cdot (1/3)] \cdot (1.6)^n \qquad [6\text{-}4]$$

Inherent in the approximations leading to the above simplified formulae is the absence of the depth of the route, H. The net effect of this parameter is relatively minor, consistent with the corresponding terms in Equations [2-1b] and [2-1d], with opposite signs (+ –), essentially canceling the net effect of this physical characteristic, especially for typical bore paths where the overall length greatly exceeds the depth.

6.31 Additional Path Curvature

The value of n, the equivalent number of additional 90° route bends, may be expressed as:

$$n = n_1 + n_2 \qquad [6\text{-}5]$$

where n_1 is the effective number of additional planned (90°) route bends, and n_2 is the cumulative curvature due to the unplanned path corrections/deviations. Figure 6-1 shows a deliberate horizontal (planar) bend of 45° to the right, in order to avoid an obstacle or follow a utility right-of-way, followed by another 45° horizontal bend to the left. In this example, each 45° bend is equal to half of a 90° bend, corresponding to a total of ½ + ½ = 1 equivalent 90° bend, such that $n_1 = 1$.

[16] Additional (planned) route bends may also be incorporated into a maxi-HDD installation, but are considered to be less likely than for the mini-HDD operation, and are not reflected in Equations [2-1].

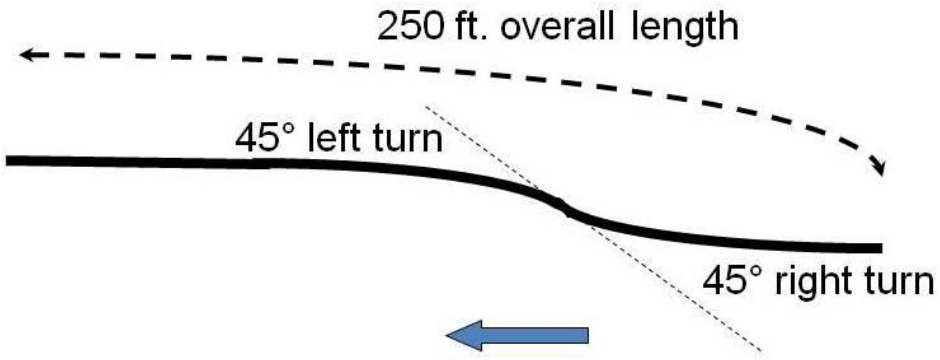

Figure 6-1. Deliberate/Planned Path Curvature

It is considerably more difficult to determine or estimate the value of the cumulative unplanned curvature, n_2, since this will vary with soil conditions, expertise of the crew, and equipment. However, in the absence other specific information, the following guideline may be used to provide a reasonable estimate of the general magnitude of the corresponding curvature of actual installed paths:

$$n_2 \approx L_{bore}\,(\text{ft}) / 500\ \text{ft.} \qquad [6\text{-}6]$$

Thus, each 500 ft of path length may result in the equivalent curvature of one 90° bend, due to path corrections, although significant variability may be anticipated, as noted. The estimate of the unplanned path curvature in Equation [6-6] is based on sample mini-HDD operations using steel drill rods of approximately 2-in. diameter.[17] Larger diameter drill rods are less flexible and would result in more gradual path deviations and corrections, and a correspondingly reduced level of path undulations. Therefore, a reduced value of n_2 should be used when applying the above procedure to a midi-HDD operation, using larger diameter rods, for which the following estimate is suggested:

$$n_2 \approx [L_{bore}\,(\text{ft}) / 500\ \text{ft.}] \cdot [2\text{-in} / \text{rod diameter (in)}] \qquad [6\text{-}7]$$

For example, a 4-in. diameter drill rod would correspond to one 90° bend every 1,000 ft. Equation [6-7] may also be applied to smaller size rods, resulting in a greater estimate of this curvature.

The general estimate in Equation [6-7] is likely conservative since the rod stiffness is disproportionally dependent on the diameter, even considering presumably greater applied bending forces, but is convenient, and consistent with an equivalent bending stress level in the steel rods. Although, in principle, this same phenomenon may be extrapolated to maxi-HDD, using corresponding larger diameter drill rods, it is considered excessively conservative, especially for such well-planned, well-controlled operations.

6.4 BUOYANT WEIGHT

The effective buoyant weight, w_b, in Equation [6-4], may be determined by the formulae in ASTM F1962 under various conditions, including empty, filled with water, or filled with drilling

[17] See DitchWitch Model 4/40A Jet Trac® Boring System Operator's Manual (1993) and DitchWitch 8/60 Jet Trac® Boring System Operator's Manual (1993), which consider drill rods of 1.75-in. and 2.25-in. diameter, respectively.

fluid. For the present simplified method, it is assumed that ballast is not employed, and the buoyant weight for the empty pipe is conservatively based on the specific gravity of the drilling fluid/slurry of 1.5. In this case, the (submerged) buoyant weight may be conveniently estimated by the following formula based on the actual outer diameter, D, and the weight of the empty pipe, w_a:

$$w_b \text{ (lbs/ft)} = 0.5 \cdot D^2 - w_a \text{ (lbs/ft)} \qquad [6\text{-}8]$$

The weight of the empty pipe may be obtained from the manufacturer specifications, depending on the nominal size and DR rating. Alternatively, Figure 6-2 provides the approximate buoyant weight for pipes of various IPS or DIPS sizes, representing an average for the two systems, using the nominal pipe size.

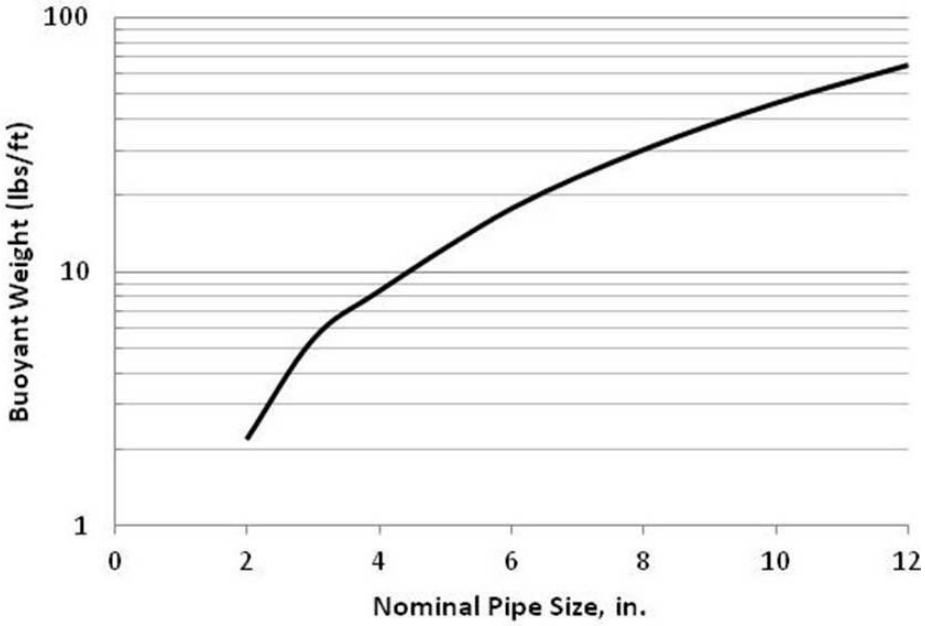

Figure 6-2. Approximate Buoyant Weight

6.5 IMPLEMENTATION

The estimated peak tension, T_D', during a mini- (or midi-) HDD installation may now be calculated and compared to the safe pull strength for the pipe. Table 6-1 shows safe pull strengths for HDPE for a variety of pipe sizes, again representing an average for the IPS and DIPS systems. These values are based on a safe pull stress of 1,400 lbs/in^2 for the PE4710 material, corresponding to a minimum tensile yield strength of 3,500 lbs/in^2 (80^{o}F) and a factor of 0.4 to limit non-recoverable viscoelastic deformation, at an assumed effective load duration of

one hour. These values also reflect a 6% typical oversize in the pipe wall thickness due to manufacturing tolerances.[18]

Table 6-1 Safe Pull Tension (lbs), HDPE (PE4710) Pipe, 1 hour

Nominal Size	Pipe Diameter to Thickness Ratio (DR)				
	7	**9**	**11**	**13.5**	**17**
2-in.	3,220	2,597			
3-in.	7,973	6,431			
4-in.	12,357	9,967	8,340	6,921	5,587
6-in.	26,118	21,066	17,628	14,629	11,809
8-in.	44,612	35,983	30,110	24,988	20,170
10-in.	68,154	54,972	45,999	38,175	30,815
12-in.	96,136	77,541	64,885	53,848	43,466

For a given nominal pipe size, the diameter of the DIPS pipe is somewhat larger than that of the IPS pipe, corresponding to greater pipe strength, but also greater buoyant weight. Thus, the use of the (average) buoyant weight in Figure 6-2 is consistent with the (average) pull strengths in Table 6-1. The use of Equation [6-8] to determine the buoyant weight, in combination with the strengths in Table 6-1, is somewhat more conservative for the DIPS size pipes and somewhat less conservative for the IPS size pipes, sizes, but is not considered significant relative to the potential variability in the pulling forces experienced in an actual installation.

6.6 COMPARISON TO FIELD DATA

The indication of the pull force imposed on the pipe during an HDD operation is sometimes deduced from information monitored at the drill rig (hydraulic pressure, ...). These loads, however, also reflect that required to overcome the drag forces on the drill string in the ground, and by the back-reamer to expand or maintain the borehole. In general, therefore, it is only that drill rig information observed at the end of the installation that may represent that the pulling force on the pipe itself, which may, or may not, be the maximum experienced. Fortunately, appropriate data that directly monitors the pull force at the leading end of the pipe does exist, based on actual field installations or related research projects.

One of the installations (Finnsson, 2004) represented a field trial of a previously commercially available product (TensiTrak™) for monitoring tension and drilling fluid pressure

[18] The MAB-7 guidelines (Plastics Pipe Institute, 2020) provide separate values for the IPS and DIPS pipes, without the 6% oversize factor.

at the leading end of the pipe.[19] A 6-in. DR 11 HDPE pipe, weighing 4.7 lbs/ft, was installed in a nominally straight, 460 ft. route ($n_1 = 0$), for which the force vs. installed length was recorded, with a generally monotonically increasing tension reaching approximately 3500 lbs at the completion of the installation. It is noted that this installation employed a *midi*-HDD rig, with 15 ft. long, 3.5-in. diameter drill rods, for which Equation [6-7] is used to estimate the unintended path curvature, n_2. The following values therefore apply:

L_{bore} = 460 ft.

D = 6.625-in. (IPS)

w_a = 4.9 lbs/ft

n_1 = 0

n_2 = [L_{bore} (ft) / 500 ft.] · [2-in / rod diameter (in)]
= [460 ft / 500 ft] · [2-in / 3.5-in]
= 0.53

$n = n_1 + n_2$
= 0.53

$w_b = 0.5 \cdot D^2 - w_a$ (lbs/ft)
= $0.5 \cdot (6.625)^2 - 4.9$ (lbs/ft)
= 17.0 lbs/ft

Thus, Equation [6-4] estimates a peak pull load of

$T_D' = [L_{bore} \cdot w_b \cdot (1/3)] \cdot (1.6)^n$
= $[460 \text{ ft} \cdot 17.0 \text{ lbs/ft} \cdot (1/3)] \cdot (1.6)^{0.53}$
= 3344 lbs

This estimate is remarkably close to the 3500 lbs measured load, and is admittedly fortuitous, considering the complicated process and uncertainties in the effective drag loads[20], as well as the variability in the gauge readings. Nonetheless, ignoring the unintentional curvature (i.e., assuming $n_2 = 0$) would result in an estimated tension of less than 2606 lbs – significantly less than that recorded, confirming the need to consider this phenomenon.

An important research project comprised three mini-HDD installations for which a 6-in. DR 11 MDPE pipe was installed twice in the same borehole, followed by an 8-in. DR 17 HDPE pipe (Knight et al, 2002); see Section 5.5. The borehole was a nominally straight 590 ft path, to a depth of 6.5 ft, with entry and exit angles of approximately 11°, and was pre-reamed as necessary to approximately 50% greater than the outer diameter of the pipe. The drill rods are assumed to be 2-in. diameter, typical for a mini-HDD rig. In general, the peak tensions were experienced prior to the end of the operations, corresponding to approximately 5620 lbs, 3370 lbs, and 5845 lbs, in the sequence described. The corresponding estimated loads, using the present methodology, are 5813, 5813, and 10,494 lbs, in that order.

[19] This product is no longer commercially available.

[20] It is recognized that the force gauge would also reflect that additional resistance at the pulling head resulting from the hydrokinetic pressure acting on the cross-sectional area. The observed pressure in this case was generally in the range of 6 – 8 psi, somewhat less than the 10 psi level assumed in Section 2.24, and corresponding to an incremental load of a few hundred pounds. Thus, the pipe itself would be subject to a pulling force somewhat less than the 3,500 lbs recorded, but again remarkably close to the estimated load.

Figure 6-3 illustrates the results for the four installations, with the actual and calculated peak tensions normalized relative to the estimated tension. The figure also shows the estimates if the unintentional curvature is ignored. Although only a limited sample, several interesting, albeit tentative, conclusions may be drawn. In general, it is necessary to consider the likelihood that there will in fact be additional route curvature, due to less than precise control in the less sophisticated mini- (or midi-) HDD process. This consideration, in combination with the conservatively high assumed value for the buoyant weight – e.g., Equation [6-8], provides a reasonable estimate of the maximum pulling force, allowing for various imperfections in the overall process. However, it is also possible that such conservatism is not always necessary, as illustrated in the last two installations of the research project (i.e., $n_2 = 0$). The reduced tension in these cases is apparently due to the improved conditions in the borehole as a result of the subsequent reuse of the same borehole, including a likely reduction in the path undulations, as the reamer makes additional passes through the original borehole.

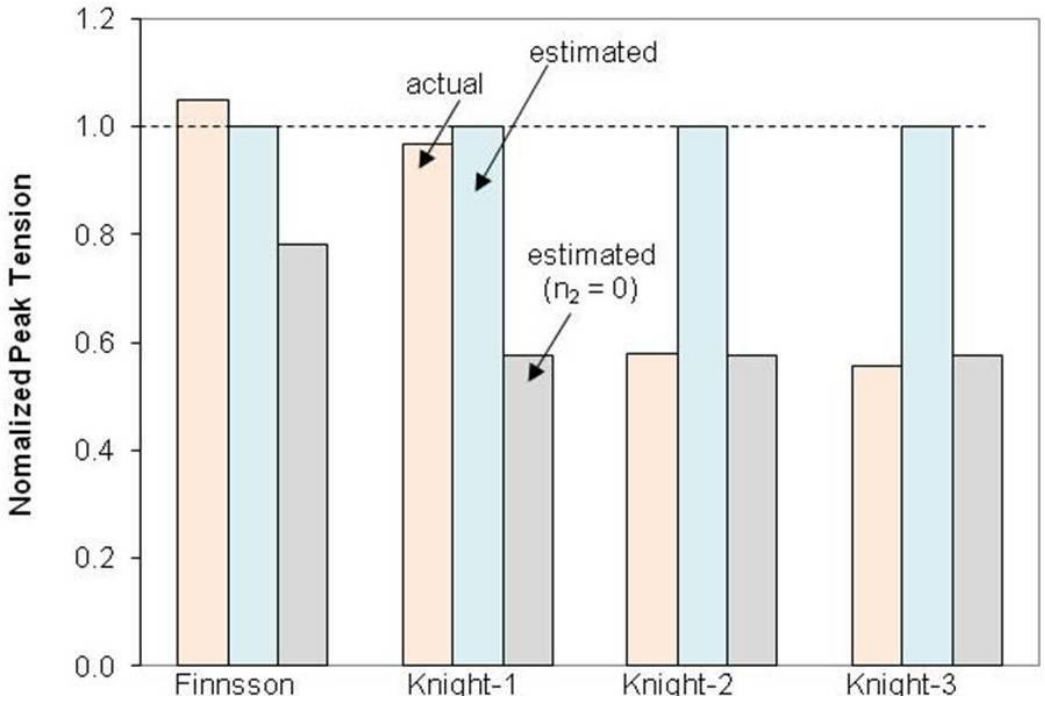

Figure 6-3. Actual vs. Estimated (Normalized) Peak Tension

6.7 SUMMARY

The basic Equations [2-1] that are applicable to a carefully engineered, well-controlled maxi-HDD operation would be relatively complicated for use in typical mini- (or midi-) HDD installations. These equations have therefore been modified for use in such cases, corresponding to Equation [6-4]. Furthermore, this simplified methodology is also more appropriate for these less-well controlled applications, as a result of path corrections and associated unplanned path curvatures, increasing the required pulling force on the pipe. **In general, therefore, this procedure should be used for these applications, rather than ASTM F1962, which does not account for this additional effect.** The validity of the proposed procedure is confirmed by application to several field installations.

CHAPTER 7
NON-LEVEL GRADE – WITHOUT BALLAST[21]

7.1 INTRODUCTION

The basic ASTM F1962 procedure for calculating the required pulling force on the pipe, including Equations [2-1], are based on the route geometry illustrated in Figure 7-1, which shows a level terrain. In principle, the formulae are also valid for non-level terrain, providing the pipe entry and exit points are at the same elevation. Nonetheless, it is not uncommon that significantly different elevations will occur in practical applications, especially over the long distance characteristic of many maxi-HDD installations. This effect is significant since the largest source of drag on the pipe is the frictional drag associated with the buoyant weight of the polyethylene pipe, with or without ballast. The buoyancy also tends to pull the pipe upwards, opposite gravity, along sloped portions of the bore path. The phenomena is complicated by the possible deployment of anti-buoyancy techniques, including (water) ballast added to the pipe interior, which application is discussed in Chapter 8.

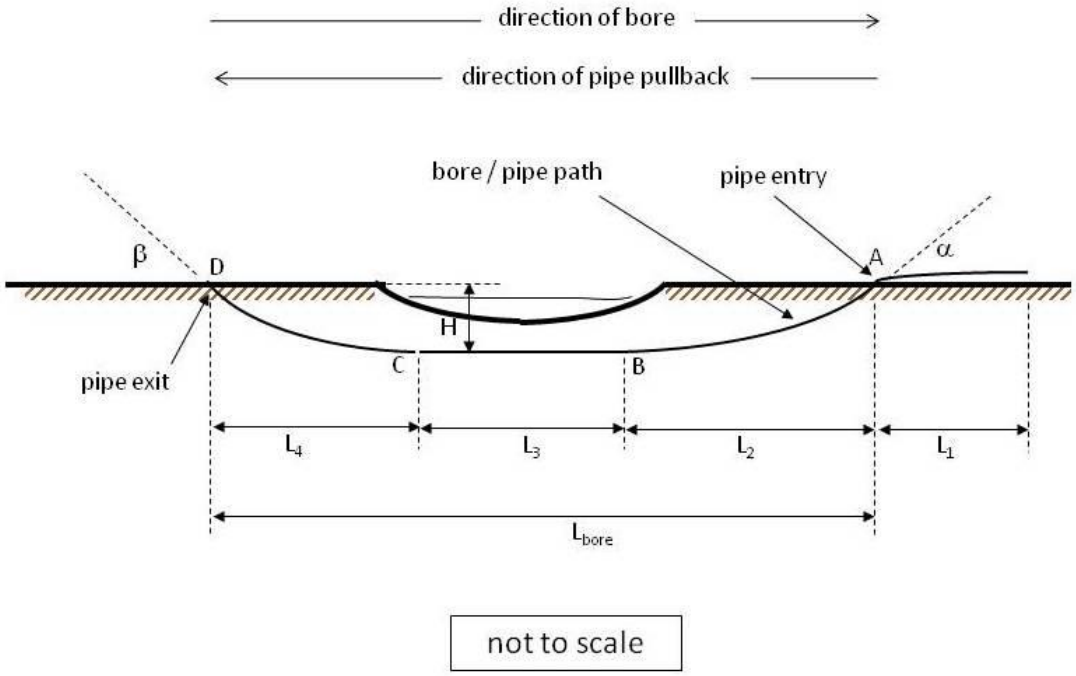

Figure 7-1. Maxi-HDD Pullback with Level Grade
(Courtesy of Outside Plant Consulting Services, Inc.)

[21] Ref. "Maxi-HDD Pull Loads for Nonlevel Grade for Polyethylene Pipe", Slavin, Najafi, and Skonberg, ASCE Journal of Pipeline Systems Engineering and Practice, May 2011 and "Maxi-HDD Pull Loads for Entry and Exit Points at Different Elevations", Slavin and Najafi, ASCE Journal of Pipeline Systems Engineering and Practice, August 2015.

7.2 GEOMETRY A

In contrast to Figure 7-1, Figure 7-2, illustrates one type of configuration, designated as Geometry A, for which the pipe entry and exit points, A and D, respectively, are at different elevations, with the pipe being pulled in a generally upward direction, towards point D. In this bore path, segment B – C remains horizontal, and H_1 and H_2 represent the vertical depth of this segment below point A and point D, respectively. For pipe entry path (A – B) and exit path (C – D), each of approximately uniform curvature, the lengths L_2 and L_4 in Figure 7-2 may be estimated as:

$$L_2 = 2H_1 / \alpha \qquad [7\text{-}1a]$$

and

$$L_4 = 2H_2 / \beta \qquad [7\text{-}1b]$$

for which the pipe entry and exit angles, α and β, respectively, are still considered to be measured relative to a horizontal plane, similar to the orientation of horizontal segment (C – D), with an additional angle ϕ representing the local slope of the surface at point A. The local angle ϕ is considered positive (+) as shown, and is not necessarily equal to the average grade between points A and D, as given by Equation [7-2]:

$$\text{Average \% Grade} = 100 \times (H_2 - H_1) / L_{bore} \qquad [7\text{-}2]$$

where it is assumed that H_1 is a minimum depth, with H_2 accordingly greater.

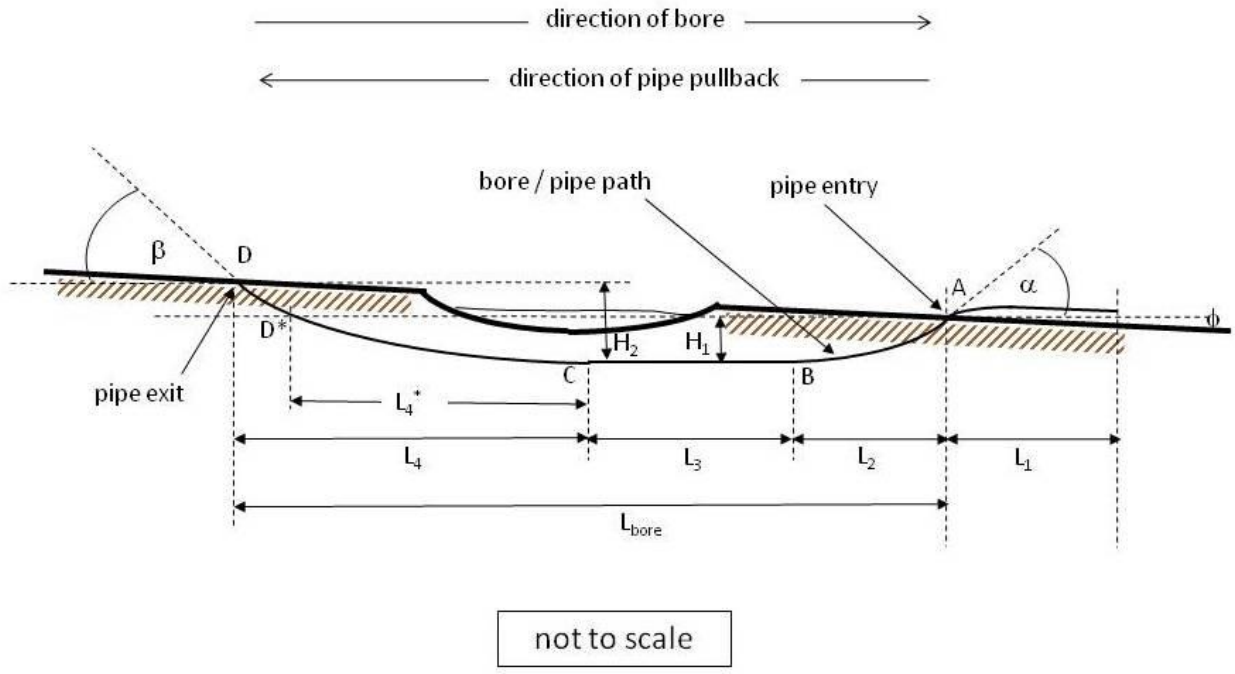

Figure 7-2. Maxi-HDD Pipe Pullback with Upward Grade – Geometry A (Courtesy of Outside Plant Consulting Services, Inc.)

The length L_4* corresponds to the (projected) distance between point C and D*, where D* represents the point at the same elevation as point A, and above which the slurry would not be expected to fill the borehole as it drains from point A, and may be estimated by:

$$L_4^* = L_4 \cdot [1 - (\Delta H / H_2)]^{½} \qquad [7\text{-}3]$$

where $\Delta H = H_2 - H_1$.

7.21 Upward Grade

Analogous to Equations [2-1] for determining the pulling forces T_A , T_B , T_C , or T_D , for a level terrain, Equations [7-4] are appropriate for an upward installation:

$$T_A = e^{\nu_a(\alpha+\phi)} \cdot (\nu_a + \phi) \cdot w_a \cdot (L_1 + L_2 + L_3 + L_4)` \qquad [7\text{-}4a]$$

$$T_B = e^{\nu_b \alpha} \cdot (T_A + \nu_b \cdot w_b \cdot L_2 + w_b \cdot \mathbf{H_1} - (\nu_a + \phi) \cdot w_a \cdot L_2 \cdot e^{\nu_a(\alpha+\phi)}) \qquad [7\text{-}4b]$$

$$T_C = T_B + \nu_b \cdot w_b \cdot L_3 - e^{\nu_b \alpha} \cdot [(\nu_a + \phi) \cdot w_a \cdot L_3 \cdot e^{\nu_a(\alpha+\phi)}] \qquad [7\text{-}4c]$$

$$T_D = e^{\nu_b \beta} \cdot (T_C + \nu_b \cdot w_b \cdot \mathbf{L_4^* + \nu_b \cdot w_a \cdot (L_4 - L_4^*)} - w_b \cdot \mathbf{H_1} + \mathbf{w_a \cdot \Delta H_2} - e^{\nu_b \alpha} \cdot [(\nu_a + \phi) \cdot w_a \cdot L_4 \cdot e^{\nu_a(\alpha+\phi)}]) \qquad [7\text{-}4d]$$

The extension of Equations [2-1] to Equations [7-4] is based on a low average grade and local angle ϕ.

The additional terms introduced into Equations [7-4] have been highlighted to emphasize the difference relative to the original basic Equations [2-1]. The incremental tension, ΔT, must again be added to each of these terms (T_A, T_B, T_C, or T_D) to account for the fluidic drag component, which also applies to the other estimates provided in this chapter.

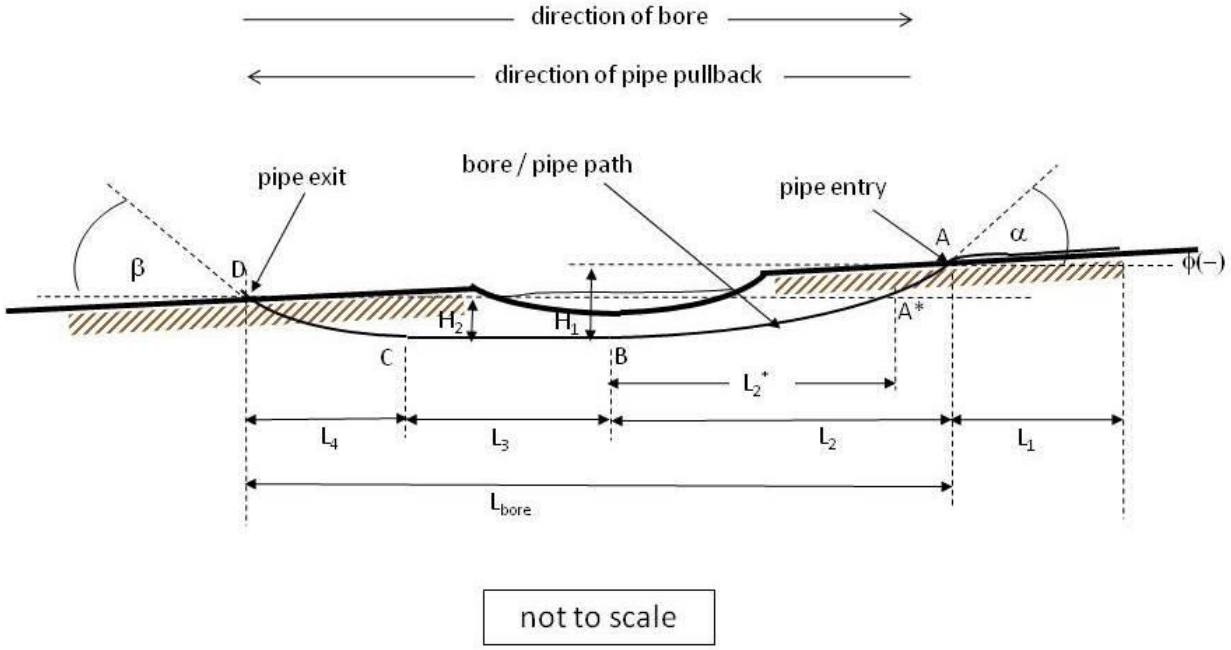

Figure 7-3. Maxi-HDD Pipe Pullback with Downward Grade – Geometry A (Courtesy of Outside Plant Consulting Services, Inc.)

7.22 Downward Grade

For a downward grade, as illustrated in Figure 7-3, the relevant equations are now:

$$T_A = e^{\nu_a(\alpha+\phi)} \cdot (\nu_a + \phi) \cdot w_a \cdot (L_1 + L_2 + L_3 + L_4) \quad [7\text{-}5a]$$

$$T_B = e^{\nu_b \alpha} \cdot (T_A + \nu_b \cdot w_b \cdot \mathbf{L_2^*} + \mathbf{\nu_b \cdot w_a\ [L_2 - L_2^*]} + w_b \cdot \mathbf{H_2} + \mathbf{w_a \cdot \Delta H} - (\nu_a + \phi) \cdot w_a \cdot L_2 \cdot e^{\nu_a(\alpha+\phi)}) \quad [7\text{-}5b]$$

$$T_C = T_B + \nu_b \cdot w_b \cdot L_3 - e^{\nu b\,\alpha} \cdot [(\nu_a + \phi) \cdot w_a \cdot L_3 \cdot e^{\nu_a(\alpha+\phi)}] \quad [7\text{-}5c]$$

$$T_D = e^{\nu_b \beta} \cdot (T_C + \nu_b \cdot w_b \cdot L_4 - w_b \cdot \mathbf{H_2} - e^{\nu_b \alpha} \cdot [(\nu_a + \phi) \cdot w_a \cdot L_4 \cdot e^{\nu_a(\alpha+\phi)}]) \quad [7\text{-}5d]$$

The length L_2^* corresponds to the (projected) distance between point B and A*, where A* represents the point at the same elevation as point D, and above which the slurry would not be expected to fill the borehole as it drains from point D, for which:

$$L_2^* = L_2 \cdot [1 + (\Delta H / H_1)]^{1/2} \quad [7\text{-}6]$$

recognizing that $\Delta H = H_2 - H_1$ is negative, and H_2 is a minimum depth, with H_1 accordingly greater.

The equations, as written, are valid for $(\nu_a + \phi) \geq 0$, or $-\phi \leq \nu_a$, for which it is noted that the local grade angle ϕ, as indicated in Figure 7-3 is considered to be negative (–), consistent with its opposite sense relative to Figure 7-2. For $(\nu_a + \phi) \leq 0$, Equation [7-5a] implies the pipe will be in compression entering (and leaving) the pipe point. If it may be assumed that the pipe can withstand the compression, Equations [7-4] may extended to the more general case by replacing the exponential term $e^{\nu_a(\alpha+\phi)}$ by the term $e^{\nu_a(\alpha+\phi)\cdot \mathrm{SIGN}(\nu_a+\phi)}$ in Equations [7 5a] through [7-5d].

7.3 GEOMETRY B

Figures 7-4 and 7-5 show an alternate configuration for which the intermediate segment B – C is oriented at the average grade angle between points A and D, designated as Ω, which is considered positive (+) for an uphill installation, and is again assumed to be low (<< 1 radian), to allow convenient approximations. This configuration is designated as Geometry B. The segment B – C is located at the uniform distance, or depth, H from the average grade line A – D. Geometry B may then be considered as a simple rotation of the basic (level grade) geometry illustrated in Figure 7-1. This geometry may be considered to be more practical than that of Geometry A, especially for large grades and correspondingly large depths at the uphill end of the bore, and also avoids possible geometric inconsistencies at large grades and relatively shallow depths.

In this case, it is convenient to define the entry and exit angles (α' and β', respectively) relative to the average grade line, similar to the orientation of inclined segment B – C, and for which $\alpha' = \alpha + \Omega$, and $\beta' = \beta - \Omega$. Furthermore, the angle ϕ' shown in Figure 7-4 now represents the incremental slope relative to the basic slope Ω, as opposed to the total local slope ϕ shown in Figure 7-2.

Similar to Equations [7-1], for pipe entry and exit paths of uniform curvature, the lengths L_2 and L_4 may be estimated as:

$$L_2 = 2H / \alpha' \qquad [7\text{-}6a]$$

and

$$L_4 = 2H / \beta' \qquad [7\text{-}6b]$$

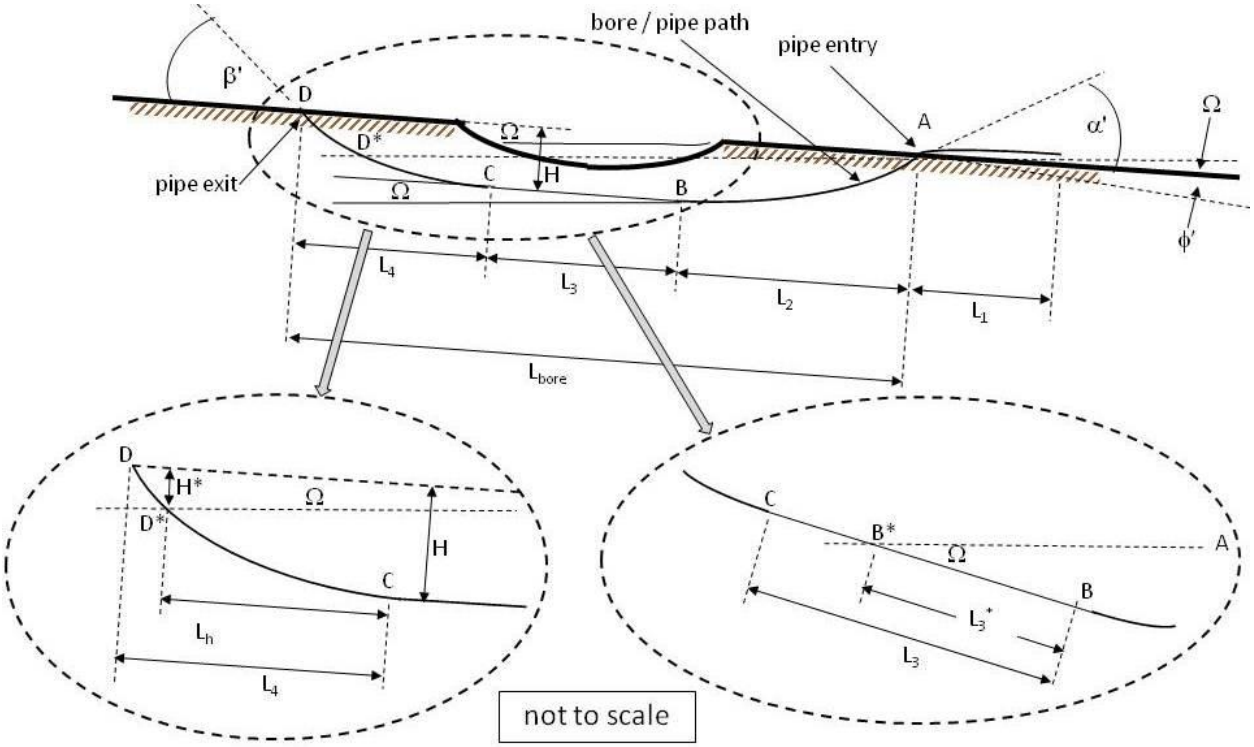

Figure 7-4. Maxi-HDD Pipe Pullback with Upward Grade – Geometry B (Courtesy of Outside Plant Consulting Services, Inc.)

The points D* or B*, located at distance L_3* or L_4* from points C or B, respectively, again correspond to the point at the same elevation as point A, and above which the slurry would not be expected to fill the borehole as it drains from point A. Whether this point occurs within segment C – D or B – C will depend upon the overall configuration, including the magnitude of the grade angle, Ω. For relatively shallow grade angles, the point of interest (D*) will fall within segment C – D, while for large grades the point (B*) would lie within the segment B – C. .It is assumed, however, that the grade angle is not sufficiently large such that the drainage point could fall within the segment A – B, which would imply that the grade angle Ω, exceeds half the entry angle. In such cases, the equations below would have to be further extended, and is beyond the scope of the present analysis. For the present analysis, it is therefore assumed that $\Omega \leq \alpha'/2$.

The generalized relationships for the distances L_3* or L_4*, for use in subsequent equations [7-9], may be expressed by:

$$L_3^* = \text{MIN}\{([H/\Omega) - L_2], L_3\} \qquad [7\text{-}7a]$$

and

$$L_4^* = L_4 \cdot [1 - (H^*/H)]^{1/2} \qquad [7\text{-}7b]$$

The term H* represents the depth at the point D* or B*, and may be shown to be approximately given by the following expressions, depending upon the grade angle Ω:

$$\begin{aligned} H^* = {} & (\theta^2/2)\cdot\{[(2/\Omega)\cdot(L_2 + L_3) - (L_4^2/H)] \\ & + ([(2/\Omega)\cdot(L_2 + L_3) - (L_4^2/H)]^2 - (4/\Omega^2)\cdot\mathbf{[}(L_2 + L_3)^2 - L_4^2])^{1/2}\} \\ & \qquad \text{for } \Omega \le H/(L_2 + L_3) \\ = {} & H \qquad \text{for } \Omega > H/(L_2 + L_3) \end{aligned} \qquad [7\text{-}8]$$

Since the entire segment B – C is at a depth of H, the depth H* at point B* would also be equal to H, and is consistent with the above condition.

7.31 Upward Grade

Equations [7-9] are applicable to Geometry B, for an upward installation, for determining tensions T_A , T_B , T_C , or T_D:

$$T_A = e^{\nu_a(\alpha' + \varphi')} \cdot (\nu_a + \mathbf{\Omega} + \phi') \cdot w_a \cdot (L_1 + L_2 + L_3 + L_4)` \qquad [7\text{-}9a]$$

$$T_B = e^{\nu_b \alpha'} \cdot (T_A + \nu_b \cdot w_b \cdot L_2 + w_b \cdot (H - \mathbf{L_2\cdot\Omega}) - (\nu_a + \mathbf{\Omega} + \phi') \cdot w_a \cdot L_2 \cdot e^{\nu_a(\alpha' + \phi')} \qquad [7\text{-}9b]$$

$$\begin{aligned} T_C = {} & T_B + \nu_b \cdot w_b \cdot \mathbf{L_3^*} + \mathbf{\nu_b \cdot w_a \cdot (L_3 - L_3^*) - \Omega \cdot [w_b \cdot L_3^* - w_a \cdot (L_3 - L_3^*)]} \\ & - e^{\nu_b \alpha'} \cdot (\nu_a + \mathbf{\Omega} + \phi') \cdot w_a \cdot L_3 \cdot e^{\nu_a(\alpha' + \varphi')}] \end{aligned} \qquad [7\text{-}9c]$$

$$\begin{aligned} T_D = {} & e^{\nu_b \beta'} \cdot (T_C + \nu_b \cdot w_b \cdot \mathbf{L_4^* + \nu_b \cdot w_a (L_4 - L_4^*)} \cdot - w_b \cdot (H \mathbf{- H^* + L_4^* \cdot \Omega}) \\ & + \mathbf{w_a \cdot [H^* + (L_4 - L_4^*)\,\Omega]} - e^{\nu_b \alpha'} \cdot [(\nu_a + \mathbf{\Omega} + \phi') \cdot w_a \cdot L_4 \cdot e^{\nu_a(\alpha' + \varphi')}]) \end{aligned} \qquad [7\text{-}9d]$$

The greater complexity of Equations [7-9], compared to Equations [7-4] for Geometry A, is the result of geometric and logical considerations, as illustrated in Figure 7-4, due to the possible location of the drainage point, A.

7.32 Downward Grade

For the downward installation shown in Figure 7-5, the following equations result:

$$T_A = e^{\nu_a(\alpha' + \varphi')} \cdot (\nu_a + \mathbf{\Omega} + \phi') \cdot w_a \cdot (L_1 + L_2 + L_3 + L_4)` \qquad [7\text{-}10a]$$

$$\begin{aligned} T_B = {} & e^{\nu_b \alpha'} \cdot (T_A + \nu_b \cdot w_b \cdot \mathbf{L_2^* + \nu_b \cdot w_a \cdot (L_2 - L_2^*) + w_b \cdot (H - H^{**} - L_2^* \cdot \Omega)} \\ & \mathbf{- w_a \cdot [H^{**} - (L_2 - L_2^*)\,\Omega]} - (\nu_a + \mathbf{\Omega} + \phi') \cdot w_a \cdot L_2 \cdot e^{\nu_a(\alpha' + \phi')} \end{aligned} \qquad [7\text{-}10b]$$

$$\begin{aligned} T_C = {} & T_B + \nu_b \cdot w_b \cdot \mathbf{L_3^{**}} + \mathbf{\nu_b \cdot w_a \cdot (L_3 - L_3^{**}) - \Omega \cdot [w_b \cdot L_3^{**} - w_a \cdot (L_3 - L_3^{**})]} \\ & - e^{\nu_b \alpha'} \cdot (\nu_a + \mathbf{\Omega} + \phi') \cdot w_a \cdot L_3 \cdot e^{\nu_a(\alpha' + \varphi')}] \end{aligned} \qquad [7\text{-}10c]$$

$$\begin{aligned} T_D = {} & e^{\nu_b \beta'} \cdot (T_C + \nu_b \cdot w_b \cdot L_4 - w_b \cdot (H \mathbf{+ L_4\cdot\Omega}) \\ & - e^{\nu_b \alpha'} \cdot [(\nu_a + \mathbf{\Omega} + \phi') \cdot w_a \cdot L_4 \cdot e^{\nu_a(\alpha' + \varphi')}]) \end{aligned} \qquad [7\text{-}10d]$$

where again $\alpha' = \alpha + \Omega$, and $\beta' = \beta - \Omega$, and Ω is understood to be negative (–) for the downhill installation, and ϕ' represents any local (negative) incremental slope at entry, in addition to that of the average grade Ω. The equations, as written, are valid for $(\nu_a + \Omega + \phi') \ge 0$, recognizing that the term $(\Omega + \phi')$ is negative, as indicated in Figure 7-5.

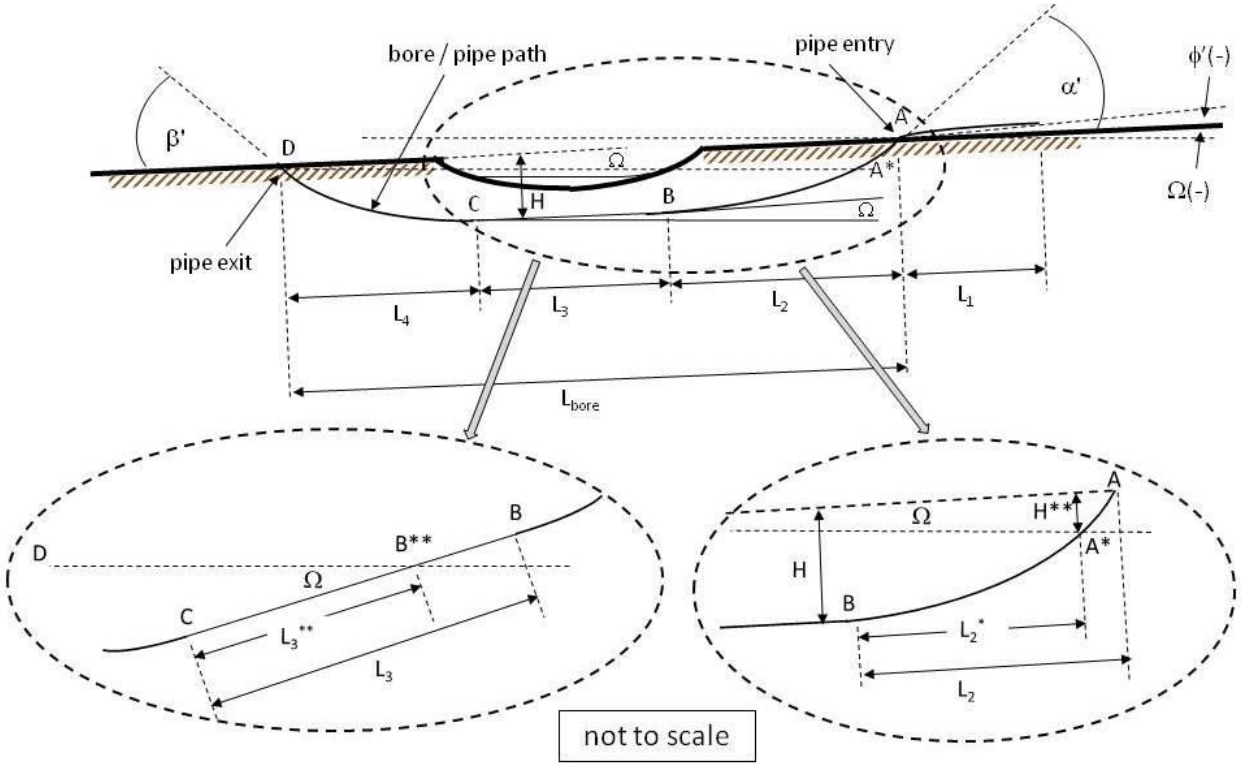

Figure 7-5. Maxi-HDD Pipe Pullback with Downward Grade – Geometry B
(Courtesy of Outside Plant Consulting Services, Inc.)

The distances L_2* and L_3**, as indicated in Figure 7-5, relate to the point A* or B**, respectively, analogous to those for the upward installation, and for which:

$$L_3^{**} = \text{MIN}\{[(H/|\Omega|) - L_4], L_3\} \quad [7\text{-}11a]$$

and

$$L_2^{*} = L_2 \cdot [1 - (H^{**}/H)]^{½} \quad [7\text{-}11b]$$

In this case, the term H** represents the depth at the point A* or B**, and may be shown to be approximately given by the following expressions, as a function of the grade angle, Ω:

and

$$\begin{aligned} H^* = {} & (\theta^2/2)\cdot\{[(2/|\Omega|)\cdot(L_3 + L_4) - (L_2^2/H)] \\ & + ([(2/|\Omega|)\cdot(L_3 + L_4) - (L_2^2/H)]^2 - (4/\Omega^2)\cdot[(L_3 + L_4)^2 - L_2^2])^{½}\} \\ & \qquad \text{for } |\Omega| \le H/(L_3 + L_4) \\ = {} & H \qquad \text{for } |\Omega| > H/(L_3 + L_4) \end{aligned} \quad [7\text{-}12]$$

Analogous to the upward grade, it is assumed that the magnitude of the grade angle is not sufficiently large such that the drainage point could fall within the segment C – D, which would imply that |Ω| exceeds half the exit angle. It is therefore assumed that $|\Omega| \le \beta'/2$.

Table 7-1 Borehole and Installation Parameters

Parameter	Value	Remarks
bore length, L_{bore}	2,500 ft	
L_1	125 ft	= 5% L_{bore}
pipe entry angle, α'	15°	0.262 radians to average grade
pipe exit angle, β'	15°	0.262 radians to average grade
Geometry A		**Figures 7-2 and 7-3**
H_1	45 ft – 295 ft	upward or downward grade
H_2	295 ft – 45 ft	upward or downward grade
minimum depth	45 ft	
average grade	± (0% to 10%)	= (H_2 – H_1) / L_{bore}
local grade, ϕ	± (0% to 10%)	= average grade
L_2	342 ft – 1614 ft	uniform curvature
L_4	1614 ft – 342 ft	uniform curvature
Geometry B		**Figures 7-4 and 7-5**
average grade, Ω	± (0% to 10%)	= ± maximum 0.10 radians (5.71°)
incremental grade, ϕ’	0%	local grade = average grade
depth, H	45 ft	uniform nominal depth
L_2	342 ft	uniform curvature
L_4	342 ft	uniform curvature
D	24.0 in.	pipe outer diameter
DR	11	2.182-in. wall thickness
D_{hole}/D	36.0 in.	50% clearance
ΔP	10 psi	incremental pressure
ΔT	2,827 lbs	= $\Delta P \cdot (\pi/8) \cdot (D_{hole}^2 - D^2)$
γ_a	0.955	HDPE
γ_b	1.2	realistic
γ_c	1.0	water ballast
w_a	61.9 lbs/ft	unsubmerged pipe weight (empty)
w_b	173.4 lbs/ft	submerged buoyant weight (without ballast)
ν_a	0.10	rollers
ν_b	0.30	within borehole

7.4 RESULTS

Table 7-1 shows the assumed values of the relevant parameters, which are generally consistent with those of the examples in previous chapters. For the present purposes, the entry and exit angles relative to the average grade, α' and β', are maintained at the fixed values indicated, independent of the magnitude of the grade itself. The magnitudes of the entry and exit angles relative to horizontal, α and β, therefore vary with the magnitude of the average grade angle. The value for the coefficient of friction within the entire length of the borehole is again at the 0.30 value, assuming the lubricating characteristics are essentially the same for the drained section.

Figure 7-6 shows the results for the tension at the end of the installation, including both upward and downward installations. (The incremental tension ΔT due to the fluidic drag is included in the results) Several interesting observations may be made regarding the required pulling force, as applicable to an installation in a non-level grade, without the use of ballast:

- An upward OR downward installation results in a lower required pulling load than that corresponding to a level grade;
- A downward installation is preferable;
- The bore path geometry will have a significant effect on the magnitude of the load reduction.

These conclusions are consistent with the reduced portions of the bore path for which the pipe is fully submerged, due to the drainage of the slurry from the borehole for a non-level grade, as well as the beneficial effect of gravity for a downward installation. The use of internal ballast, however, has a major impact on the phenomena and the related conclusions, as discussed in Chapter 8.

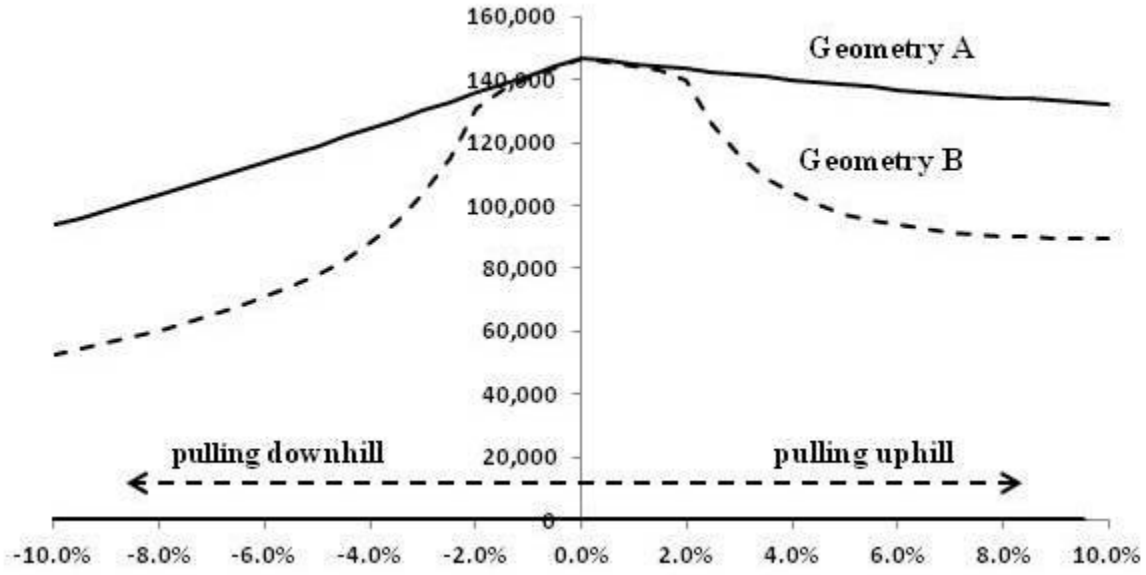

Figure 7-6. Tension vs. Average Grade, without Ballast (45 ft Minimum Depth)

CHAPTER 8
NON-LEVEL GRADE – WITH BALLAST[22]

8.1 INTRODUCTION

The analysis and results in Chapter 7 illustrate the significant effect of a non-level grade on the estimated pulling force for a maxi-HDD installation. These results only considered applications without the use of anti-buoyancy techniques. However, the use of internal liquid ballast is routinely employed during the installation of HDPE pipes in long bores for the purpose of reducing the buoyant weight and corresponding frictional drag, thereby maintaining the pull forces within acceptable levels. It is therefore of interest to investigate the potential magnitude of the required forces when employing ballast in installations with a non-level grade.

Although it is possible to allow the drilling slurry to enter the pipe and provide efficient ballast, water is commonly used to avoid contamination. In this case, the leading (pulling) end of the pipe is sealed to prevent the slurry from entering. When the water is inserted into the pipe, at the trailing end, as it is pulled into the borehole, it may generally be assumed that the pipe will be filled with water along the entire belowground length, but this assumption may not be true for a non-level grade, as discussed below. However, it is assumed that the pipe is continuously filled with water, as the installation proceeds, with any excess water flowing out of the open (tail) end of the pipe.

8.2 GEOMETRY A

Figure 8-1 is similar to that of Figure 7-2 in Chapter 7, for an upward installation, but adds the additional dimension, L_h, corresponding to the point D_h located at the level of the internal water ballast which depends on the magnitude of the differential height ($H_2 - H_1$) in relation to the height, h, of a column of water that can be supported by atmospheric pressure; i.e., approximately 34 ft.[23] The horizontal portion of the segment $D_h - D$, drained of internal ballast, is determined by the distance $L_4 - L_h$, with L_h indicated in Figure 8-1 and given by:

$$L_h = L_4 \cdot \{ 1 - MAX [(\Delta H - h)/H_2, 0] \}^{½} \qquad [8\text{-}1]$$

[22] Ref. "Maxi-HDD Pull Loads in Non-level Grade for Polyethylene Pipe Including Ballast", Slavin,, Najafi and Skonberg, ASCE Pipelines 2011 Conference and "Maxi-HDD Pull Loads for Entry and Exit Points at Different Elevations", Slavin and Najafi, ASCE Journal of Pipeline Systems Engineering and Practice, August 2015.

[23] The partial retraction of water within the pipe reduces the internal pressure at its leading end to below atmospheric, presumably corresponding to a vacuum. This effect is contrary to the additional benefit internal ballast in reducing the pipe's vulnerability to collapse by offsetting the external hydrostatic pressure of the slurry at increasing depths. This condition should be evaluated during the design process, using the methodology in ASTM F1962, especially for relatively thin-walled pipe and/or if exposed over an extended period of time.

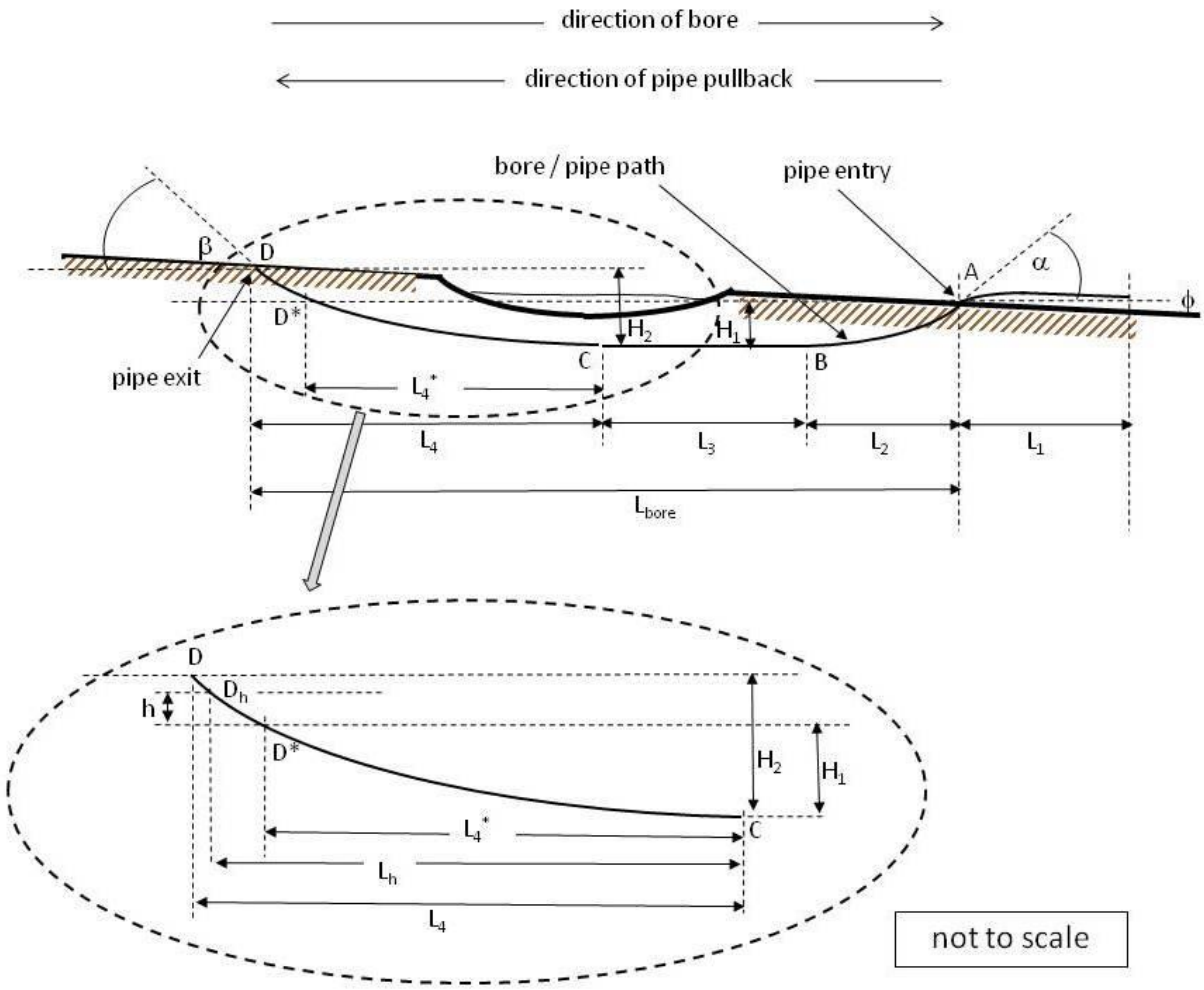

Figure 8-1. Maxi-HDD Pipe Pullback with Upward Grade, with Ballast – Geometry A (Courtesy of Outside Plant Consulting Services, Inc.)

8.21 Upward Grade

Similar to Equations [7-4], the generalized governing equations for an upward grade, considering the effect of slurry drainage from the borehole, as well as the retraction of the water ballast within the pipe, become:

$$T_A = e^{\nu_a(\alpha+\phi)} \cdot (\nu_a + \phi) \cdot w_a \cdot (L_1 + L_2 + L_3 + L_4)` \quad [8\text{-}2a]$$

$$T_B = e^{\nu_b \alpha} \cdot (T_A + \nu_b \cdot w_b^{\,1} \cdot L_2 + w_b \cdot \mathbf{H_1} - (\nu_a + \phi) \cdot w_a \cdot L_2 \cdot e^{\nu_a(\alpha+\phi)}) \quad [8\text{-}2b]$$

$$T_C = T_B + \nu_b \cdot w_b^{\,1} \cdot L_3 - e^{\nu_b \alpha} \cdot [(\nu_a + \phi) \cdot w_a \cdot L_3 \cdot e^{\nu_a(\alpha+\phi)}] \quad [8\text{-}2c]$$

$$\begin{aligned} T_D = {} & e^{\nu_b \beta} \cdot (T_C + \nu_b \cdot w_b^{\,1} \cdot \mathbf{L_4^* + \nu_b \cdot w_a^{\,1} \cdot (L_h - L_4^*) + \nu_b \cdot w_a \cdot (L_4 - L_h)} \\ & - w_b \cdot \mathbf{H_1} + \mathbf{w_a^{\,1} \cdot MIN\,[\Delta H, h]} + \mathbf{w_a \cdot \{MAX\,[\Delta H, h] - h\}} \\ & - e^{\nu_b \alpha} \cdot [(\nu_a + \phi) \cdot w_a \cdot L_4 \cdot e^{\nu_a(\alpha+\phi)}]) \end{aligned} \quad [8\text{-}2d]$$

where the various terms are as previously defined and $w_b^{\,1}$ is the (upward) buoyant weight with ballast and $w_a^{\,1}$ is the (downward) weight of the pipe, due to gravity, when filled with the water ballast.

Equation [8-2d] is more complicated than Equation [7-4d] since it accounts for a combination of possible interactions, including the drainage of the slurry external to the pipe and the retraction of the water internal to the pipe. The individual terms in this equation account for the frictional drag resulting from the forces within the borehole responding to the (upward) buoyant weight in section C – D*, the (downward, gravity) weight of the relatively heavy water-filled pipe in section D* – D_h, and the (downward, gravity) weight of the empty pipe in section D_h – D. The three other terms that include the heights (H_1, ΔH, h) account for the tendency of the net buoyancy or weight (gravity) to decrease or increase the required force in these corresponding sections.

8.22 Downward Grade

Figure 8-2 is identical to Figure 7-3 in Chapter 7, for a downward installation, indicating there are no additional phenomena associated with the presence of the internal ballast. In practice, however, the relevant weights are dramatically different, including the greatly reduced (upward) buoyant weight, w_b^1, in the sections between points A* and D, as well as the (downward, gravity) weight, w_a^1, of the relatively heavy water-filled pipe in section A* – A. Both of these effects tend to reduce the required pulling force.

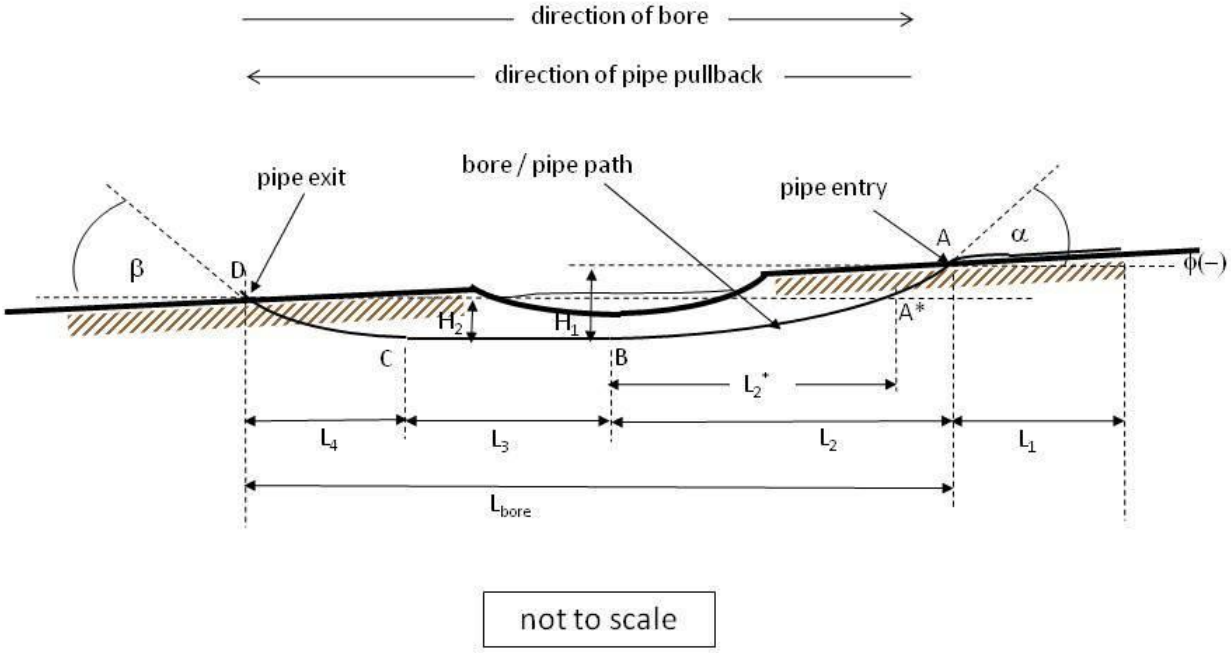

Figure 8-2. Maxi-HDD Pipe Pullback with Downward Grade, with Ballast – Geometry A (Courtesy of Outside Plant Consulting Services, Inc.)

The appropriate equations are now:

$$T_A = e^{\nu_a(\alpha+\phi)} \cdot (\nu_a + \phi) \cdot w_a \cdot (L_1 + L_2 + L_3 + L_4) \quad [8\text{-}3a]$$

$$T_B = e^{\nu_b \alpha} \cdot (T_A + \nu_b \cdot w_b^1 \cdot \mathbf{L_2^*} + \mathbf{\nu_b \cdot w_a^1\ [L_2 - L_2^*]} + w_b^1 \cdot \mathbf{H_2} + \mathbf{w_a^1} \cdot \mathbf{\Delta H} - (\nu_a + \phi) \cdot w_a \cdot L_2 \cdot e^{\nu_a(\alpha+\phi)}) \quad [8\text{-}3b]$$

$$T_C = T_B + \nu_b \cdot w_b^1 \cdot L_3 - e^{\nu_b \alpha} \cdot [(\nu_a + \phi) \cdot w_a \cdot L_3 \cdot e^{\nu_a(\alpha+\phi)}] \quad [8\text{-}3c]$$

$$T_D = e^{\nu_b \beta} \cdot (T_C + \nu_b \cdot w_b^1 \cdot L_4 - w_b^1 \cdot \mathbf{H_2} - e^{\nu_b \alpha} \cdot [(\nu_a + \phi) \cdot w_a \cdot L_4 \cdot e^{\nu_a(\alpha+\phi)}]) \quad [8\text{-}3d]$$

The equations, as written, are valid for $(\nu_a + \phi) \geq 0$, or $-\phi \leq \nu_a$, for which it is again noted that the local grade angle, ϕ, as indicated in Figure 8-2 is considered to be negative.

8.3 GEOMETRY B

Figure 8-3 is similar to that of Figure 7-4 in Chapter 7, for the alternate Geometry B for an upward installation. In this case, there is the additional dimension, L_h, as well as L_h', corresponding to the points D_h and D_h', respectively, and are located at the level of the internal water ballast as it may retract within the leading end of the pipe, in relation to the height, h, of a column of water that can be supported by atmospheric pressure. This allows for the possibility that the level of the water ballast may be within either segment C – D or B – C.

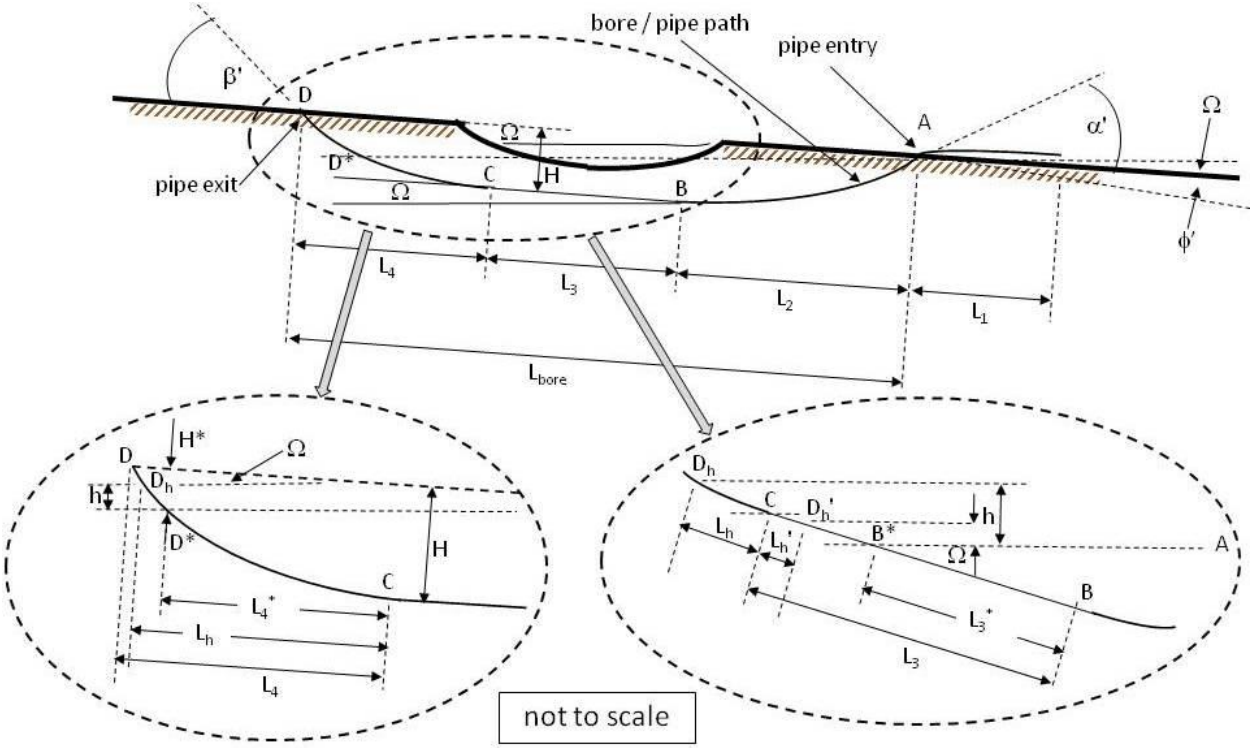

Figure 8-3. Maxi-HDD Pipe Pullback with Upward Grade, with Ballast – Geometry B (Courtesy of Outside Plant Consulting Services, Inc.)

The distances L_h and L_h' may be determined by:

$$L_h' = \text{MAX}\{ [(L_3 - L_3^*) - h/\Omega], 0\} \quad [8\text{-}4]$$

and

$$L_h = L_4 \cdot \{1 - [H^* - \text{MIN}(H^*, \text{MAX}\{[h - (L_3 - L_3^*)\,\Omega], 0\})]/H\}^{1/2} \quad [8\text{-}5]$$

8.31 Upward Grade

Considering an uphill installation (Figure 8-3) for Geometry B, and the use of internal water ballast, the following equations result:

$$T_A = e^{\nu_a(\alpha' + \varphi')} \cdot (\nu_a + \Omega + \phi') \cdot w_a \cdot (L_1 + L_2 + L_3 + L_4)` \quad [8\text{-}6a]$$

$$T_B = e^{\nu_b \alpha'} \cdot (T_A + \nu_b \cdot w_b \cdot L_2 + w_b \cdot (H - \mathbf{L_2 \cdot \Omega}) - (\nu_a + \Omega + \phi') \cdot w_a \cdot L_2 \cdot e^{\nu_a(\alpha' + \phi')} \quad [8\text{-}6b]$$

$$\begin{aligned} T_C = {} & T_B + \nu_b \cdot w_b \cdot \mathbf{L_3^*} + \mathbf{\nu_b \cdot w_a^1 \cdot (L_3 - L_3^* - L_h')} + \mathbf{\nu_b \cdot w_a \cdot L_h'} \\ & - \mathbf{\Omega \cdot [w_b \cdot L_3^* - w_a^1 \cdot (L_3 - L_3^* - L_h') - w_a \cdot L_h']} \\ & - e^{\nu_b \alpha'} \cdot (\nu_a + \Omega + \phi') \cdot w_a \cdot L_3 \cdot e^{\nu_a(\alpha' + \varphi')}] \end{aligned} \quad [8\text{-}6c]$$

$$\begin{aligned} T_D = {} & e^{\nu_b \beta'} \cdot (T_C + \nu_b \cdot w_b \cdot \mathbf{L_4^* + \nu_b \cdot w_a^1 \cdot (L_h - L_4^*) + \nu_b \cdot w_a (L_4 - L_h)} \cdot \\ & - w_b \cdot (H - \mathbf{H^* + L_4^* \cdot \Omega}) \\ & + \mathbf{w_a^1 \cdot MIN\{ [H^* + (L_h - L_4^*)\,\Omega], MAX\{ [h - (L_3 - L_3^*)\Omega], 0 \} \}} \\ & \mathbf{+ w_a \cdot MAX\{[H^* + (L_4 - L_h)\Omega - MIN\{[H^* + (L_h - L_4^*)\Omega], MAX\{[h - (L_3 - L_3^*)\Omega], 0\}\}\}, 0\}} \\ & - e^{\nu_b \alpha'} \cdot [(\nu_a + \Omega + \phi') \cdot w_a \cdot L_4 \cdot e^{\nu_a(\alpha' + \varphi')}]) \end{aligned} \quad [8\text{-}6d]$$

where the various terms are again as previously defined, and, as before (Section 7.3), are valid for $\Omega \leq \alpha'/2$. Equations [8-6} are even more complex than the comparable equations of Section 7.31, due to the additional parameter, h, associated with the height of the water ballast.

8.32 Downward Grade

Similar to the downward installation for Geometry A, Figure 8-4 is identical to Figure 7-5 in Chapter 7, for a downward grade, but for which the relevant weights include the greatly reduced -gravity) weight, w_a^1, of the relatively heavy water-filled pipe in section A* – A. As before, both of these effects tend to reduce the required pulling force compared to the case without ballast.

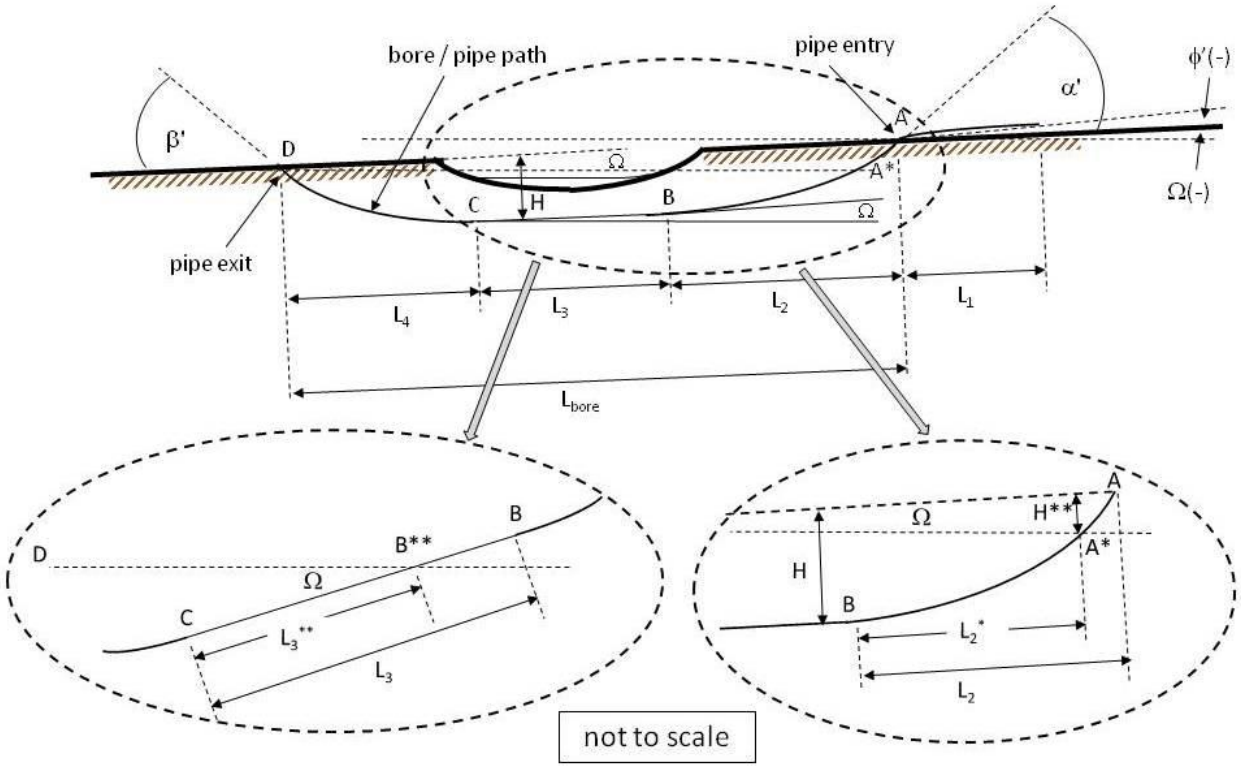

Figure 8-4. Maxi-HDD Pipe Pullback with Downward Grade, with Ballast – Geometry B (Courtesy of Outside Plant Consulting Services, Inc.)

For the downward installation shown in Figure 8-4, the following equations apply:

$$T_A = e^{\nu_a(\alpha' + \varphi')} \cdot (\nu_a + \Omega + \phi') \cdot w_a \cdot (L_1 + L_2 + L_3 + L_4)` \quad [8\text{-}7a]$$

$$T_B = e^{\nu_b \alpha'} \cdot (T_A + \nu_b \cdot w_b^{\,1} \cdot \mathbf{L_2^*} + \boldsymbol{\nu_b \cdot w_a^{\,1} \cdot (L_2 - L_2^*)} + \mathbf{w_b^{\,1} \cdot (H - H^{**} - L_2^* \cdot \Omega)} - \mathbf{w_a^{\,1} \cdot [H^{**} - (L_2 - L_2^*)\Omega]} - (\nu_a + \Omega + \phi') \cdot w_a \cdot L_2 \cdot e^{\nu_a(\alpha' + \phi')} \quad [8\text{-}7b]$$

$$T_C = T_B + \nu_b \cdot w_b^{\,1} \cdot \mathbf{L_3^{**}} + \boldsymbol{\nu_b \cdot w_a^{\,1} \cdot (L_3 - L_3^{**}) - \Omega \cdot [w_b^{\,1} \cdot L_3^{**} - w_a^{\,1} \cdot (L_3 - L_3^{**})]} - e^{\nu_b \alpha'} \cdot (\nu_a + \Omega + \phi') \cdot w_a \cdot L_3 \cdot e^{\nu_a(\alpha' + \varphi')} \quad [8\text{-}7c]$$

$$T_D = e^{\nu_b \beta'} \cdot (T_C + \nu_b \cdot w_b^{\,1} \cdot L_4 - w_b^{\,1} \cdot (H + \mathbf{L_4 \cdot \Omega}) - e^{\nu_b \alpha'} \cdot [(\nu_a + \Omega + \phi') \cdot w_a \cdot L_4 \cdot e^{\nu_a(\alpha' + \varphi')}]) \quad [8\text{-}7d]$$

As previously, Ω and ϕ' are negative, as shown, and it is assumed $|\Omega| \leq \beta'/2$.

8.4 RESULTS AND OBSERVATIONS

The assumed values of the relevant parameters are those in Table 7-1, supplemented by the values in Table 8-1 for the effective weights, corresponding to the use of internal water ballast. (The effective weights without ballast are again shown for comparison.)

Table 8-1 Effective Weights of Pipe

Parameter	Value	Remarks
w_a	61.9 lbs/ft	unsubmerged weight (empty)
w_a[1]	**193.1 lbs/ft**	**unsubmerged weight (with ballast)**
w_b	173.4 lbs/ft	submerged buoyant weight (empty)
w_b[1]	**42.1 lbs/ft**	**submerged buoyant weight (with ballast)**

Figures 8-5 and 8-6 show the results for the tension at the end of the installation, including both upward and downward installations, for the basic geometries characterized in Table 7-1, including a 2500 ft long bore path and (minimum) depth of 45 ft. The following immediate observations may be made regarding the effect of a non-level grade, with or without the use ballast:

- Whereas the use of water ballast dramatically reduces the required installation force for a level grade, this not necessarily true for an installation with a significant grade;
- The magnitude of the load reduction, if any, will depend on the bore path geometry.

These interesting results are due to the effect of the relatively heavy water-filled pipe in drained sections of the bore path for which the pipe is not submerged in drilling fluid. This corresponds to an increase in frictional drag, hindering the installation, as well as greater downward forces due to gravity, which may hinder (upward grade) or help (downward grade) the installation process. Whereas Figure 8-5 shows a significant benefit when using Geometry A (with ballast), whether pulling upward or downward, the more likely configuration of Geometry B is considerably more complicated with respect to the potential benefits. Indeed, for the example installation with this the latter configuration, Figure 8-6 shows that the load reduction (with ballast) essentially vanishes at grade angles of several percent, and even indicates that the use of ballast for a downward installation, using ballast, exceeds that without ballast. This effect is further exaggerated for a longer, 5000 ft bore path, as illustrated in Figure 8-7 for which the largest estimated pull force corresponds to a downward installation, using internal water ballast, compared to an upward installation and/or the absence of such ballast.

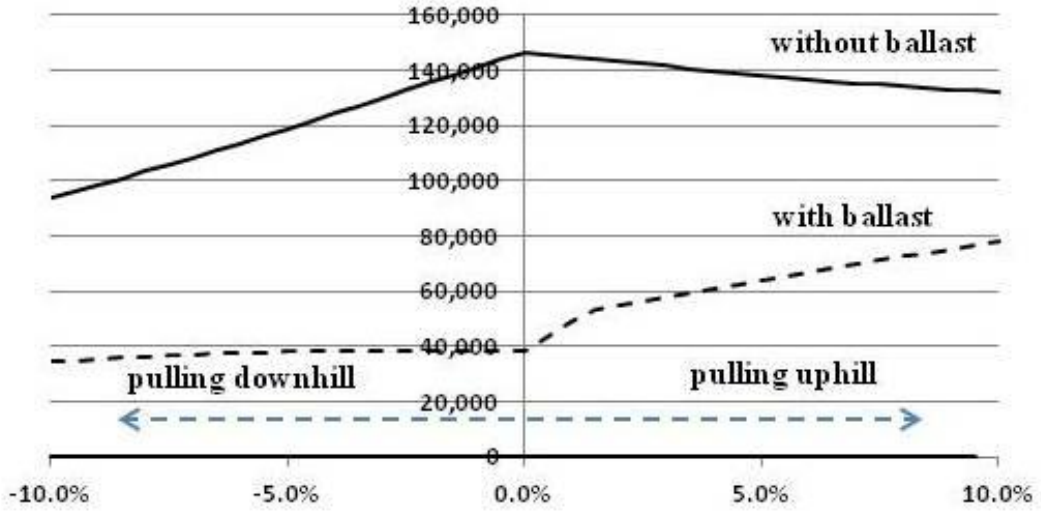

Figure 8-5. Tension vs. Average Grade, Geometry A (2,500 ft)

In other words, the intuitively most favorable method of installation – pulling downward, and deploying internal water ballast – may actually be the most difficult, with respect to the required pull force on the product pipe itself. This suggests that the use of internal water ballast may be counter-productive for a relatively high grade, depending on the bore path details. Therefore, for applications characterized by a relatively large average grade, it may be advisable, depending on the bore path details, to *forego the use of the ballast*, thereby considerably simplifying the process.

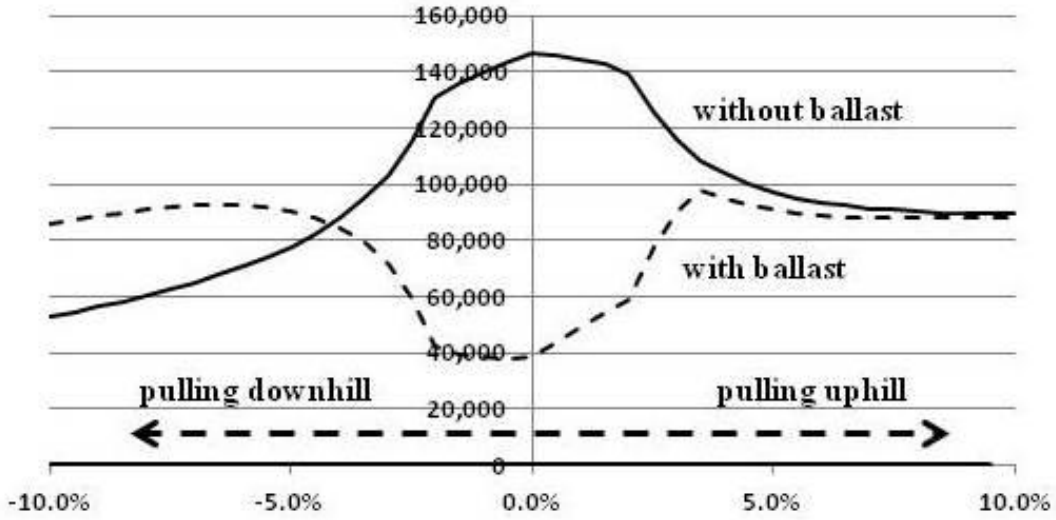

Figure 8-6. Tension vs. Average Grade, Geometry B (2,500 ft)

Although these results are based on particular geometries and parametric values, for which the quantitative results will not be universally applicable, the general observations are significant, and, provide an improved understanding of the various phenomena. For a particular

application of interest, the formulae for the generic geometries used herein may possibly be used to estimate the required pull force for various installation parameters, as appropriate. For significantly different bore path configurations, similar principles may be used to develop corresponding formulae, or other available HDD planning and design methods may be applied to investigate the issues addressed in this investigation. However, it is important to note that the observations regarding the relative benefits regarding the direction of pulling, in combination with the possible use of internal water ballast, are based entirely on anticipated tensile loads. Potential issues related to the removal of spoils during the initial boring or back-reaming operations, and other possible issues related to the direction of operation, have not been considered in the investigations.

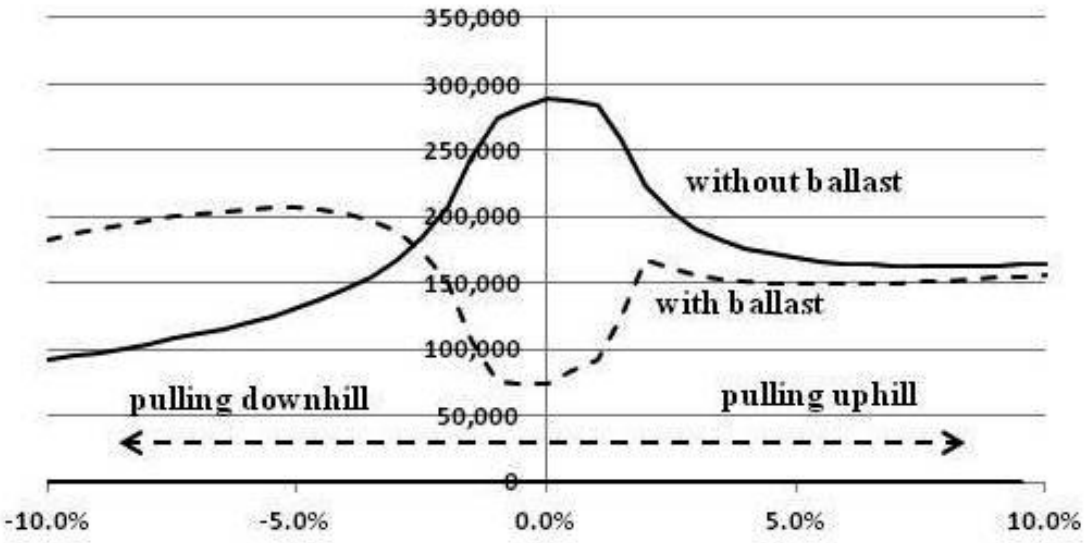

Figure 8-7. Tension vs. Average Grade, Geometry B (5000 ft)

GLOSSARY

The following definitions supplement the dictionary definitions, which may not always be sufficient for the purposes of this manual.

ballast: material to offset the (upward) buoyancy effects produced by a fluid on an relatively light, possibly hollow, object; e.g., water within a hollow pipe.; see "buoyant weight".

bending stiffness: a measure of the resistance of a long object, such as a pipe, to lateral deflection, quantified by the product of the "elastic modulus" (E) and "cross-section moment of inertia" area (I), or "EI".

borehole: the path belowground path or cavity created by the drilling process.

buoyant weight: the net (effective) upward force on an object submerged in a fluid, equal to the (upward) buoyant force less the (downward) gravitational force.

capstan effect: the amplification of the tension on a rope, cable or flexible pipe pulled around a curved surface, due to the normal reaction force at the surface, resulting from the tension vectors, and corresponding frictional drag; see "frictional drag".

clearance: the space between the product pipe and borehole wall; quantitatively equal to the borehole diameter minus the pipe outer diameter.

coefficient of friction: the ratio of the drag force at a surface to the local (normal/perpendicular) reaction force; see "frictional drag"; see "Coulomb friction".

complete bend: a uniform curvature (constant radius) of sufficient angular extent such that a pipe within the curve conforms to the curvature of the bend

Coulomb friction: a type of surface friction for which the magnitude of the force resisting movement is linearly proportional to the normal force at the surfaces; see "coefficient of friction".

Cross-section area moment of inertia: the geometric property of a cross-section which, in combination with the elastic modulus, determines the bending stiffness of a beam or pipe.

density: the weight per unit volume of a solid, liquid or gaseous material; e.g., lbs/ft^3.

depth: the vertical distance of a belowground object from the ground or water surface directly above.

Dimension Ratio (DR): the ratio of the pipe outer diameter to the wall thickness.

Ductile Iron Pipe Sizes (DIPS): standard pipe sizes based on the outer diameter, originally intended for specification of ductile iron pipe, but also used for specifying the outer diameter of other type pipe, including polyethylene.

drilling fluid: the liquid used to penetrate the soil, remove cuttings, and provide borehole stability, lubrication and cooling during a drilling or boring operation; typically under high pressure but low volume for HDD operations.

elastic: the property of a material relating the force required to produce a deformation, from which the material fully recovers when the load is removed; see **viscoelastic**.

elastic modulus: the linear relationship between the force required to produce a (temporary) elastic deformation and the magnitude of the deformation; see **elastic** and **viscoelastic**.

entry angle: as usually expressed in degrees, the angle of the drill rods entering the ground at the drill rig, or the angle of the product pipe being pulled into the completed borehole at the end of the bore path opposite the drill rig, depending upon the context; the entry angle at the drill rig is the exit angle of the pipe at the end of its installation, and the exit angle at the drill rig is the entry angle of the pipe at the beginning of its installation.

exit angle: see "entry angle".

fluidic drag: the force at the surface of an object exerted by a fluid on the surface, acting in the direction of the relative motion of the fluid to the surface.

frictional drag: the force at the surface of an object resisting its movement in the direction of a pulling force; typically assumed to be proportional to the local reaction force at the surface; see "coefficient of friction".

grade: the slope of terrain, measured by the vertical rise per unit horizontal (projected) distance, expressed as a percentage.

HDPE: high density polyethylene.

hydrokinetic pressure: the liquid pressure at the leading end of the pipe, due to the pumping of the drilling fluid.

Iron Pipe Sizes (IPS): standard pipe sizes based on the outer diameter, originally intended for specification black iron pipe, but now also used for specifying the outer diameter of other type pipe, including polyethylene.

Maxi-HDD: a category of horizontal directional drilling using very large machines with corresponding drilling and placement capabilities.

Midi-HDD: a category of horizontal directional drilling using machines of size and capability intermediate to that of mini-HDD and maxi-HDD.

Mini-HDD: a category of horizontal directional drilling using relatively small machines with corresponding drilling and placement capabilities.

PRC method: an analytic method for estimating the pull load on a steel pipe during an HDD operation, developed by developed by the Pipeline Research Committee of the American Gas Association.

safe pull (tensile) stress (SPS): the allowable tensile stress level for the HDPE pipe, to limit non-recoverable viscoelastic deformation, based on the inherent material strength, load duration and material temperature.

safe pull (force, tension) strength: the tensile force on the cross-section of the pipe, based on the safe pull stress (SPS), but ignoring any local bending stresses.

slurry: the combination of drilling fluid and soil cuttings resulting from an HDD drilling operation; also referred to as "mud".

specific gravity: the ratio of the density of a material to that of water (approximately 62.4 lbs/ft^3).

tail load: the restraining force at the entrance to a bend around which a rope, cable or flexible pipe is pulled.

viscoelastic: the property of materials, such as polyethylene, to deform under load, due to a combination of recoverable ("elastic") deformation and non-recoverable deformation, where the latter (permanent or temporary) deformation is a function of load duration; see **elastic**.

viscosity: the resistance of a fluid to flow along a surface, corresponding to a shear (drag) force acting at the surface.

REFERENCES

Adedamola, A. and Knight, M.A. (2002). "Applicability of Methods Used to Estimate Pipe-Slurry Fluidic Drag Force During HDD Pipe Installations", North American Society for Trenchless Technology, NO-DIG 2002

ASCE (2014). *Manual and Reports on Engineering Practice No. 108, Pipeline Design for Installation by Horizontal Directional Drilling*, American Society of Civil Engineers, Second Edition, 2005.

AWWA (2020) *PE Pipe – Design and Installation,* M55, American Water Works Association, Second Edition, 2020.

Baumert, M., Allouche, E., and Moore, I. (2005). "Drilling Fluid Considerations in Design of Engineered Horizontal Directional Drilling Installations", International Journal of Geomechanics., December 2005.

Bayat, A., Lawrence, K., Knight, M. and Rubeiz, C. (2011). "New Generation of Design Tools for Directional Drilling Projects", International Conference on Pipelines and Trenchless Technology, 2011.

Buller, F.H. (1949). "Pulling Tension During Cable Installation in Ducts or Pipes", General Electric Review, August 1949.

Cheng, E. and Polak, M.A. (2007). "Theoretical Model for Calculating Pulling Loads for Pipes in Horizontal Directional Drilling", Tunnelling and Underground Space Technology, 2007.

Duyvestyn, G. (2009). "Comparison of Predicted and Observed HDD Installation Loads for Various Calculation Methods", North American Society for Trenchless Technology, NO-DIG 2009.

El-Chazli, G., Hinchberger, S., Baumert, M. and Allouche, E.N. (2005). "Experimental Investigation of Borehole and Surface Friction Coefficients During HDD Investigations", North American Society for Trenchless Technology, NO-DIG 2005.

Faghih, A., Yaolin, Y., Bayat, A. and Osbak, M. (2015). "Fluidic Drag Estimation in Horizontal Directional Drilling Based on Flow Equations", ASCE Journal of Pipeline Systems Engineering and Practice, November 2015.

Finnsson, S. (2004). "TensiTrak™ – A Tension Load and Drilling Fluid Pressure-Monitoring Device for Horizontal Directional Drilling Installations", North American Society for Trenchless Technology, NO-DIG 2004.

Griffioen, W. (1993). *Installation of Optical Cables in Ducts*, Plumettaz SA, 1993.

Hair & Associates, Capozzoli & Associates, and Stress Engineering Services (1995). "Installation of Pipelines by Horizontal Directional Drilling, an Engineering Design Guide", Pipeline Research Committee, American Gas Association, April 15, 1995.

Hair, J., *Installation of Pipelines by Horizontal Directional Drilling Design Guide*, PR-277-144507-Z01, Pipeline Research Council International, 2015.

HDD Consortium, (2008). *Horizontal Directional Drilling – Good Practices Guidelines*, 3rd Edition, North American Society for Trenchless Technology.

Huey, D.P., Hair, J.D. and McLeod, K.B. (1996). "Installation Loading and Stress analysis Involved with Pipelines Installed by Horizontal Directional Drilling", North American Society for Trenchless Technology, NO-DIG 96.

Knight, M.A., Duyvestyn, G.M., and Polak, M.A. (2002). "Horizontal Directional Drilling Installation Loads on Polyethylene Pipes", North American Society for Trenchless Technology, NO-DIG 2002.

Knight, M.A. and Adedamola, A. (2003). "Are Designers Overestimating the Maximum HDD Pull Load?", Presentation at Underground Construction Technology Conference, 2003.

Performance Pipe (2007). *Field Handbook*, Performance Pipe, Bulletin PP-901, August 2007.

Petroff, L. (2004) "Horizontal Directional Installation of Polyethylene Pipe", ASCE Pipelines 2004 Conference.

Petroff, L. (2006). "Designing Polyethylene Water Pipe for Directional Drilling Applications Using ASTM F 1962", North American Society for Trenchless Technology, NO-DIG 2006.

Petroff, L.J. (2010). "Directional Drilling Design with ASTM F1962: A Decade of Success", ASCE 2010 Pipelines Conference.

Plastics Pipe Institute (2008). *The Plastics Pipe Institute Handbook of Polyethylene Pipe*, Second Edition, 2008.

Plastics Pipe Institute (2020). *MAB Guidelines for Use of Mini-Horizontal Directional Drilling for Placement of HDPE (PE4710) Pipe in Municipal Applications*, MAB-7, 2020.

Plastics Pipe Institute. PPI Boreaid™, http://ppiboreaid.com.

PipeEng. "Reinvent Pipeline Engineering Tools", https://pipeeng.com/hdd.html.

Puckett, J.S. (2003). Analysis of Theoretical Versus Actual HDD Pulling Loads, ASCE Pipelines 2003 Conference.

PWPipe (2000). "PVC C900 High Pressure Water Pipe", PWPipe, April 2000.

Rabiei, M., Yi, Y., Bayat, A., and Cheng, R. (2016). "General Method for Pullback Force Estimation for Polyethylene Pipes in Horizontal Directional Drilling", ASCE Journal of Pipeline Systems Engineering and Practice, January 2016.

Rabiei, M., Yi, Y., Bayat, A., Cheng, R. and Osbak, M. (2017). "Estimation of Hydrokinetic Pressure and Fluidic Drag Changes during Pipe Installations via HDD Based on Identifying Slurry-Flow Pattern Change within a Borehole", ASCE Journal of Pipeline Systems Engineering and Practice, November 2017.

Rifenburg, R.C. (1953). "Pulling Pipeline Design for Pipe-Type Feeders", Transaction AIEE Power Apparatus and Systems, Vol. 72, Part III, 1953.

Roark, R.J. (1943). "Formulas for Stress & Strain", Second Edition, McGraw-Hill, 1943.

Slavin, L.M. (2007). "Simplified Methodology for Selecting Polyethylene Pipe for Mini (or Midi) – HDD Applications", ASCE Pipelines 2007 Conference.

Slavin, L.M. (2010). “Parametric Dependency and Trends of HDD Pull Loads”, ASCE Journal of Pipeline Systems Engineering and Practice, May 2010.

Slavin, L.M. and Petroff, L. (2010). “Discussion of ASTM F 1962 or “How are the Pulling Load Formulas Derived and How are they Used?’ ”, North American Society for Trenchless Technology, NO DIG 2010.

Slavin, L.M., Najafi, M. and Skonberg, E.R. (2011). “Maxi-HDD Pull Loads for Nonlevel Grade for Polyethylene Pipe”, ASCE Journal of Pipeline Systems Engineering and Practice, May 2011.

Slavin, L.M., Najafi, M. and Skonberg, E.R. (2011a). “Maxi-HDD Pull Loads in Non-Level Grade for Polyethylene Pipe Including Ballast”, ASCE Pipelines 2011 Conference.

Slavin, L.M. and Najafi, M. (2012). “Effect of Pipe Stiffness on Maxi-HDD Pull Loads”, ASCE Journal of Pipeline Systems Engineering and Practice, February 2012.

Slavin, L.M. and Najafi, M. (2015). Maxi-HDD Pull Loads for Entry and Exit Points at Different Elevations”, ASCE Journal of Pipeline Systems Engineering and Practice, August 2015.

Slavin, L.M. and Scholl, J. (2014). “Which Method to Use When Estimating Maxi-HDD Installation Loads − ASTM F1962 or the PRCI Method?”, ASCE Pipelines 2014 Conference.

Svetlik, H.E. (1995). “Polyethylene Pipe Design for Directional-Drillings and River-Crossings”, North American Society for Trenchless Technology, NO-DIG 1995.

Vermeer Corporation. BoreAid®.

Xiao, S., Li, L. and Wu, S. (2012). “Calculations and Analysis of Pullback Force in Horizontal Directional Drilling”, International Conference on Pipelines and Trenchless Technology, 2012.

Young, W.C. (1989). “Roark’s Formulas for Stress & Strain”, Sixth Edition, McGraw-Hill, 1989.

Zeng, C., Jia, Z., Kong, Y. and Han, Y, (2013) “Estimating Pull-back Force of Horizontal Directional Drilling in Medium and Coarse Sand”, ASCE Pipelines 2013 Conference.